

# Continuous and discontinuous Galerkin finite element methods of variational Boussinesq water-wave models

M. Sc. thesis.

O.R. Koop

*University of Twente*

*Department of Applied Mathematics*

*Group of Numerical Analysis and Computational Mechanics*

October 4, 2006



*Supervisors:*

Dr. Ir. O. Bokhove (University of Twente)

Ir. G. Klopman (University of Twente)

*Committee:*

Dr. Ir. O. Bokhove

Ir. G. Klopman

Dr. R.M.J. van Damme

Ir. S. Rhebergen

M.Sc. D. Hurdle



## Abstract

There are many reasons to investigate the propagation of surface water waves in the sea. In this report Boussinesq models are studied, that can be applied for modeling free-surface waves propagating from the deep sea up into the surf zone. These models can become fairly complex and improving linear frequency dispersion properties of these Boussinesq models often invoke difficult higher-order terms in the resulting partial differential equations [18].

Among others, Broer [7, 8], Broer et al.[9]and Klopman et al.[19] propose, based on the variational principle for potential flows proposed by Luke [27], variational Boussinesq models to describe potential flows with dispersion. The advantage of these models is that energy is conserved and guaranteed to be positive, while mixed higher order spatial and temporal derivatives are avoided. The cost of this is that we additional unknown quantities, with associated elliptic partial differential equations, that are relatively simple to solve numerically [20].

In this report three variational models are considered, namely those of Luke [27], Klopman et al. [19] and Whitham [37], and they are extended including surface tension effects. Additionally, we integrated the motion of the fluid domain boundaries with our variational principles describing the fluid motion. We compare the linear dispersion relations of the three models and draw the conclusions that the Klopman variational Boussinesq model approximates the exact linear dispersion obtained from Luke variational principle for potential flow, better than the Whitham model.

We numerically solve the Whitham and Klopman variational Boussinesq models in time using a continuous Galerkin finite element method. To simulate the propagation of the discontinuous jump that occurs when waves are breaking, we propose a discontinuous Galerkin finite element method. In this progress of this report, a discontinuous Galerkin approach was successfully applied to the linear Klopman variational Boussinesq model. This approach can be followed to formulate a discontinuous Galerkin finite element discretization to solve the fully nonlinear model.

In this report it is shown that breaking waves do not occur in Whitham's variational Boussinesq model for waves propagating over a horizontal seabed. Further, we consider the weakly nonlinear Klopman VBM, i.e. neglecting higher-order waves-slope effects, and it is shown that waves described by this model can not break as well. Further research on the fully nonlinear Klopman variational Boussinesq model is required. In this report we draw some conclusions and state recommendations, particularly on how to construct a discontinuous Galerkin FEM to solve the fully nonlinear Klopman variational Boussinesq model numerically.



## Preface

The research in this M.Sc. thesis has been conducted at the University of Twente. I did my research within the department of Applied Mathematics in the group Numerical Analysis and Computational Mechanics. I chose the Boussinesq water-wave models as the subject of my thesis, because since I was a small child I have been interested in water motion. Waterfalls, breaking waves and waves moving up and down the beaches have always intrigued me. I enjoy being in the water as my main hobbies are waterpolo and swimming. Moreover, I find the beauty of solving practical problems with such an abstract tool as mathematics, combined with the power of numerical methods to solve practical problems, very appealing.

First of all I would like to thank Onno Bokhove, for his everlasting enthusiasm, his straightforward manner, his criticism and teaching me to become a better research worker. I would like to thank Gert Klopman, for the fruitful discussions we had and his help investigating the model that he et al. proposed. I would like to thank both supervisors for the pleasant co-operation and for their efforts correcting and looking over my thesis.

Furthermore I would like to thank Chris Klaij, Vyjaja Ambati and Sander Rhebergen for their helpful suggestions on the lifting operators and getting acquainted with  $\LaTeX$ 2e and C++. Moreover, I would like to thank Sander for overlooking the chapter on discontinuous Galerkin and being a member of the committee. Furthermore, I would like to thank Ruud van Damme and David Hurdle for their willingness to serve on the committee.

Marieke and Renske, I really had a pleasant time with you in the *afstudeerkamer*, thank you. Bernhard, Chris, Diana, Fedderik, Mariëlle, Sander and all others with whom I spent my daily lunch, thank you for the pleasant time.

A special word of thanks to my parents, Jeanie and Henk, for their love and care, for their everlasting support and understanding: Thank you. Arjen and Emily, I am really happy having you as brother and "schone zus" and I have enjoyed the time we have spent in Enschede. Which city will follow hereafter?! Shelly, thank you for everything!

Olger Koop

Enschede, Octobre 2006



# Contents

<b>Abstract</b>	<b>iii</b>
<b>Preface</b>	<b>v</b>
<b>List of Figures</b>	<b>ix</b>
<b>Nomenclature</b>	<b>xi</b>
<b>1 Introduction</b>	<b>1</b>
1.1 Motivation . . . . .	1
1.2 Mathematical model . . . . .	1
1.3 Numerical computation . . . . .	2
<b>2 Variational principles for water waves</b>	<b>3</b>
2.1 Introduction . . . . .	3
2.2 Luke’s variational principle for free-surface potential flow . . . . .	3
2.3 Klopman’s variational Boussinesq model (KVBM) . . . . .	7
2.4 Whitham’s variational Boussinesq model (WVBM) . . . . .	10
2.5 Comparison of dispersion relations . . . . .	11
2.6 Moving boundaries in the KVBM . . . . .	16
2.7 Conclusion . . . . .	18
<b>3 Numerical modeling: continuous Galerkin</b>	<b>19</b>
3.1 Introduction . . . . .	19
3.2 Whitham’s Boussinesq variational principle . . . . .	19
3.3 Assembly of global nodes . . . . .	21
3.4 Klopman’s variational Boussinesq model . . . . .	24
3.5 Assembly of global nodes . . . . .	25
3.6 Time integration . . . . .	28
3.7 Conclusion . . . . .	29
<b>4 Numerical Modeling: Discontinuous Galerkin</b>	<b>31</b>
4.1 Introduction . . . . .	31
4.2 Finite element discretization . . . . .	31
4.3 Linear shallow water system . . . . .	34
4.4 Numerical Fluxes . . . . .	36
4.5 Elliptic equations . . . . .	37
4.6 Linearized Klopman model . . . . .	38
4.7 Conclusion . . . . .	41
<b>5 Verification</b>	<b>43</b>
5.1 Introduction . . . . .	43
5.2 Shallow water equations . . . . .	43
5.3 Whitham’s variational Boussinesq model . . . . .	47
5.4 Klopman’s variational Boussinesq model . . . . .	49
5.5 Small amplitude waves in the KVBM . . . . .	50
5.6 Large amplitude waves in the KVBM . . . . .	52
5.7 Conclusion . . . . .	52
<b>6 Investigation into wave breaking and linear dispersion</b>	<b>55</b>
6.1 Introduction . . . . .	55

6.2	Wave breaking . . . . .	55
6.3	Linear dispersion . . . . .	58
<b>7</b>	<b>Conclusions</b>	<b>61</b>
<b>8</b>	<b>Recommendations</b>	<b>63</b>
	<b>References</b>	<b>65</b>
<b>A</b>	<b>Nonlinear shallow water equations with discontinuous Galerkin</b>	<b>68</b>
A.1	Non-linear shallow water equations . . . . .	68
A.2	DG discretization with polynomials of degree 1 . . . . .	68
A.3	Algebraic system of equations . . . . .	68
<b>B</b>	<b>Klopman’s variational Boussinesq discontinuous Galerkin discretization</b>	<b>71</b>
B.1	DG discretization with polynomials of degree 1 . . . . .	71
B.2	Algebraic system of equations . . . . .	71
<b>C</b>	<b>Brezzi’s approach</b>	<b>73</b>
C.1	Fixed boundary conditions . . . . .	73
C.2	Periodic boundary conditions . . . . .	73
C.3	Conclusion . . . . .	73
<b>D</b>	<b>Periodic wave solutions for WVBM model</b>	<b>75</b>
D.1	Model equations . . . . .	75
D.2	Periodic solutions . . . . .	75
D.3	Integrations . . . . .	75
D.4	Model closure . . . . .	76
D.5	Further investigation into the periodic wave solutions . . . . .	77
D.6	Numerical solution . . . . .	78

## List of Figures

2.2.1 Parameters describing potential flow. . . . .	3
2.3.1 Parameters describing the fluid (KVBM/WVBM). . . . .	8
2.5.1 Dispersion relations for two types of Boussinesq-models . . . . .	12
2.5.2 Dispersion relations with surface tension for various (small) water depths . . . . .	14
3.2.1 Subdivision into $N$ elements $K_j$ of the horizontal domain $D_h$ . . . . .	19
3.2.2 Linear basis functions for continuous Galerkin finite elements . . . . .	20
4.2.1 Discretization for the DG FEM . . . . .	32
5.2.1 Initial sinusoidal wave profile . . . . .	44
5.2.2 Three time integration methods for linear SWE. . . . .	45
5.2.3 Nonlinear SWE (deep water, CG FEM). . . . .	46
5.2.4 Nonlinear SWE (deep water, DG FEMs). . . . .	46
5.3.1 Nonlinear WVBM, small amplitude (CG FEM). . . . .	48
5.3.2 Nonlinear WVBM, cnoidal wave . . . . .	49
5.3.3 Nonlinear WVBM, matlab BVP . . . . .	49
5.5.1 Small amplitude waves KVBM; Surface height and energy . . . . .	51
5.6.1 Large amplitude waves in linear KVBM; Surface height and velocity potential . . . . .	53
6.2.1 Nonlinear WVBM; sinusoidal wave . . . . .	56
6.2.2 Weakly nonlinear KVBM; sinusoidal wave . . . . .	57
6.3.1 Linear KVBM and linear SW; (DG) . . . . .	59
D.6.1 Numerical solution of the WVBM . . . . .	80



## Nomenclature

$\phi(x, y, z, t)$	The velocity potential of a particle located at $(x, y, z)$ at time $t$ .
$\lambda$	Wavelength
$c$	Wave speed
$T$	Time period
$\kappa$	Wave number
$\eta$	Wave elevation
$d$ and $h_0$	Waterdepth
$h_b(x)$	Vertical position of the seabed
$h(x)$	Height of the water with respect to the seabed
$E_k$	Kinetic energy
$E_p$	Potential energy
$\omega$	Wave frequency
$C_e^{(0)}, C_e^{(\gamma)}$	Phase speed without or with surface tension effects
$\mathcal{L}$	Lagrangian functional
$C_0^\infty(\Omega)$	Set of testfunctions on $\Omega$ with compact support in $\Omega$
$u$	Horizontal flow velocity
$\partial_x^n = \frac{\partial^n}{\partial x^n}$	$n$ - th order partial derivative (same for $y$ - and $z$ -direction).
$\frac{d}{dt}[f(x(t), t)]$	Total derivative of $f$ with respect to $t$ .
$\partial_t[f(x, t)]$	Partial derivative of $f$ with respect to it's second argument $t$ .
$\nabla = (\partial_x, \partial_y, \partial_z)$	in the 3D case or $(\partial_x, \partial_z)$ in the 2D case
$\nabla = (\partial_x, \partial_y)$	First order horizontal derivatives (in the 3D case).
$\bar{S}$	Surrounding surface of a volume
$S_f$	Free surface
$D_h$	Horizontal domain
$\partial D_h$	Boundary of the domain $D_h$
$L^p(\Omega)$	Space of Lebesgue integrable functions; $\{v \mid (\int_\Omega  v ^p \, d\Omega)^{1/p} < \infty\}$
$H_g^1(\Omega)$	Hilbert space $\{v \in L^2(\Omega) \mid \partial_x v \in L^2(\Omega), v _{\partial D_h} = g\}$
$N$	Number of elements (= number of nodes -1)
$\chi$	Global basisfunction
$\hat{\phi}$	Trial function for $\phi$
$\hat{h}$	Trial function for $h$
$\hat{K}$	Reference element; $K = \{\xi \in (-1, 1)\}$
$\Theta$	Local basis function
$M^{-1}$	Inverse of matrix $M$
$I_N$	Unity matrix of size $[N \times N]$
$\Gamma, \Gamma_i, \Gamma_b$	Set of all, internal and boundary faces respectively
$[\cdot]$	The jump at a face
$\{\{\cdot\}\}$	The average at a face
$F_j(\zeta)$	Map from the reference element to the element-interval $K_j$
$v_x = \frac{dv}{dx}$	First order spatial derivative with respect to its only argument
$\mathcal{R}(\phi)$	Global lifting operator
$\mathcal{R}_s$	Local lifting operator
$\eta^e$	Local lifting operator weight (dependent on the element size)
$N_s$	Number of faces adjacent to an element
$S, S_L, S_R$	Face, Face left or right of an element



# 1 Introduction

## 1.1 Motivation

There are many reasons to investigate free-surface water waves propagation in the sea, such as the necessity to predict the motion of the water-surface at a certain place and time and to deduce the effects when waves reach shores which is of much interest for coastal defenses. Waves reaching the entrance of a harbor are of much interest for both harbor designers and vessel constructors. Propagating waves may threaten offshore oil rigs.

The recent devastation of the shores and cities of South-Asia and East-Africa by a tsunami (December 2004) is a striking example where the origination and propagation of waves is of particular interest. The tsunami was excited by a fault movement<sup>1</sup> in the Indian Ocean near the Indonesian island of Sumatra. Reconstruction of the seabed movement at the time of fault motion is crucial for scientific understanding of tsunami excitation and developing coastal warning systems. Furthermore, predicting the propagation of tsunamis and tsunami wave trains may indicate which regions are relatively safe and which coastal regions are threatened the most when tectonic activity is measured.

Wave prediction and reconstruction can be achieved in various ways. Field data can be observed to gain real scale statistical information. A laboratory setting can be used to simulate a full-scale problem and to validate theoretical models. Lastly, mathematical models can be developed to understand and predict water waves.

In this report we consider Boussinesq models that aim to accurately model waves propagation from the deep sea to the surf-zone [25]. An important question is, whether waves in the Boussinesq models are capable to break, i.e. develop jumps in the surface elevation. Further challenges will then be to cope with the breaking of the waves numerically and to model flooding and drying of waves reaching the shore.

## 1.2 Mathematical model

Waves of Boussinesq type account for dispersion<sup>2</sup> and nonlinearity [17]. Ideally, Boussinesq models can be applied to water waves occurring from deep water to the surf zone, without any extensions of the model. The model is valid for long waves with a depth to wavelength ratio of  $h/\lambda \ll 1$  [25]. Over the years the original Boussinesq formulation (Peregrine, 1967 [30]) has been extended to improve the dispersion properties of the model and to adapt for bathymetric influences. See for an overview the work of Madsen et al. [25] and Kirby [17]. Extensions are generally made by introducing complex high-order mixed spatial and temporal derivatives. Further, many Boussinesq-type models are not derived from variational principles and do not satisfy positive-definite energy conservation [19], while the original (potential-flow) models do conserve positive-definite energy [27].

Therefore, we start from a variational approach to account for the conservation of energy [19]. The complete complex dynamics of the system is now captured in two scalar quantities, namely the velocity potential and the kinematic energy [21]. Furthermore, the variational principle provides a weak formulation, which is easily transferred into a finite element weak formulation.

In this report three variational Boussinesq models are studied. Firstly, Luke's variational principle [27] for the full three dimensional potential flow is investigated. Luke's variational principle allows us to compare the dispersion relations of the two Boussinesq models with the exact dispersion relation of the potential flow model.

The second variational model is derived by Klopman et al. [19] and is an approximation of

---

<sup>1</sup>Fault movement was the actual cause of both the tsunami and the earth quake.

<sup>2</sup>Dispersion is a phenomenon that causes the wave to separate into components with different frequencies and wavelengths, due to the dependency of the celerity of these components on its wavelength and/or its frequency.

Luke's variational principle. Within this model energy is conserved and is positive-definite. This model is applicable for fully non-linear water waves of Boussinesq-type and has improved dispersion characteristics for propagating wave-groups such as tsunami wave-trains as compared to classical Boussinesq-type equations.

The third variational Boussinesq model is derived by Whitham [37], resulting (under additional approximations) in the original Boussinesq (partial differential) equations formulated by Peregrine [30]. It is a further simplification relative to Luke's and Klopman's variational principle.

In this report surface tension effects are included in the three variational models. These effects are not negligible in small water-depths [23] and are easily included in a variational principle. This has the advantage that the mathematical models can be validated eventually with a laboratory test in which surface tension is important.

In this report we introduce moving boundaries for the Klopman's variational Boussinesq model in order to capture flooding and drying effects in the model.

### 1.3 Numerical computation

The wave propagation described by the two variational Boussinesq models is solved numerically. The variational models lead to weak variational forms, that are used to conduct the weak formulations of the continuous Galerkin finite element method. We compare the numerical results with approximate the original Boussinesq equations [11], called cnoidal waves<sup>3</sup>.

Instead of investigating shoaling effects we will simulate breaking waves by initially considering very steep linear wave solutions in our non-linear model [36]. When a wave is breaking, the water surface shows a discontinuous jump. To be able to solve the propagation of a discontinuous jump numerically we propose a discontinuous Galerkin method.

---

<sup>3</sup>A cnoidal wave is a periodic analytical solution to the Korteweg-de Vries (KdV) equations, which is a propagating, shape invariant solution in both space and time.

## 2 Variational principles for water waves

### 2.1 Introduction

Considering fluids with the assumption of conservation of energy enables us here to formulate a variational principle. We assume the fluids to be incompressible. Neglecting air pressure, Luke's principle [27] varies the total energy for potential flow, which is the addition of the kinetic energy  $E_k$  and potential energy  $E_p$  as the basis of his principle. This principle completely describes the fluid motion at the free surface and incorporates appropriate boundary conditions for free surface flows. Taking variations results in partial differential equations, which are called the Euler-Lagrange equations and which are the governing equations of motion for our system. In the next section §2.2, we consider Luke's principle including surface tension for nonlinear potential flow. Thereafter, we will derive the exact linear dispersion relation for potential flow.

In section 2.3, we consider a variational principle for Klopman et al.'s [19] nonlinear conservative Boussinesq equations extended with surface tension. This variational principle is deduced by approximating the vertical structure of the velocity potential. As a result, the kinetic energy term is changed relative to Luke's variational principle. Surface tension effects are included in the model and the linear dispersion relation is derived.

In section 2.4 we consider the simpler Whitham Boussinesq model. We again include surface tension in the model and we derive the linear dispersion relation.

Finally, in section 2.5 the three dispersion relations are compared for deep water and for relatively small water depth, as compared with the wave length. For long waves the surface tension effects can be neglected, for short waves the effects of surface tension must be included.

Finally, in section 2.7 some conclusions are drawn.

### 2.2 Luke's variational principle for free-surface potential flow

We consider a fluid layer with surface tension in three dimensions extending over a horizontal domain  $(x, y) \in D_h$  and in the vertical direction  $z$ , see figure 2.2.1. The solenoidal<sup>4</sup> velocity is

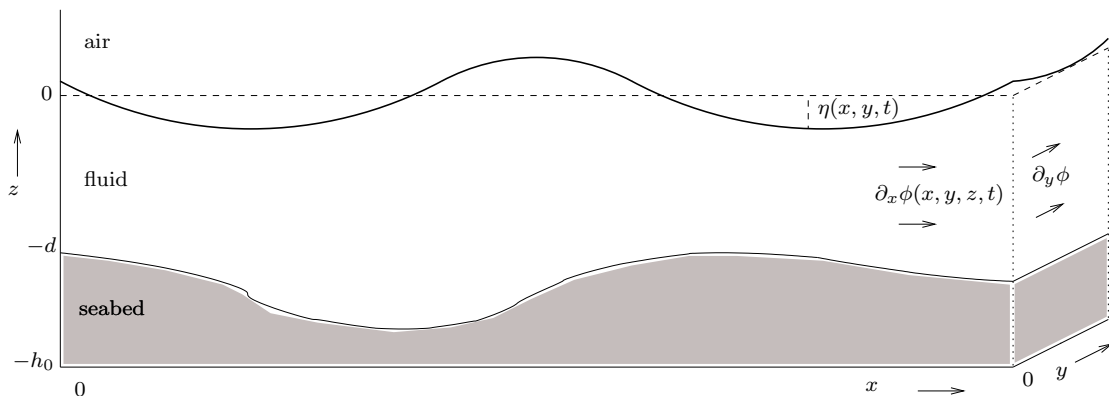


Figure 2.2.1: Parameters describing the free surface  $\eta(x, y, t)$  of the fluid moving in a horizontal velocity  $\mathbf{v} = \nabla\phi(x, y, z, t)$  above a varying seabed  $z = -d(x, y)$  in an horizontal domain  $(x, y) \in D_h$ .

given by  $\mathbf{v} = \nabla\phi(x, y, z, t)$ , where  $\phi(x, y, z, t)$  is the velocity potential and  $\nabla = (\partial_x, \partial_y, \partial_z)^T$  the three dimensional gradient. We write  $|\nabla\phi|^2 = (\partial_x\phi)^2 + (\partial_y\phi)^2 + (\partial_z\phi)^2$ . Surface tension is a force that tends to minimize the area of the free surface. The surface tension  $\gamma$  is measured in Newton per meter [ $Nm^{-1}$ ] and is defined as the intensity of the molecular attraction per

<sup>4</sup>The divergence of a vector in a solenoidal field  $\nabla \cdot \mathbf{v}$  is equal to zero; the fluid is irrotational.

unit length along any line in the surface [29]. In the following we will write  $\gamma = \gamma'/\rho$ . The kinetic  $E_k$  and potential energy  $E_{pot}$  are of the form

$$\rho E_k = \iint_{D_h} \int_{-d}^{\eta(x,y,t)} \frac{1}{2} \rho |\nabla \phi|^2 dz dx dy \quad (2.1)$$

$$\rho E_{pot} = \iint_{D_h} \int_{-d}^{\eta(x,y,t)} \rho g z dz + \gamma \rho (\sqrt{1 + (\partial_x \eta)^2 + (\partial_y \eta)^2} - 1) dx dy \quad (2.2)$$

with  $\rho$  the constant density of the fluid,  $\eta(x, y, t)$  the surface elevation,  $d(x, y)$  the still water depth at  $(x, y)$ , and  $g$  the gravitational acceleration. The first order horizontal derivatives are denoted as  $\nabla = (\partial_x, \partial_y)^T$ , with the transpose  $(\cdot)^T$ . We define Hamilton's principle for potential flow with the action functional  $\mathcal{L}_f$ :

$$0 = \delta \mathcal{L}_f(\phi, \phi_s, \eta) = \delta \int_{t_0}^{t_1} L_f(\phi, \phi_s, \eta) dt \quad (2.3)$$

$$\text{with } L_f = \iint_{D_h} \rho \phi_s \partial_t \eta dx dy - \mathcal{H} \quad (2.4)$$

$$\text{and } \mathcal{H} = E_k + E_{pot}. \quad (2.5)$$

Here,  $\phi_s = [\phi]_{z=\eta}$  is the evaluation of  $\phi$  on the free surface  $z = \eta$  [27] and  $L_f$  is the Lagrangian. This action functional is known as Luke's principle (Luke, 1967) for  $\gamma = 0$ , in the form as given by Miles [27]. We vary (2.3):

$$0 = \delta \int_{t_0}^{t_1} L_f(\phi, \phi_s, \eta) dt \quad (2.6)$$

$$= \lim_{\epsilon \downarrow 0} \frac{1}{\epsilon} \left\{ \int_{t_0}^{t_1} L_f(\phi + \epsilon \delta \phi, \phi_s + \epsilon \delta \phi_s, \eta + \epsilon \delta \eta) - L_f(\phi, \phi_s, \eta) dt \right\} \quad (2.7)$$

$$= \lim_{\epsilon \downarrow 0} \frac{1}{\epsilon} \left\{ \int_{t_0}^{t_1} \iint_{D_h} \underbrace{[(\phi_s + \epsilon \delta \phi_s) \partial_t (\eta + \epsilon \delta \eta)]}_{\mathbf{A}} - \int_{-d}^{\eta + \epsilon \delta \eta} \underbrace{\frac{1}{2} |\nabla(\phi + \epsilon \delta \phi)|^2}_{\mathbf{B}} dz \right. \\ \left. - \underbrace{\frac{1}{2} g (\eta + \epsilon \delta \eta)^2}_{\mathbf{C}} - \underbrace{\gamma \sqrt{1 + |\nabla(\eta + \epsilon \delta \eta)|^2}}_{\mathbf{D}} dx dy \right. \\ \left. - \iint_{D_h} \underbrace{[\phi_s \partial_t \eta]}_{\mathbf{A}} - \int_{-d}^{\eta} \underbrace{\frac{1}{2} |\nabla \phi|^2}_{\mathbf{B}} dz - \underbrace{\frac{1}{2} g \eta^2}_{\mathbf{C}} + \underbrace{\gamma \sqrt{1 + |\nabla \eta|^2}}_{\mathbf{D}} dx dy dt \right\}. \quad (2.8)$$

The linearity property of variational problems allows us to write out expressions per term more elaborately [35]. Integrating with respect to time, terms **A** in (2.8) can be rewritten as:

$$\int_{t_0}^{t_1} \iint_{D_h} \delta \phi_s \partial_t \eta + \phi_s \partial_t \delta \eta dx dy dt = \int_{t_0}^{t_1} \iint_{D_h} \delta \phi_s \partial_t \eta - \delta \eta \partial_t \phi_s dx dy dt, \quad (2.9)$$

where we used that  $\delta \eta(t_0) = \delta \eta(t_1) = 0$ , since  $\delta \eta$  belong to the set of test functions  $C_0^\infty(D_h)$ , which is the set of admissible elements. We rewrite terms **B** by splitting the integration

domain  $[-d, \eta + \epsilon\delta\eta]$  in the two intervals  $[-d, \eta]$  and  $[\eta, \eta + \epsilon\delta\eta]$ . We get for the first interval  $[-d, \eta]$  using Gauss's law:

$$\iint_{D_h} \int_{-d}^{\eta} (\nabla\phi \cdot \nabla\delta\phi) \, dV = - \iint_{D_h} \int_{-d}^{\eta} \delta\phi \nabla^2\phi \, dV + \oint_{\bar{S}} \delta\phi \nabla\phi \cdot \mathbf{n} \, dS, \quad (2.10)$$

with  $\bar{S}$  the (closed) surrounding boundaries of the volume  $V = [D_h] \times [-d, \eta]$  and with  $dV = dx \, dy \, dz$ . The boundary  $\bar{S}$  includes the seabed, the vertical boundaries on the edges of the horizontal domain  $D_h$  (for example a wall at  $x = x_0$ ), and the free surface boundary  $S_f$  at  $z = \eta$ . We adjust our infinitesimal surface element  $dS$  with respect to the surface we are integrating over. We again evaluate  $\delta\phi$  at the free surface with  $\delta\phi_s$ . The free surface parametrized as the surface  $s = 0$  with  $s = \eta - z$  and we obtain for the normal vector on the free surface the following expression:

$$\mathbf{n} = \frac{\nabla s}{|\nabla s|} = \frac{(\partial_x\eta, \partial_y\eta, -1)^T}{\sqrt{(\partial_x\eta)^2 + (\partial_y\eta)^2 + 1}}. \quad (2.11)$$

Combining this with evaluating  $\delta\phi$  on the free surface, the boundary integral of equation (2.10) becomes:

$$\oint_{\bar{S}} \delta\phi \nabla\phi \cdot \mathbf{n} \, dS = \iint_{\bar{S} \setminus S_f} \delta\phi \nabla\phi \cdot \mathbf{n} \, dS + \iint_{S_f} \delta\phi_s [\nabla\phi \cdot \nabla\eta - \partial_z\phi] \, dx \, dy \quad (2.12)$$

For the second contribution to  $\mathbf{B}$ , i.e. the interval  $[\eta, \eta + \epsilon\delta\eta]$ , we obtain:

$$\lim_{\epsilon \downarrow 0} \frac{1}{\epsilon} \iint_{D_h} \int_{\eta}^{\eta + \epsilon\delta\eta} \frac{1}{2} |\nabla(\phi + \epsilon\delta\phi)|^2 \, dV \quad (2.13a)$$

$$= \lim_{\epsilon \downarrow 0} \frac{1}{\epsilon} \iint_{D_h} \int_{\eta}^{\eta + \epsilon\delta\eta} \frac{1}{2} |\nabla\phi|^2 \, dV + \lim_{\epsilon \downarrow 0} \iint_{D_h} \int_{\eta}^{\eta + \epsilon\delta\eta} \nabla\phi \cdot \nabla\delta\phi \, dV \quad (2.13b)$$

$$= \iint_{D_h} \frac{\delta\eta}{2} |\nabla\phi|_{z=\eta}^2 \, dx \, dy, \quad (2.13c)$$

where we applied Taylor expansions around  $z = \eta$  in going from (2.13b) to (2.13c). Terms  $\mathbf{D}$  in equation (2.8) are approximated with Taylor expansions around  $\epsilon = 0$ :

$$\lim_{\epsilon \downarrow 0} \frac{1}{\epsilon} \iint_{D_h} \gamma \sqrt{1 + |\nabla(\eta + \epsilon\delta\eta)|^2} - \gamma \sqrt{1 + |\nabla\eta|^2} \, dx \, dy \quad (2.14a)$$

$$= \lim_{\epsilon \downarrow 0} \iint_{D_h} \frac{\gamma\epsilon}{\epsilon} \left( \frac{\nabla(\eta + \epsilon\delta\eta) \cdot \nabla(\delta\eta)}{\sqrt{1 + |\nabla(\eta + \epsilon\delta\eta)|^2}} \right) \, dx \, dy \quad (2.14b)$$

$$= \iint_{D_h} \gamma \frac{\nabla\eta \cdot \nabla(\delta\eta)}{\sqrt{1 + |\nabla\eta|^2}} \, dx \, dy \quad (2.14c)$$

$$= - \iint_{D_h} \gamma\delta\eta \left[ \frac{\eta_x}{\sqrt{1 + |\nabla\eta|^2}} \right]_x + \gamma\delta\eta \left[ \frac{\eta_y}{\sqrt{1 + |\nabla\eta|^2}} \right]_y \, dx \, dy, \quad (2.14d)$$

where  $\eta_x = \partial\eta/\partial x$ . We used Gauss' law from (2.14c) to (2.14d) and used that  $\delta\eta$  is arbitrary. With the (derived) expressions for  $\mathbf{A}$  to  $\mathbf{D}$ , we obtain for equation (2.8):

$$\begin{aligned}
0 = & \int_{t_0}^{t_1} \iint_{D_h} -\delta\eta \partial_t \phi_s + \delta\phi_s \partial_t \eta - g\eta \delta\eta - \delta\eta \frac{1}{2} |\nabla\phi|_{z=\eta}^2 \\
& + \delta\phi_s [\nabla\phi \cdot \nabla\eta - \partial_z \phi]_{z=\eta} + \int_{-d}^{\eta} \delta\phi \nabla^2 \phi \, dz - [\delta\phi \nabla\phi \cdot \mathbf{n}]_{\bar{S}\setminus S_f} \\
& + \gamma \delta\eta \left( \left[ \frac{\eta_x}{\sqrt{1+|\nabla\eta|^2}} \right]_x + \left[ \frac{\eta_y}{\sqrt{1+|\nabla\eta|^2}} \right]_y \right) \, dx dy \, dt.
\end{aligned} \tag{2.15}$$

Note that the subscript  $S_f$  indicates the free surface, while  $\bar{S}$  denotes all the surrounding surfaces. The variational problem states that  $\mathcal{L}(\phi, \phi_s, \eta)$  is stationary with respect to the independent variables  $\delta\phi$ ,  $\delta\phi_s$  and  $\delta\eta$  [35], and thus we obtain the following expressions:

$$\begin{aligned}
& \int_{t_0}^{t_1} \iiint_{D_h} \int_{-d}^{\eta} \delta\phi \nabla^2 \phi \, dz \, dx \, dy + [\delta\phi \nabla\phi \cdot \mathbf{n}]_{\bar{S}\setminus S_f} \, dt = 0 \\
& \Rightarrow \delta\phi : \nabla^2 \phi = 0 \text{ for } z \in [-d, \eta] \cap (x, y) \in D_h
\end{aligned} \tag{2.16}$$

$$\text{and } \delta\phi : \nabla\phi \cdot \mathbf{n} = 0 \text{ at } \bar{S}\setminus S_f \tag{2.17}$$

$$\begin{aligned}
& \int_{t_0}^{t_1} \iiint_{D_h} \delta\phi_s (\partial_t \eta + \nabla\phi \cdot \nabla\eta - \partial_z \phi) \, dx \, dy \, dt = 0 \\
& \Rightarrow \delta\phi_s : \partial_t \eta + \nabla\phi \cdot \nabla\eta - \partial_z \phi = 0 \text{ at } z = \eta;
\end{aligned} \tag{2.18}$$

$$\begin{aligned}
& \int_{t_0}^{t_1} \iint_{D_h} \delta\eta \left\{ -\partial_t \phi_s - g\eta - \frac{1}{2} |\nabla\phi|_{z=\eta}^2 \right. \\
& \quad \left. + \gamma \left( \left[ \frac{\eta_x}{\sqrt{1+|\nabla\eta|^2}} \right]_x + \left[ \frac{\eta_y}{\sqrt{1+|\nabla\eta|^2}} \right]_y \right) \right\} \, dx dy \, dt = 0 \\
& \Rightarrow \delta\eta : \partial_t \phi + g\eta + \frac{1}{2} |\nabla\phi|^2 \\
& \quad - \gamma \left[ \frac{\eta_x}{\sqrt{1+|\nabla\eta|^2}} \right]_x - \gamma \left[ \frac{\eta_y}{\sqrt{1+|\nabla\eta|^2}} \right]_y = 0 \text{ at } z = \eta.
\end{aligned} \tag{2.19}$$

Expression (2.16) implies that the fluid is incompressible (Laplace's equations) and denotes conservation of mass. Expression (2.17) states that no particle of the fluid can move through the seabed and the wall. The natural boundary condition (2.17) is also known as Neumann's boundary condition. In expression (2.18) the free surface kinematic free surface boundary condition [16] is given, which expresses that matter does not leave the fluid through the free surface (for example, there is no evaporation). Expression (2.19) represents the free surface dynamic free boundary condition, which is the so-called Bernoulli equation, evaluated at the free surface [16].

### 2.2.1 Linear dispersion for potential flow

We sketch the derivation of the exact linear dispersion relation for potential flow over a horizontal seabed, as in [23], but now with surface tension. We translate the surface elevation

$\eta$  to  $h + h_b$ , see figure 2.3.1, and the seabed  $-d$  to  $h_b$  in order to compare the models later. The two boundary conditions in one dimension regarding the free surface in potential flow read, as seen in section 2.2:

$$\partial_t h + \partial_x \phi \partial_x h - \partial_z \phi = 0 \text{ at } z = h_0, \quad (2.20)$$

$$\partial_t \phi + gh + \frac{1}{2}(\partial_x \phi)^2 - \gamma \left[ \frac{h_x}{\sqrt{1 + (h_x)^2}} \right]_x = 0 \text{ at } z = h + h_b. \quad (2.21)$$

We rewrite the  $\gamma$ -term

$$\gamma \left[ \frac{h_x}{\sqrt{1 + (h_x)^2}} \right]_x = \gamma \frac{h_{xx}}{(1 + (h_x)^2)^{\frac{3}{2}}} \quad (2.22)$$

and we linearize around the free surface  $z = h_0$ :

$$\partial_t h - \partial_z \phi = 0 \text{ at } z = h + h_b \quad (2.23)$$

$$\partial_t \phi + g(h - h_0) - \gamma h_{xx} = 0 \text{ at } z = h_0. \quad (2.24)$$

Combining the two linear boundary conditions and with a constant seabed, such that  $\partial_t h_b = 0$ , we obtain

$$\partial_t^2 \phi + g \partial_z \phi - \gamma \partial_z \partial_x^2 \phi = 0 \text{ at } z = h_0. \quad (2.25)$$

With Stokes' first-order theory [23] we can write the velocity potential as

$$\phi(x, z, t) = \Phi(z) e^{i(\kappa x - \omega t)}, \quad (2.26)$$

which satisfies Laplace's equation  $\nabla^2 \phi = 0$  and we may write

$$\Phi(x, z, t) = \Phi_0 \cosh[\kappa z], \quad (2.27)$$

since as  $\phi$  is a solution to Laplace's equation, so is its complex conjugate. Substituting this in the free-surface boundary condition (2.25) yields the exact linear dispersion relation

$$-\omega \phi + g \tanh[\kappa z] \phi + \gamma \kappa^3 \tanh[\kappa z] \phi = 0 \text{ at } z = h_0 \quad \Leftrightarrow \quad (2.28)$$

$$\omega^2 = (g + \gamma \kappa^2) \kappa \tanh(\kappa h_0). \quad (2.29)$$

We get the following Taylor expansion in  $\kappa$ , around the long-wave limit  $\kappa = 0$ :

$$\omega^2 = gh_0 \kappa^2 - \left(\frac{1}{3}gh_0^3 - \gamma h_0\right) \kappa^4 + \left(\frac{2}{15}gh_0^5 - \frac{1}{3}\gamma h_0^3\right) \kappa^6 - \left(\frac{17}{315}gh_0^7 - \frac{2}{15}\gamma h_0^5\right) \kappa^8 + \mathcal{O}(\kappa^{10}). \quad (2.30)$$

### 2.3 Klopman's variational Boussinesq model (KVBM)

We consider the fluid layer in two dimensions with horizontal  $x$ -axis and vertical  $z$ -axis, see figure 2.3.1. The fluid velocity is now given by  $(u, v) \equiv (\partial_x \phi, \partial_z \phi)$  and we change the definition for the free surface elevation  $\eta(x, t)$  to the total water height  $h(x, t) + h_b(x)$  by translation over  $h_0$ , such that  $-d$  equals the seabed height  $h_b(x)$ . This choice is convenient when modeling free surface waves that may run up, for example, beaches, or where dry patches of land may appear. Now we make the following Ansatz for the potential  $\phi(x, z, t)$ , motivated by the parabolic vertical structure of the velocity potential found in conventional Boussinesq models for water waves over a horizontal bed [19]:

$$\phi(x, z, t) = \varphi(x, t) + f(z)\psi(x, t), \quad (2.31)$$

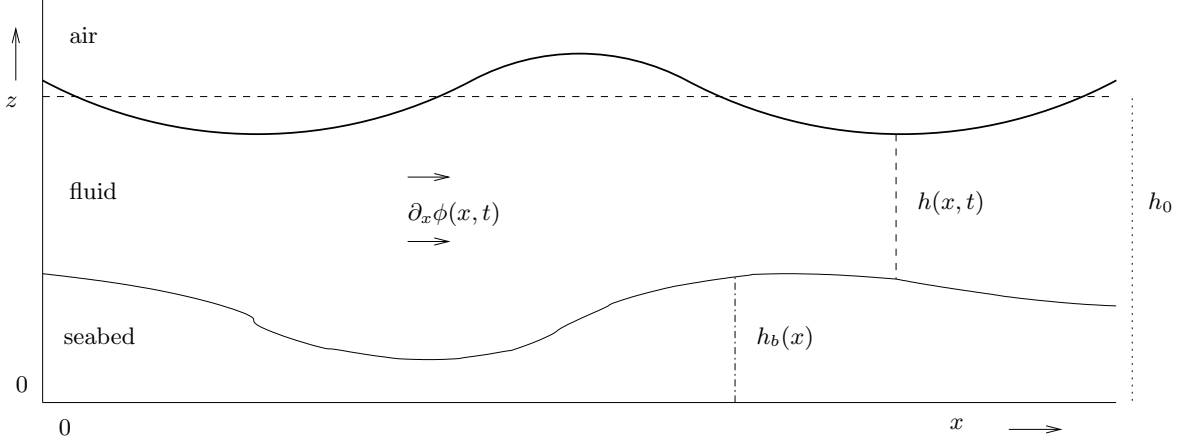


Figure 2.3.1: Parameters describing the free surface  $h(x, t)$  of the fluid moving with horizontal velocity  $\partial_x \phi$  above a varying seabed  $h_b(x)$  in an horizontal domain  $x \in D_h$  for the Klopman and Whitham variational Boussinesq model.

where  $\phi = \varphi$  at the free surface  $z = h(x, t) + h_b(x)$  and

$$f(z) = (z - h - h_b)(z + h - h_b). \quad (2.32)$$

We take this choice because we only want time derivatives of  $h(x, t)$  and  $\varphi(x, t)$  to appear in the Euler-Lagrange equations. Further, the form of the vertical structure function  $f(z)$  is motivated by the fact, that for long waves over a horizontal bed, the cosh-function of equation (2.27) becomes, to a good approximation, a parabolic function with its derivative equal to zero at the sea bed. The assumption that  $\partial_z \phi = 0$  at  $z = h_b$  for a (locally) horizontal seabed is a good approximation for small bottom slopes [19]. Under the assumption of a mildly sloping bottom, i.e. assuming spatial derivatives of  $h_b(x)$  are small and thus neglected, and under the assumption that wave slopes are small  $\partial_x(h + h_b - h_0) \ll 1$  we have a weakly nonlinear model and the velocity components become:

$$\partial_x \phi = \partial_x \varphi + f(z) \partial_x \psi \quad \text{and} \quad \partial_z \phi = 2(z - h_b) \psi. \quad (2.33)$$

When we substitute these expressions into the energy  $\mathcal{H}$  in (2.3):

$$\mathcal{H} = \int_{D_h} \left\{ \int_{h_b}^{h+h_b} \frac{1}{2} [(\partial_x \phi)^2 + (\partial_z \phi)^2] dz + \frac{1}{2} g (h - h_0)^2 \right\} dx. \quad (2.34)$$

we find for the modified energy  $\mathcal{H}_b$  in the two dimensional case:

$$\mathcal{H} = \int_{D_h} \left\{ \int_{h_b}^{h+h_b} \frac{1}{2} [(\partial_x \varphi + f(z) \partial_x \psi)^2 + f'(z)^2 \psi^2] dz + \frac{1}{2} g (h - h_0)^2 \right\} dx \quad (2.35a)$$

$$= \int_{D_h} \left\{ \frac{1}{2} h \partial_x \varphi - \frac{2}{3} h^3 \partial_x \varphi \partial_x \psi + \frac{4}{15} h^5 (\partial_x \psi)^2 + \frac{2}{3} h^3 \psi^2 + \frac{1}{2} g (h - h_0)^2 \right\} dx \quad (2.35b)$$

$$= \int_{D_h} \left\{ \frac{1}{2} h \left[ \partial_x \varphi - \frac{2}{3} h^2 \partial_x \psi \right]^2 + \frac{2}{45} h^5 (\partial_x \psi)^2 + \frac{2}{3} h^3 \psi^2 + \frac{1}{2} g (h - h_0)^2 \right\} dx. \quad (2.35c)$$

We can define the action functional  $\mathcal{L}_b$  for the energy  $\mathcal{H}_b$  and the first variation is

$$0 = \delta \int_{t_0}^{t_1} \left\{ \int_{D_h} \varphi \partial_t h dx - \mathcal{H} \right\} dt. \quad (2.36)$$

Taking variations with respect to  $\varphi$ ,  $h$  and  $\psi$  gives:

$$0 = \int_{t_0}^{t_1} \int_{D_h} \delta\varphi \partial_t h - \partial_x \delta\varphi \left[ h \partial_x \varphi - \frac{2}{3} h^3 \partial_x \psi \right] \quad (2.37a)$$

$$+ \varphi \partial_t \delta h - \delta h \left( \frac{1}{2} (\partial_x \varphi)^2 - 2h^2 \partial_x \varphi \partial_x \psi + \frac{4}{3} h^4 (\partial_x \psi)^2 + 2h^2 \psi^2 + g(h - h_0) \right) \quad (2.37b)$$

$$+ \partial_x \delta\psi \left[ \frac{2}{3} h^3 \partial_x \varphi - \frac{8}{15} h^5 \partial_x \psi \right] - \frac{4}{3} \delta\psi h^3 \psi \, dx \, dt. \quad (2.37c)$$

Partial integration with respect to time and space results in the variational derivative:

$$0 = \int_{t_0}^{t_1} \int_{D_h} \delta\varphi \left( \partial_t h + \partial_x \left[ h \partial_x \varphi - \frac{2}{3} h^3 \partial_x \psi \right] \right) \quad (2.38a)$$

$$- \delta h \left( \partial_t \varphi + \frac{1}{2} (\partial_x \varphi)^2 - 2h^2 \partial_x \varphi \partial_x \psi + \frac{4}{3} h^4 (\partial_x \psi)^2 + 2h^2 \psi^2 + g(h - h_0) \right) \quad (2.38b)$$

$$- \delta\psi \left( \partial_x \left[ \frac{2}{3} h^3 \partial_x \varphi - \frac{8}{15} h^5 \partial_x \psi \right] + \frac{4}{3} h^3 \psi \right) \, dx \, dt, \quad (2.38c)$$

where we used that  $\delta\varphi$  and  $\delta h$  are elements of  $C_0^\infty(D_h)$ . The variational principle states that  $\mathcal{L}_b$  is stationary with respect to the independent variables  $\varphi$ ,  $h$  and  $\psi$ . We replace the flow velocity variable  $u \equiv \partial_x \varphi$  and obtain the Euler-Lagrange equations, from (2.38a)

$$\delta\varphi : \partial_t h + \partial_x \left[ hu - \frac{2}{3} h^3 \partial_x \psi \right] = 0, \quad (2.39)$$

from (2.38b), and differentiating with respect to  $x$ ,

$$\delta h : \partial_t u + \partial_x \left[ \frac{1}{2} u^2 - 2h^2 u \partial_x \psi + \frac{4}{3} h^4 (\partial_x \psi)^2 + 2h^2 \psi^2 + g(h - h_0) \right] = 0, \quad (2.40)$$

and from (2.38c)

$$\delta\psi : \partial_x \left[ \frac{2}{3} h^3 u - \frac{8}{15} h^5 \partial_x \psi \right] + \frac{4}{3} h^3 \psi = 0. \quad (2.41)$$

### 2.3.1 Klopman Variational Boussinesq model including surface tension

We now consider the expressions derived previously including surface tension. Note that  $\nabla\eta = \nabla h = \partial_x h$  in the one dimensional case. The energy equation (2.35a) now reads:

$$\mathcal{H} = \int_{D_h} \left\{ \int_{h_b}^{h+h_b} \frac{1}{2} [(\partial_x \varphi + f \partial_x \psi)^2 + (f' \psi)^2] dz + \frac{1}{2} g(h - h_0)^2 + \gamma (\sqrt{1 + (\partial_x h)^2} - 1) \right\} dx. \quad (2.42)$$

Analogous to Luke's variational principle, due to the linearity property [35], this contributes in a term which occurs in the first variation of  $\delta h$ . The governing equations now read (with the respective varied variables):

$$\delta\varphi : \partial_t h + \partial_x \left[ hu - \frac{2}{3} h^3 \partial_x \psi \right] = 0, \quad (2.43a)$$

$$\delta h : \partial_t u + \partial_x \left[ \frac{1}{2} u^2 - 2h^2 u \partial_x \psi + \frac{4}{3} h^4 (\partial_x \psi)^2 + 2h^2 \psi^2 + g(h - h_0) - \gamma \left[ \frac{h_x}{\sqrt{1 + (\partial_x h)^2}} \right] \right] = 0 \quad (2.43b)$$

$$\delta\psi : \partial_x \left[ \frac{2}{3} h^3 u - \frac{8}{15} h^5 \partial_x \psi \right] + \frac{4}{3} h^3 \psi = 0. \quad (2.43c)$$

### 2.3.2 Linear dispersion for Klopman Variational Boussinesq model

We obtain the following linearized equations of the Boussinesq model of subsection 2.3.1, for a constant mean-water depth  $h_0$ :

$$\partial_t h + h_0 \partial_x u - \frac{2}{3} h_0^2 \partial_x^3 \psi = 0, \quad (2.44a)$$

$$\partial_t u + g \partial_x h - \gamma \partial_x^3 h = 0, \quad (2.44b)$$

$$\frac{2}{3} h_0^3 \partial_x u - \frac{8}{15} h_0^5 \partial_x^2 \psi + \frac{4}{3} h_0^3 \psi = 0. \quad (2.44c)$$

We introduce solutions  $h(x, t) = \tilde{h} e^{i(\kappa x - \omega t)}$ ,  $u(x, t) = \tilde{u} e^{i(\kappa x - \omega t)}$  and  $\psi = \tilde{\psi} e^{i(\kappa x - \omega t)}$  to the linear system (2.44), and to find the dispersion relation:

$$\frac{h_0 \omega^2}{g} = \left(1 + \frac{\gamma \kappa^2}{g}\right) (\kappa h_0)^2 \frac{1 + \frac{1}{15} (\kappa h_0)^2}{1 + \frac{2}{5} (\kappa h_0)^2}. \quad (2.45)$$

We get the following Taylor expansion in  $\kappa$

$$\omega^2 = g h_0 \kappa^2 - \left(\frac{1}{3} g h_0^3 - \gamma h_0\right) \kappa^4 + \left(\frac{2}{15} g h_0^5 - \frac{1}{3} \gamma h_0^3\right) \kappa^6 - \left(\frac{4}{75} g h_0^7 - \frac{2}{15} \gamma h_0^5\right) \kappa^8 + \mathcal{O}(\kappa^{10}). \quad (2.46)$$

### 2.4 Whitham's variational Boussinesq model (WVBM)

Finally, we consider the following one dimensional simplified variational principle  $\mathcal{L}_s$  introduced by Whitham [37], equation (1.7):

$$\mathcal{L}_s(h, \partial_t h, \partial_x \phi) = \int_{t_0}^{t_1} \int_{D_h} \phi \partial_t h - \frac{1}{2} h (\partial_x \phi)^2 + \frac{1}{6} h_0 (\partial_t h)^2 - \frac{1}{2} g (h - h_0)^2 \, dx \, dt \quad (2.47)$$

with  $h_0(x)$  the height of the water when the fluid is at rest. Taking variations with respect to  $\phi$  and  $h$ , we obtain the Euler-Lagrange equation:

$$\begin{aligned} 0 &= \delta \int_{t_0}^{t_1} \int_{D_h} \phi \partial_t h - \frac{1}{2} h (\partial_x \phi)^2 + \frac{1}{6} (\partial_t h)^2 - \frac{1}{2} g (h - h_0)^2 \, dx \, dt \\ &= \int_{t_0}^{t_1} \int_{D_h} \delta \phi \partial_t h - h \partial_x \phi \partial_x \delta \phi + \phi \partial_t \delta h - \frac{1}{2} \delta h (\partial_x \phi)^2 + \frac{1}{3} h_0 \partial_t h \partial_t \delta h - g (h - h_0) \delta h \, dx \, dt \\ &= \int_{t_0}^{t_1} \int_{D_h} \delta \phi (\partial_t h + \partial_x [h \partial_x \phi]) - \delta h \left( \partial_t \phi + \frac{1}{2} (\partial_x \phi)^2 + g (h - h_0) + \frac{1}{3} h_0 \partial_t^2 h \right) \, dx \, dt, \end{aligned} \quad (2.48)$$

where we integrated by parts with respect to time and space from (2.4) to (2.48) and we used the arbitrariness of  $\delta \phi$  and  $\delta h$ . Taking the first variations we obtain the following governing equations:

$$\delta \phi : \partial_t h + \partial_x [h \partial_x \phi] = 0, \quad (2.49a)$$

$$\delta h : \partial_t \phi + \frac{1}{2} (\partial_x \phi)^2 + \frac{1}{3} h_0 \partial_t^2 h + g (h - h_0) = 0. \quad (2.49b)$$

Introducing the horizontal velocity  $u \equiv \partial_x \phi$  we rewrite the equations of motion in the form:

$$\partial_t h + \partial_x [hu] = 0, \quad (2.50a)$$

$$\partial_t u + \partial_x \left[ \frac{1}{2} u^2 + g(h - h_0) + \frac{1}{3} h_0 \partial_t^2 h \right] = 0. \quad (2.50b)$$

Note that expression (2.50a) is a kinematic condition concerning conservation of mass and expression (2.50b) is a dynamic condition, which denotes conservation of momentum. Without the term  $\frac{1}{3} \partial_t^2 h$  we have the non-linear shallow water equations:

$$\partial_t h + \partial_x [hu] = 0, \quad (2.51a)$$

$$\partial_t u + \partial_x \left[ \frac{1}{2} u^2 + g(h - h_0) \right] = 0. \quad (2.51b)$$

#### 2.4.1 Whitham variational Boussinesq model including surface tension

Analogous to the derivation in section 2.3.1 we obtain for the Whitham Boussinesq model the following equations:

$$\partial_t h + \partial_x [hu] = 0, \quad (2.52a)$$

$$\partial_t u + \partial_x \left[ \frac{1}{2} u^2 + g(h - h_0) + \frac{1}{3} h_0 \partial_t^2 h - \gamma \left[ \frac{h_x}{\sqrt{1 + (h_x)^2}} \right] \right] = 0. \quad (2.52b)$$

#### 2.4.2 Linear dispersion for the original Whitham Boussinesq-model

We linearize the governing equations of the Whitham Boussinesq-model, in the same way as considered in section 2.4:

$$\partial_t h + h_0 \partial_x u = 0, \quad (2.53a)$$

$$\partial_t u + g \partial_x h + \frac{1}{3} h_0 \partial_t^2 \partial_x h - \gamma \partial_x^3 h = 0. \quad (2.53b)$$

We introduce solutions  $h(x, t) = \tilde{h} e^{i(\kappa x - \omega t)}$  and  $u(x, t) = \tilde{u} e^{i(\kappa x - \omega t)}$ . Substituting these into the linear system (2.53) we observe that they satisfy the dispersion relation:

$$\frac{h_0 \omega^2}{g} = \left( 1 + \frac{\gamma}{g} \kappa^2 \right) \frac{(\kappa h_0)^2}{1 + \frac{1}{3} (\kappa h_0)^2}. \quad (2.54)$$

We get the following Taylor expansion in  $\kappa$ , around  $\kappa = 0$ :

$$\begin{aligned} \omega^2 = g h_0 \kappa^2 - \left( \frac{1}{3} g h_0^3 - \gamma h_0 \right) \kappa^4 + \left( \frac{1}{9} g h_0^5 - \frac{1}{3} \gamma h_0^3 \right) \kappa^6 \\ - \left( \frac{1}{27} g h_0^7 - \frac{1}{9} \gamma h_0^5 \right) \kappa^8 + \mathcal{O}(\kappa^{10}). \end{aligned} \quad (2.55)$$

### 2.5 Comparison of dispersion relations

In this subsection we compare the three models derived for 2D. The Taylor expansions around  $\kappa = 0$  of the linear dispersion relations of the three models that we studied, are the following:

1. Full potential flow<sup>5</sup>, as derived from Luke's variational principle:

$$\begin{aligned} \omega_{Pot}^2 = \frac{g}{h_0} \left( (h_0 \kappa)^2 - \frac{1}{3} (h_0 \kappa)^4 + \frac{2}{15} (h_0 \kappa)^6 - \frac{17}{315} (h_0 \kappa)^8 \right) \\ + \frac{\gamma}{h_0^3} \left( (h_0 \kappa)^4 - \frac{1}{3} (h_0 \kappa)^6 + \frac{2}{15} \gamma (h_0 \kappa)^8 \right) + \mathcal{O}(\kappa^{10}), \end{aligned} \quad (2.56)$$

---

<sup>5</sup>Taylor approximation of the exact linear dispersion relation.

2. Klopman variational Boussinesq Model (KVBM):

$$\omega_K^2 = \frac{g}{h_0} \left( (h_0\kappa)^2 - \frac{1}{3}(h_0\kappa)^4 + \frac{2}{15}(h_0\kappa)^6 - \frac{17}{315}(h_0\kappa)^8 \right) + \frac{\gamma}{h_0^3} \left( (h_0\kappa)^4 - \frac{1}{3}(h_0\kappa)^6 + \frac{2}{15}(h_0\kappa)^8 \right) + \mathcal{O}(\kappa^{10}) \quad \text{and} \quad (2.57)$$

3. Whitham variational Boussinesq Model (WVBM):

$$\omega_W^2 = \frac{g}{h_0} \left( (h_0\kappa)^2 - \frac{1}{3}(h_0\kappa)^4 + \frac{1}{9}(h_0\kappa)^6 - \frac{1}{27}(h_0\kappa)^8 \right) + \frac{\gamma}{h_0^3} \left( (h_0\kappa)^4 - \frac{1}{3}(h_0\kappa)^6 + \frac{1}{9}(h_0\kappa)^8 \right) + \mathcal{O}(\kappa^{10}). \quad (2.58)$$

### 2.5.1 Comparison of dispersion relations without surface tension effects

We neglect surface tension effects,  $\gamma = 0$ . When comparing the Taylor expansions of the dispersion relations, we see that the Klopman variational Boussinesq model is of order  $\mathcal{O}(\kappa^{10})$  and the original Whitham Boussinesq-model is of order  $\mathcal{O}(\kappa^4)$  compared with the exact dispersion relation. In fact, the linear dispersion relation of the KVBM is the same relation as for the Boussinesq equations with improved linear dispersion of Madsen et al. [25].

We will first consider the dispersion relations without surface tension effects,  $\gamma = 0$ . In figure 2.5.1 we plot the dispersion relations<sup>6</sup> of the three models for small  $\kappa h_0$ , where  $\kappa = 2\pi/\lambda$ . Long waves are represented by  $\kappa h_0 \rightarrow 0$  and for  $\kappa h_0 \gg 1$  we have short waves relative to the water depth. For long waves the three dispersion relation denoted by defining  $\Omega(\kappa) = \omega$

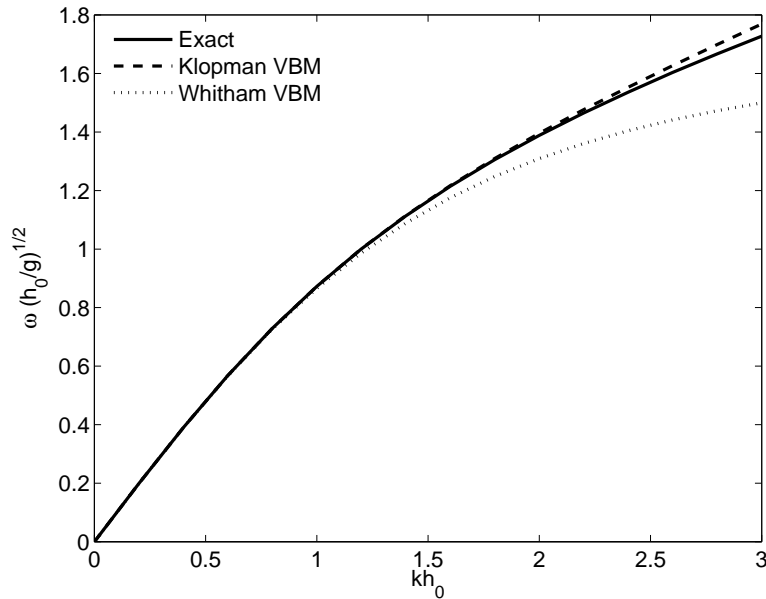


Figure 2.5.1: Dispersion relations:  $\omega\sqrt{h/g}$  as a function of  $\kappa h_0$ , for the Klopman and Whitham Boussinesq-models and the exact dispersion relation. water depth  $h_0 = 10\text{m}$ .

of equations (1)-(3) yield a group velocity  $V_{group}(\kappa)$  equal to  $\partial\Omega(\kappa)/\partial\kappa$ . For infinitesimal waves it is shown by Klopman et al. [19] that for waves up to  $\kappa h_0 = \pi$  the phase speed  $\Omega_K(\kappa)/\sqrt{gh_0}$  of the Klopman variational Boussinesq model has a relative error,

$$\frac{\Omega_K(\kappa)/\kappa}{\Omega_{exact}(\kappa)/\kappa} - 1, \quad (2.59)$$

<sup>6</sup>Partly reconstruction of figure 5.1a in [20].

less than 3%<sup>7</sup> compared to the exact phase speed. For the original Whitham variational Boussinesq model we have that the relative error,

$$\frac{\Omega_W(\kappa)/\kappa}{\Omega_{exact}/\kappa} - 1, \quad (2.60)$$

is equal to 15%<sup>8</sup> for  $\kappa h_0 = \pi$ . The equality  $\kappa h_0 = \pi$  is particularly important if we like to investigate breaking waves. For smaller water depths and around this  $\kappa$  it is where we consider waves propagating from deep water into shallow water. For the nonlinear shallow water-wave model propagating waves will break eventually. Note that Vinje and Brevig [36] investigated the breaking of nonlinear shallow water waves with an initial sinusoidal wave profile, at a ratio of  $\kappa h_0 = 0.53 * (2\pi)$  [36]. Due to the accurate approximation of the exact phase speed we have that the linear Klopman variational Boussinesq model holds for waves propagating up to the edge of the deep-water zone. Moreover, it is particularly interesting to investigate within the non-linear Klopman variational Boussinesq model whether waves will eventually start to break in the presence of dispersion.

### 2.5.2 Comparison of dispersion relations with surface tension effects

Now we include surface tension effects in our dispersion relations. We investigate surface tension effects since they affect the velocity of propagating waves. In figure 2.5.2 we plot the linear dispersion relations for  $\gamma' = 7.4 \cdot 10^{-2} \text{ Nm}^{-1}$  and  $\gamma = \gamma'/\rho$ , since we eliminated the water density  $\rho$  previously. This is an experimental value for water in contact with air at  $15.6^\circ\text{C}$  [29]. We take  $\rho = 1.0 \cdot 10^{-3}$ . This figure is partly a reproduction of fig. 57 in [23]. We observe that the Klopman variational Boussinesq model more closely resembles the exact dispersion relation including surface tension. In table 2.5.1 and figure 2.5.2 this has been made more explicitly. In table 2.5.1 the relative error of the phase speeds of the KVBM  $C_k^{(\gamma)}$  and WVBM  $C_w^{(\gamma)}$  with the exact phase speed  $C_e^{(\gamma)}$  are given:

Observe that in the KVBM with surface tension the error is bigger, as compared with the Whitham formulation for longer waves.

Now the question arises if it is always appropriate to include surface tension effects. Denoting the phase speed when neglecting surface tension effects by  $C^{(0)}$  and the phase speed with surface tension effects by  $C^{(\gamma)}$ , we can calculate the relative error by

$$\frac{C_e^{(\gamma)}}{C_e^{(0)}} - 1 = \frac{g + \kappa^2 \gamma}{g} - 1 \quad (2.61)$$

since  $C_e^{(0)} \sim g$  and  $C^{(\gamma)} \sim g + \kappa^2 \gamma$  for a certain waterdepth  $h_0$  and wavenumber  $\kappa$  and again  $\gamma = \gamma'/\rho$  with  $\gamma' = 7.4 \cdot 10^{-2} \text{ Nm}^{-1}$  and  $\rho$  the water density, here  $1000 \text{ kg m}^{-3}$ . For wavelengths  $\lambda$  equal to  $2\pi/\kappa$  the relative error is : We added the third column ( $h_0 = 5 \text{ cm}$ ) in table to compare the results with figure 2.5.1. Lighthill [23] states that in general surface tension is negligible for water waves  $\lambda > 7 \text{ cm}$ ; from (2.5.2) we see that the phase speed has a relative error of 0.061 %. Longer waves propagate as pure gravity waves.

When including surface tension effects we may conclude that for the region where surface tension effects are important, the KVBM including surface tension shows smaller relative errors than the WVBM.

<sup>7</sup>We found a relative error of 2.79%.

<sup>8</sup>The actual error was  $-14.7\%$ , which implicitly yields that propagating waves will be dissipated and will not be dispersed.

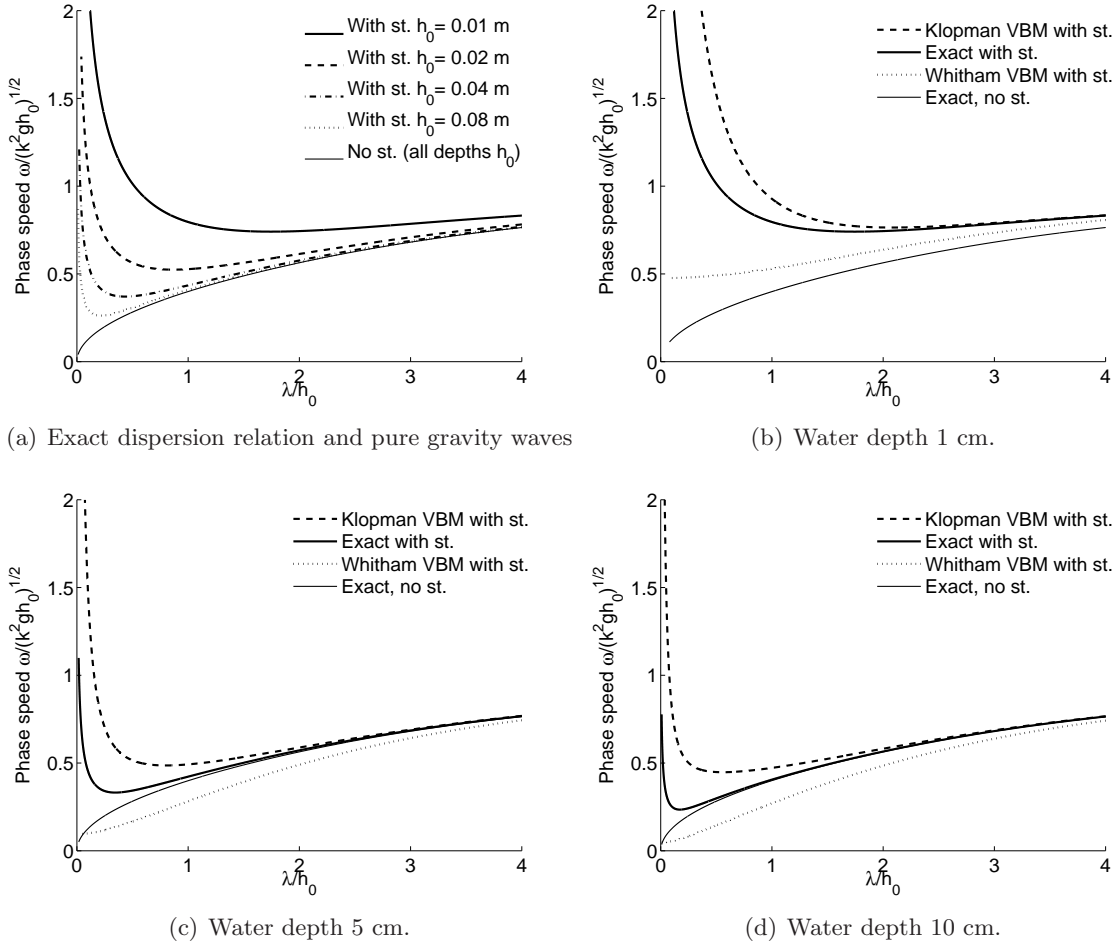


Figure 2.5.2: Phase speed  $\omega/(\kappa\sqrt{gh})$  plotted against the ratio  $2\pi/(\kappa h_0) = \lambda/h_0$  for small water depths  $h_0$ . Here: Surface tension (st.) parameter  $\gamma = 7.4 \times 10^{-2} \text{Nm}^{-1}$  for water in contact with air at  $15.6^\circ\text{C}$ . For reference the pure gravity wave at this water depth is plotted. (a) the exact dispersion relation including surface tension effects for various water depths. Presented are the dispersion relations for the KVBM, WVBM and the exact model including surface tension effects at depth b)  $h_0 = 1$  cm, c)  $h_0 = 5$  cm and d)  $h_0 = 10$  cm.

$h_0$ [cm]	$\lambda$ [cm]	$C_e^{(\gamma)}$ [m/s]	$C_k^{(\gamma)}$	$C_k^{(\gamma)}/C_e^{(\gamma)} - 1$	$C_w^{(\gamma)}$	$C_w^{(\gamma)}/C_e^{(\gamma)} - 1$
1.0	1.0	0.125	0.146	16.578 %	0.083	-33.386 %
	2.0	0.176	0.181	2.794 %	0.151	-14.264 %
	4.0	0.239	0.240	0.187 %	0.232	-3.059 %
	7.0	0.280	0.280	0.012 %	0.278	-0.530 %
	10.0	0.295	0.295	0.002 %	0.294	-0.148 %
	14.0	0.303	0.303	0.000 %	0.303	-0.042 %
	20.0	0.308	0.308	0.000 %	0.308	-0.010 %
5.0	1.0	0.125	0.288	130.264 %	0.039	-69.1449 %
	2.0	0.177	0.293	65.810 %	0.077	-56.5613 %
	4.0	0.250	0.313	25.057 %	0.151	-39.6463 %
	7.0	0.331	0.356	7.761 %	0.252	-23.7148 %
	10.0	0.394	0.405	2.794 %	0.338	-14.2638 %
	14.0	0.462	0.466	0.847 %	0.428	-7.4348 %
	20.0	0.535	0.536	0.187 %	0.519	-3.0586 %
1.0	1.0	0.125	0.405	224.116%	0.0273	-78.157%
	2.0	0.177	0.407	130.264%	0.0545	-69.145%
	4.0	0.250	0.414	65.810%	0.1086	-56.561%
	7.0	0.331	0.434	31.191%	0.1877	-43.235%
	10.0	0.395	0.461	16.578%	0.2632	-33.386%
	14.0	0.467	0.504	7.761%	0.3566	-23.715%
	20.0	0.558	0.573	2.794%	0.4782	-14.264%

Table 2.5.1: Phase speeds of the exact dispersion relation including surface tension effects  $C_e^{(\gamma)/\kappa}$  compared with the phase speed of the KVBM  $C_k^{(\gamma)/\kappa}$  and WVBM  $C_w^{(\gamma)/\kappa}$ . The relative errors are computed for several wavelengths at various water depths. Here  $h_0$  is the water depth,  $\kappa$  the wave number and  $\lambda$  the wavelength.

$\lambda$ [cm]	$C_e^{(\gamma)}/C_e^{(0)} - 1$	$\kappa h_0$
1.0	2.978 %	31.4159
2.0	0.745 %	15.7080
4.0	0.186 %	7.8540
7.0	0.061 %	4.4880
10.0	0.030 %	3.1416
14.0	0.015 %	2.2440
20.0	0.007 %	1.5708

Table 2.5.2: Relative error of the exact phase speeds compared with the exact wavespeed including surface tension effects.

## 2.6 Moving boundaries in the KVBM

The three variational models that we investigated previously were all considered on a horizontal domain with a fixed horizontal extent. When we consider a fluid layer which is flooding and drying on a seabed  $h_b(x)$  with a slope, the fluid boundaries may not be fixed in time. Moreover, a part of the seabed may fall dry when the fluid is moving away creating distinct patches of fluid. On the other hand, distinct fluid patches may merge and flood a land patch in between. The horizontal domain now becomes  $D_h = [x_L(t), x_R(t)]$  for example and the action functional becomes

$$0 = \delta \mathcal{L}(\varphi, h, \psi, x_L, x_R) = \delta \int_{t_0}^{t_1} L(\varphi, h, \psi, x_L, x_R) dt. \quad (2.62)$$

We illustrate the moving boundary condition for the Klopman Boussinesq-model [19]. We choose the Lagrangian density  $L$  as

$$L(\phi, h, \psi, x_L, x_R) = \int_{x_L(t)}^{x_R(t)} \phi \partial_t h - \mathcal{H} dx, \quad (2.63)$$

where  $\mathcal{H}$  was derived in equation (2.35c):

$$\mathcal{H}(\varphi, h\psi) = \frac{1}{2}h \left[ \partial_x \varphi - \frac{2}{3}h^2 \partial_x \psi \right]^2 + \frac{2}{45}h^5 (\partial_x \psi)^2 + \frac{2}{3}h^3 \psi^2 + \frac{1}{2}g(h + h_b)^2 - \frac{1}{2}gh_b^2. \quad (2.64)$$

Taking variations with respect to  $\phi$ ,  $h$ ,  $\psi$ ,  $x_L$  and  $x_R$  we have

$$0 = \int_{t_0}^{t_1} \int_{x_L(t)}^{x_R(t)} \delta \varphi \partial_t h - \partial_x \delta \varphi \left[ h \partial_x \varphi - \frac{2}{3}h^3 \partial_x \psi \right] \quad (2.65a)$$

$$+ \underbrace{\varphi \partial_t (\delta h)}_{\mathbf{E}} - \delta h \left( \frac{1}{2}(\partial_x \varphi)^2 - 2h^2 \partial_x \varphi \partial_x \psi + \frac{4}{3}h^4 (\partial_x \psi)^2 + 2h^2 \psi^2 + g(h + h_b) \right) \quad (2.65b)$$

$$+ \partial_x \delta \psi \left[ \frac{2}{3}h^3 \partial_x \varphi - \frac{8}{15}h^5 \partial_x \psi \right] - \frac{4}{3} \delta \psi h^3 \psi dx \quad (2.65c)$$

$$+ \lim_{\epsilon \downarrow 0} \frac{1}{\epsilon} \int_{x_R}^{x_R + \epsilon \delta x_R} (\varphi + \epsilon \delta \varphi) \partial_t (h + \epsilon \delta h) - \mathcal{H}_b(\varphi + \epsilon \delta \varphi, h + \epsilon \delta h, \psi + \epsilon \delta \psi) dx \quad (2.65d)$$

$$+ \lim_{\epsilon \downarrow 0} \frac{1}{\epsilon} \int_{x_L}^{x_L + \epsilon \delta x_L} (\varphi + \epsilon \delta \varphi) \partial_t (h + \epsilon \delta h) - \mathcal{H}_b(\varphi + \epsilon \delta \varphi, h + \epsilon \delta h, \psi + \epsilon \delta \psi) dx dt. \quad (2.65e)$$

For the integrals terms at the boundaries  $x_L(t)$  and  $x_R(t)$ , terms (2.65d) and (2.65e) we have:

$$\begin{aligned} & \int_{t_0}^{t_1} \lim_{\epsilon \downarrow 0} \frac{1}{\epsilon} \int_{x_R}^{x_R + \epsilon \delta x_R} (\varphi + \epsilon \delta \varphi) \partial_t (h + \epsilon \delta h) - \mathcal{H}_b(\varphi + \epsilon \delta \varphi, h + \epsilon \delta h, \psi + \epsilon \delta \psi) dx \\ & + \lim_{\epsilon \downarrow 0} \frac{1}{\epsilon} \int_{x_L}^{x_L + \epsilon \delta x_L} (\varphi + \epsilon \delta \varphi) \partial_t (h + \epsilon \delta h) - \mathcal{H}_b(\varphi + \epsilon \delta \varphi, h + \epsilon \delta h, \psi + \epsilon \delta \psi) dx dt \\ & = \int_{t_0}^{t_1} [\varphi \partial_t h]_{x=x_R(t)} \delta x_R - [\varphi \partial_t h]_{x=x_L(t)} \delta x_L dt. \quad (2.66) \end{aligned}$$

since the water levels  $h(x_R(t), t)$ ,  $h(x_L(t), t)$  are equal to zero at the fluid boundary. The term  $\mathbf{E}$ ,  $\varphi \partial_t (\delta h)$  requires special treatment, since the boundaries are now time dependent.

We have the following relation to rewrite term  $\varphi\partial_t(\delta h)$ :

$$\int_{t_0}^{t_1} \frac{d}{dt} \int_{x_L(t)}^{x_R(t)} \varphi \delta h \, dx = \int_{t_0}^{t_1} \left\{ \int_{x_L(t)}^{x_R(t)} \underbrace{\delta h \partial_t \varphi}_{\mathbf{F}} + \underbrace{\varphi \partial_t (\delta h)}_{\mathbf{E}} \, dx + [\varphi \delta h]_{x=x_R(t)} \frac{dx_R(t)}{dt} - [\varphi \delta h]_{x=x_L(t)} \frac{dx_L(t)}{dt} \right\} dt, \quad (2.67)$$

where  $\mathbf{F}$  is the term that completes the terms (2.65a)-(2.65c) to regain the variational derivative resulting in the governing equations in the fluid domain, as collected in (2.38). We express  $\mathbf{E}$  explicitly using the above relation and we substitute  $\mathbf{E}$  in (2.65b).

We combine the terms at the boundaries with the boundary terms (2.65d) and (2.65e). At the boundary  $x_R(t)$ , we have for  $\delta x_R$  and  $\delta h$  the following relation:

$$\delta h \Big|_{x_R(t)} = \partial_x h \Big|_{x=x_R(t)} \delta x_R(t), \quad (2.68)$$

and similarly for  $x = x_L(t)$ . Combining the remaining terms with respect to (2.38), we have:

$$0 = \int_{x_L(t)}^{x_R(t)} \varphi \delta h \, dx \Big|_{t_0}^{t_1} + \int_{t_0}^{t_1} \delta x_R \left[ \varphi \partial_t h + \varphi \partial_x (h) \frac{dx_R(t)}{dt} \right]_{x=x_R(t)} \quad (2.69a)$$

$$- \delta x_L \left[ \varphi \partial_t h + \varphi \partial_x (h) \frac{dx_L(t)}{dt} \right]_{x=x_L(t)} dt. \quad (2.69b)$$

Observe that everywhere in the fluid we have conservation of mass

$$\partial_t h + \partial_x (h \partial_x \varphi) = 0 \quad (2.70)$$

and we have that  $h(x_R(t), t) = h(x_L(t), t) = 0$  at the boundaries. Substitution of the above relations and using the arbitrariness of the variables  $\delta x_L$ ,  $\delta x_R$  we obtain conditions for the moving boundaries

$$\delta x_R : \varphi (\partial_x \varphi) (\partial_x h) - \varphi (\partial_x h) \frac{dx_R(t)}{dt} = 0 \quad \text{at } x = x_R(t), \quad (2.71)$$

$$\delta x_L : -\varphi (\partial_x \varphi) (\partial_x h) + \varphi (\partial_x h) \frac{dx_L(t)}{dt} = 0 \quad \text{at } x = x_L(t), \quad (2.72)$$

which is simplified to

$$\delta x_R : \partial_x \varphi - \frac{dx_R(t)}{dt} = 0 \quad \text{at } x = x_R(t), \quad (2.73)$$

$$\delta x_L : \partial_x \varphi - \frac{dx_L(t)}{dt} = 0 \quad \text{at } x = x_L(t). \quad (2.74)$$

Together with equations (2.39), (2.40) and (2.41) these conditions govern the Klopman variational Boussinesq model for fluid boundaries that can move in time.

## 2.7 Conclusion

In this section we have studied variational principles for free surface water waves, where the total energy  $\mathcal{H}$  is the basis of an action functional and where  $\mathcal{H}$  varies per model. The following three variational principles have been studied:

1. Luke's variational principle for (3D) non-linear potential flow [27].
2. Klopman's variational Boussinesq model (1D) [19].
3. Whitham's variational Boussinesq model (1D) [37].

We have included surface tension effects by adding an extra term in the total energy  $\mathcal{H}$ . For all three principles the Euler-Lagrange equations were derived which govern the fluid surface motion. Comparing the linear dispersion relations we conclude that the Klopman variational Boussinesq model approximates the exact dispersion relation better than the Whitham variational Boussinesq model.

In the region where initial sinusoidal waves start to break [36], we find that the relative error of the KVBM is small compared to the exact linear dispersion relation.

Furthermore, surface tension effects can be approximated more accurately with the KVBM in water depths where surface tension effects may not be neglected, i.e. for short waves with  $\lambda < 10$  cm.

We conclude that for longer waves propagating over deeper water the Klopman Boussinesq variational is equivalent to the Boussinesq formulations of Madsen [25]. The advantage of the KVBM is that energy is conserved and guaranteed to be positive-definite. Furthermore, moving boundaries of the fluid domain can be nicely incorporated, such that the physics of flooding and drying is described easily.

### 3 Numerical modeling: continuous Galerkin

#### 3.1 Introduction

To approximate the solutions of the governing equations derived in section 2 we use the continuous Galerkin finite element method, which is also known as Ritz-Galerkin method. In this method we formulate a weak formulation of the Boundary Value Problems that we observe. Discretizing the equations offers the possibility to obtain the approximated solution numerically.

First we discretize Whitham's variational Boussinesq formulation by using the arbitrariness of the variational derivatives with respect to each variable. Note that they are elements of the test function-space  $C_0^\infty(D_h)$  on the domain, which can be restricted to the test functions on each element  $K_i$  with the test function space  $C_0^\infty(K_i)$ . Hereby we then formulate the finite element weak formulations.

In section 3.3 the assembly of the discretized system is considered. First the linearized shallow water model is considered, then the nonlinear shallow water model and finally the Boussinesq term is included, where we used an auxiliary variable to treat the second-order time derivative. Then a non-flat seabed is introduced, which enables us to test if waves will start to break.

In section 3.6 time-integration methods are proposed, namely the total variation diminishing Runge-Kutta 3 and 4 method and the symplectic Störmer-Verlet method.

In section 3.7 some conclusions are drawn.

#### 3.2 Whitham's Boussinesq variational principle

For the Whitham Boussinesq-model including surface tension (including the  $\gamma$ -term, section 2.4) the variational formulation  $\mathcal{L}_s$  was

$$0 = \delta \int_{t_0}^{t_1} \int_{D_h} L_s(h, \phi) \, dx dt \quad (3.1)$$

$$= \delta \int_{t_0}^{t_1} \int_{D_h} \phi \partial_t h - \frac{1}{2} h (\partial_x \phi)^2 + \frac{1}{6} h_0 (\partial_t h)^2 - \frac{1}{2} g (h - h_0)^2 - \gamma (\sqrt{1 + (\partial_x h)^2} - 1) \, dx dt. \quad (3.2)$$

Solving the system with a finite element method requires that we partition the horizontal domain  $D_h = x \in (x_L, x_R)$  with elements to approximate the solution. We introduce the partitioning  $T_h$  existing of  $N$  open elements  $K_j = \{x | x \in (x_j, x_{j+1})\}$  where  $x_i$  and  $x_{j+1}$  are the so-called nodes. The result is a tessellation

$$T_h = \{K_i | \cup_{i=1}^N \bar{K}_i = \bar{D}_h \text{ and } K_i \cap K_j = \emptyset \text{ if } i \neq j, 1 \leq i, j \leq N\} \quad (3.3)$$

with  $\bar{K}_i$  the closure of element  $K_i$ . This discretization is illustrated by figure 3.2.1.

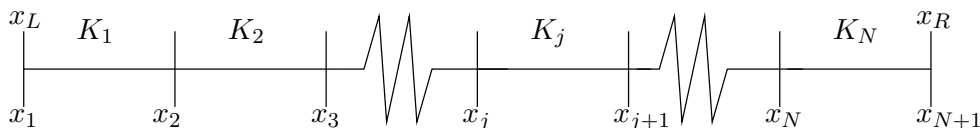


Figure 3.2.1: Subdivision into  $N$  elements  $K_j$  of the horizontal domain  $D_h$ .

We introduce global Galerkin basis-functions  $\chi_j(x) \in P^n(D_h)$ , which means that they are continuous, have compact support on  $D_h$  and are polynomials of degree  $n$  [6]. We choose linear basis-functions  $\chi_j(x) = 1$  on global node  $j$  and zero at the other nodes, see figure 3.2.2. For convenience we consider periodic boundaries, such that node  $x_1 = x_{N+1}$  and we consider

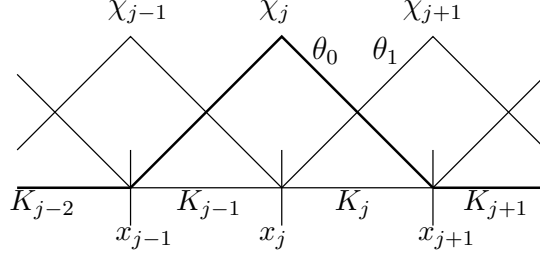


Figure 3.2.2: Linear basis functions for continuous Galerkin finite element methods; thick line is  $\chi_j(x)$ .

the surrounding elements  $K_N$  and  $K_1$  for node  $x_1$ . We approximate the unknown functions of the system on the nodes  $x_j$ ,  $j = 1, \dots, N + 1$  with trial-functions  $\hat{h}(t)$  and  $\hat{\phi}(t)$  for  $h(x, t)$  and  $\phi(x, t)$  respectively in terms of the basis-functions  $\chi_j$  [5]

$$h(x, t) \cong \hat{h}(x, t) = \sum_{j=1}^{N+1} \chi_j(x) H_j(t), \quad \phi(x, t) \cong \hat{\phi}(x, t) = \sum_{j=1}^{N+1} \chi_j(x) \Phi_j(t) \quad (3.4)$$

where  $\chi_j$  is only non-zero in the elements  $K_{j-1}$  and  $K_j$ . In element  $K_k$  the basis-functions  $\chi_k$  and  $\chi_{k+1}$  are considered, since the other basis-functions are zero. It is convenient to introduce the element basis functions  $\theta_m$  ( $m = 0, 1$ ), such that  $\theta_0(x) = \chi_k(x)$  and  $\theta_1(x) = \chi_{k+1}(x)$  for  $x \in K_k$ . The representation of the trial functions  $\hat{\phi}(x, t)$  and  $\hat{h}(x, t)$  can now be written as

$$\hat{\phi}(x, t) = \Phi_k(t)\theta_0(x) + \Phi_{k+1}(t)\theta_1(x) \quad x \in K_k, \quad (3.5a)$$

$$\hat{h}(x, t) = H_k(t)\theta_0(x) + H_{k+1}(t)\theta_1(x) \quad x \in K_k. \quad (3.5b)$$

When we consider a non-flat seabed, we may represent the still water level  $h_0(x)$  with:

$$\hat{h}_0(x) = H_{0,k}\theta_0(x) + H_{0,k+1}\theta_1(x) \quad x \in K_k. \quad (3.6)$$

### 3.2.1 Discretized variational formulation

Neglecting surface tension, the discretized variational formulation is the substitution of (3.5) and (3.6) in (3.1):

$$\begin{aligned} 0 = \delta \int_{t_0}^{t_1} \sum_{k=1}^N \int_{x_k}^{x_{k+1}} & (\Phi_k\theta_0 + \Phi_{k+1}\theta_1) \left( \frac{dH_k}{dt}\theta_0 + \frac{dH_{k+1}}{dt}\theta_1 \right) \\ & - \frac{1}{2} (H_k\theta_0 + H_{k+1}\theta_1) \left( \Phi_k \frac{d\theta_0}{dx} + \Phi_{k+1} \frac{d\theta_1}{dx} \right)^2 + \frac{1}{6} h_0 \left( \frac{dH_k}{dt}\theta_0 + \frac{dH_{k+1}}{dt}\theta_1 \right)^2 \\ & - \frac{1}{2} g (H_k\theta_0 + H_{k+1}\theta_1 - h_0(x_k)\theta_0 - h_0(x_{k+1})\theta_1)^2 dx dt. \end{aligned} \quad (3.7)$$

We may now vary with respect to the variables  $H_k(t)$ ,  $H_{k+1}(t)$ ,  $\Phi_k(t)$  and  $\Phi_{k+1}(t)$  over the elements  $K_k$ . The first variation with respect to  $\delta\Phi_k(t)$  and  $\delta\Phi_{k+1}(t)$  is:

$$\begin{aligned} 0 = \sum_{k=1}^N \int_{K_k} & (\delta\Phi_k\theta_0 + \delta\Phi_{k+1}\theta_1) \left( \frac{dH_k}{dt}\theta_0 + \frac{dH_{k+1}}{dt}\theta_1 \right) \\ & - (H_k\theta_0 + H_{k+1}\theta_1) \left( \Phi_k \frac{d\theta_0}{dx} + \Phi_{k+1} \frac{d\theta_1}{dx} \right) (\delta\Phi_k \frac{d\theta_0}{dx} + \delta\Phi_{k+1} \frac{d\theta_1}{dx}) dx \end{aligned} \quad (3.8)$$

and with respect to  $\delta H_k(t)$  and  $\delta H_{k+1}(t)$  is:

$$\begin{aligned}
0 = & \sum_{k=1}^N \int_{K_k} (\delta H_k \theta_0 + \delta H_{k+1} \theta_1) \left( \frac{d\Phi_k}{dt} \theta_0 + \frac{d\Phi_{k+1}}{dt} \theta_1 \right) \\
& + \frac{1}{2} (\delta H_k \theta_0 + \delta H_{k+1} \theta_1) \left( \Phi_k \frac{d\theta_0}{dx} + \Phi_{k+1} \frac{d\theta_1}{dx} \right)^2 \\
& + \frac{1}{3} h_0 (\delta H_k \theta_0 + \delta H_{k+1} \theta_1) \left( \frac{d^2 H_k}{dt^2} \theta_0 + \frac{d^2 H_{k+1}}{dt^2} \theta_1 \right) \\
& + g (\delta H_k \theta_0 + \delta H_{k+1} \theta_1) (H_k \theta_0 + H_{k+1} \theta_1 - H_{0,k} \theta_0 - H_{0,k+1} \theta_1) dx. \quad (3.9)
\end{aligned}$$

### 3.3 Assembly of global nodes

In this section an assembly framework is created that we can use to calculate the fully discretized variational formulation. The assembly framework results in an algebraic system. Using the arbitrariness of the variational derivatives,  $\delta H_k, \delta \Phi_k \in C_0^\infty(K_{k-1} \cup K_k)$ , we are able to collect the function values in element  $K_{k-1}$  and  $K_k$  that contribute to the function values at node  $x_k$ .

We start with the linearized shallow water model. Then we include nonlinear terms that play a role in the shallow water formulations. Thereafter we consider the discrete variational formulation for the Boussinesq model as derived in the previous section. For each step the total energy of the system is considered.

#### 3.3.1 Discrete linearized shallow water variational formulation

When we linearize the system (3.8, 3.9) around the still water position  $z = h_0$  and neglect the higher order time derivatives, we obtain the following discrete system principle for the linearized shallow water equations;

$$\begin{aligned}
0 = & \sum_{k=1}^N \int_{K_k} (\theta_0 + \theta_1) \left( \frac{dH_k}{dt} \theta_0 + \frac{dH_{k+1}}{dt} \theta_1 \right) \\
& - h_0 \left( \Phi_k \left( \frac{d\theta_0}{dx} \right)^2 + \Phi_{k+1} \left( \frac{d\theta_1}{dx} \right)^2 + (\Phi_k + \Phi_{k+1}) \frac{d\theta_0}{dx} \frac{d\theta_1}{dx} \right) dx \quad (3.10a)
\end{aligned}$$

$$\begin{aligned}
0 = & \sum_{k=1}^N \int_{K_k} (\theta_0 + \theta_1) \left( \frac{d\Phi_k}{dt} \theta_0 + \frac{d\Phi_{k+1}}{dt} \theta_1 \right) \\
& + g (\theta_0 + \theta_1) (H_k \theta_0 + H_{k+1} \theta_1 - H_{0,k} \theta_0 - H_{0,k+1} \theta_1) dx, \quad (3.10b)
\end{aligned}$$

where we used the arbitrariness of the variational derivatives. These relationships can be simplified as follows. We transform the integrals over the element  $K_k$  into integrals over the reference element  $\tilde{K} = [0, 1]$  with local basis-functions  $\hat{\theta}_0 = 1 - \xi$ ,  $\hat{\theta}_1 = \xi$ ,  $\xi \in \tilde{K}$ . We are now able to reformulate the integrals over elements  $K_k$  with respect to the reference element  $\tilde{K}$ :

$$A_{mn}^k = |K_k| \int_0^1 \hat{\theta}_m \hat{\theta}_n d\xi, \quad B_{mn}^k = |K_k| \int_0^1 \frac{d\hat{\theta}_m}{dx} \frac{d\hat{\theta}_n}{dx} d\xi, \quad (3.11)$$

with  $|K_k| = x_{k+1} - x_k$  the length of the element  $K_k$  and  $\{m, n\} = \{0, 1\}$ . These integrals over the reference element can be computed with Gauss' two-point formula, which is exact for linear polynomials [24]. The representations  $\hat{\phi}$  and  $\hat{h}$  in (3.5) evaluated on the elements  $K_k$ , together with the evaluation of the inner-products on the reference element (3.11), gives us a linear system per node  $k$ :

$$A_{10}^{k-1} \frac{dH_{k-1}}{dt} + (A_{11}^{k-1} + A_{00}^k) \frac{dH_k}{dt} + A_{01}^k \frac{dH_{k+1}}{dt}$$

$$= h_0 \left( B_{10}^{k-1} \Phi_{k-1} + (B_{11}^{k-1} + B_{00}^k) \Phi_k + B_{01}^k \Phi_{k+1} \right), \quad (3.12a)$$

$$\begin{aligned} A_{10}^{k-1} \frac{d\Phi_{k-1}}{dt} + (A_{11}^{k-1} + A_{00}^k) \frac{d\Phi_k}{dt} + A_{01}^k \frac{d\Phi_{k+1}}{dt} \\ = -g \left( A_{10}^{k-1} (H_{k-1} - H_{0,k-1}) + (A_{11}^{k-1} + A_{00}^k) (H_k - H_{0,k}) + A_{01}^k (H_{k+1} - H_{0,k+1}) \right) \end{aligned} \quad (3.12b)$$

with the stillwater height  $h_0$  constant in time. We can write this system using mass matrix  $M_A$  and stiffness matrix  $M_B$  as follows:

$$M_A \frac{dH}{dt} = h_0 M_B \Phi \quad (3.13a)$$

$$M_A \frac{d\Phi}{dt} = -g M_A (H - h_0), \quad (3.13b)$$

where  $M_A$  and  $M_B$  are tri-diagonal matrices with the exception of the first and last row, where boundary condition are playing a role. Since  $M_A$  is invertible we can write the system as follows:

$$\frac{dH}{dt} = h_0 M_A^{-1} M_B \Phi \quad (3.14a)$$

$$\frac{d\Phi}{dt} = -g (H - h_0), \quad (3.14b)$$

Integration over time can be done using the third-order Runge-Kutta method, see §3.6. The spatial averaged energy  $\bar{\mathcal{H}}(t)$  for the linearized shallow water variational formulation is given by:

$$\begin{aligned} \bar{\mathcal{H}}(t) = \frac{1}{\lambda} \sum_k \int_{K_k} \frac{1}{2} h_0 \left( \Phi_k \frac{d\theta_0}{dx} + \Phi_{k+1} \frac{d\theta_1}{dx} \right)^2 \\ + \frac{1}{2} g (H_k \theta_0 + H_{k+1} \theta_1 - H_{0,k} \theta_0 - H_{0,k+1} \theta_1)^2 dx. \end{aligned} \quad (3.15)$$

### 3.3.2 Discrete shallow water variational formulation

The discrete nonlinear shallow water system can be obtained from the discretized variational formulation described by system (3.8, 3.9). The discretized shallow water system reads:

$$\begin{aligned} 0 = \sum_{k=1}^N \int_{K_k} (\delta \Phi_k \theta_0 + \delta \Phi_{k+1} \theta_1) \left( \frac{dH_k}{dt} \theta_0 + \frac{dH_{k+1}}{dt} \theta_1 \right) \\ - (H_k \theta_0 + H_{k+1} \theta_1) \left( \Phi_k \frac{d\theta_0}{dx} + \Phi_{k+1} \frac{d\theta_1}{dx} \right) (\delta \Phi_k \frac{d\theta_0}{dx} + \delta \Phi_{k+1} \frac{d\theta_1}{dx}) dx \end{aligned} \quad (3.16a)$$

$$\begin{aligned} 0 = \sum_{k=1}^N \int_{K_k} (\delta H_k \theta_0 + \delta H_{k+1} \theta_1) \left( \frac{d\Phi_k}{dt} \theta_0 + \frac{d\Phi_{k+1}}{dt} \theta_1 \right) \\ + \frac{1}{2} (\delta H_k \theta_0 + \delta H_{k+1} \theta_1) \left( \Phi_k \frac{d\theta_0}{dx} + \Phi_{k+1} \frac{d\theta_1}{dx} \right)^2 \\ + g (\delta H_k \theta_0 + \delta H_{k+1} \theta_1) (H_k \theta_0 + H_{k+1} \theta_1 - H_{0,k} \theta_0 - H_{0,k+1} \theta_1) dx. \end{aligned} \quad (3.16b)$$

For convenience we introduce the element integration

$$D_{mnp}^k = |K_k| \int_0^1 \hat{\theta}_m \frac{d\hat{\theta}_n}{dx} \frac{d\hat{\theta}_p}{dx} d\xi. \quad (3.17)$$

Assembly of the elements  $K_{k-1}$  and  $K_k$  around  $x_k \in D_h$  using the arbitrariness of the variables  $\delta\Phi$  and  $\delta H$  results in the following system:

$$A_{10}^{k-1} \frac{dH_{k-1}}{dt} + (A_{11}^{k-1} + A_{00}^k) \frac{dH_k}{dt} + A_{01}^k \frac{dH_{k+1}}{dt} \quad (3.18a)$$

$$\begin{aligned} &= h_0 \left( B_{10}^{k-1} \Phi_{k-1} + (B_{11}^{k-1} + B_{00}^k) \Phi_k + B_{01}^k \Phi_{k+1} \right) \\ &\quad + D_{010}^{k-1} H_{k-1} \Phi_{k-1} + D_{011}^{k-1} H_{k-1} \Phi_k + D_{110}^{k-1} H_k \Phi_{k-1} + D_{111}^{k-1} H_k \Phi_k, \\ &\quad + D_{000}^k H_k \Phi_k + D_{001}^k H_k \Phi_{k+1} + D_{100}^k H_{k+1} \Phi_k + D_{101}^k H_{k+1} \Phi_{k+1}, \end{aligned}$$

$$A_{10}^{k-1} \frac{d\Phi_{k-1}}{dt} + (A_{11}^{k-1} + A_{00}^k) \frac{d\Phi_k}{dt} + A_{01}^k \frac{d\Phi_{k+1}}{dt} \quad (3.18b)$$

$$\begin{aligned} &= -g \left( A_{10}^{k-1} (H_{k-1} - H_{0,k-1}) + (A_{11}^{k-1} + A_{00}^k) (H_k - H_{0,k}) + A_{01}^{k-1} (H_{k+1} - H_{0,k+1}) \right) \\ &\quad - \frac{1}{2} D_{100}^{k-1} (\Phi_{k-1})^2 - \frac{1}{2} D_{101}^{k-1} \Phi_{k-1} \Phi_k - \frac{1}{2} D_{110}^{k-1} \Phi_k \Phi_{k-1} - \frac{1}{2} D_{111}^{k-1} (\Phi_k)^2 \\ &\quad - \frac{1}{2} D_{000}^k (\Phi_k)^2 - \frac{1}{2} D_{001}^k \Phi_k \Phi_{k+1} - \frac{1}{2} D_{010}^k \Phi_{k+1} \Phi_k - \frac{1}{2} D_{011}^k (\Phi_{k+1})^2 \end{aligned}$$

We rewrite this assembly in terms of solution vectors as follows

$$M_A \frac{dH}{dt} = h_0 M_B \Phi + M_D(H) \Phi \quad (3.19a)$$

$$M_A \frac{d\Phi}{dt} = -g M_A (H - h_0) - \frac{1}{2} M_E(\Phi) \Phi, \quad (3.19b)$$

where  $M_D(H(t))$  is denoted for periodic boundaries ( $x_1 \equiv x_{N+1}$ ) by

$$M_D = \quad (3.20)$$

$$\begin{bmatrix} MD_2^1 & MD_3^1 & 0 & \dots & \dots & 0 & MD_1^N \\ MD_1^2 & MD_2^2 & MD_3^2 & \dots & \dots & \dots & \emptyset \\ \dots & \dots & \dots & \dots & \dots & \dots & \dots \\ \emptyset & \dots & MD_1^k & MD_2^k & MD_3^k & \dots & \emptyset \\ \dots & \dots & \dots & \dots & \dots & \dots & \dots \\ \emptyset & \dots & \dots & \dots & MD_1^{N-1} & MD_2^{N-1} & MD_3^{N-1} \\ MD_3^1 & 0 & \dots & \dots & 0 & MD_1^N & MD_2^N \end{bmatrix}$$

with

$$MD_1^k(H(t)) = D_{010}^{k-1} H_{k-1}(t) + D_{110}^{k-1} H_k(t) \quad (3.21a)$$

$$MD_2^k(H(t)) = D_{011}^{k-1} H_{k-1}(t) + D_{111}^{k-1} H_k(t) + D_{000}^k H_k(t) + D_{100}^k H_{k+1}(t) \quad (3.21b)$$

$$MD_3^k(H(t)) = D_{001}^k H_k(t) + D_{101}^k H_{k+1}(t). \quad (3.21c)$$

Similarly, matrix  $M_E(\Phi(t))$  is denoted by  $ME_{i,j}(\Phi) = MD_{i,j}(\Phi)$ ,  $i, j \in [1, \dots, N]$  with coefficients computed as follows:

$$ME_1^k(\Phi(t)) = D_{100}^{k-1} \Phi_{k-1}(t) D_{110}^{k-1} \Phi_k(t) \quad (3.22a)$$

$$ME_2^k(\Phi(t)) = D_{101}^{k-1} \Phi_{k-1}(t) + D_{111}^{k-1} \Phi_k(t) + D_{000}^k \Phi_k(t) + D_{010}^k \Phi_{k+1}(t) \quad (3.22b)$$

$$ME_3^k(\Phi(t)) = D_{001}^k \Phi_k(t) + D_{011}^k \Phi_{k+1}(t). \quad (3.22c)$$

Note that in the assembly of the nonlinear terms in (3.19a) and (3.19b), the matrix coefficients  $MD_1^k$  (3.21a) and  $ME_1^k$  (3.22a) are multiplied by  $\Phi_{k-1}$ . Similarly, the coefficients  $MD_2^k$  (3.21b) and  $ME_2^k$  (3.22b) are multiplied by  $\Phi_k$  and finally  $MD_3^k$  (3.21c) and  $ME_3^k$  (3.22c) are multiplied by  $\Phi_{k+1}$ .

The spatial averaged energy  $\bar{\mathcal{H}}(t)$  for the shallow water variational formulation is given by:

$$\begin{aligned} \bar{\mathcal{H}}(t) = & \frac{1}{\lambda} \sum_k \int_{K_k} \frac{1}{2} (H_k \theta_0 + H_{k+1} \theta_1) \left( \Phi_k \frac{d\theta_0}{dx} + \Phi_k \frac{d\theta_1}{dx} \right)^2 \\ & + \frac{1}{2} g (H_k \theta_0 + H_{k+1} \theta_1 - H_{0,k} \theta_0 - H_{0,k+1} \theta_1)^2 dx. \end{aligned} \quad (3.23)$$

### 3.3.3 Discrete Whitham variational Boussinesq formulation

Equivalently to the previous formulations for the shallow water model the Whitham Boussinesq model can be discretized. The Boussinesq model includes the second-order time derivative of the wave elevation,  $\partial_t^2 \eta(x, t)$  in (3.9). The system to be solved now reads:

$$M_A \frac{dH}{dt} = h_0 M_B \Phi + M_D(H) \Phi \quad (3.24a)$$

$$M_A \frac{d\Phi}{dt} + \frac{1}{3} h_0 M_A \frac{d^2 H}{dt^2} = -g M_A (H - h_0) - \frac{1}{2} M_E(\Phi) \Phi, \quad (3.24b)$$

For convenience, write  $\frac{d^2 H}{dt^2} = \frac{d}{dt} \left( \frac{dH}{dt} \right)$  and introducing  $F = \Phi + \frac{1}{3} h_0 \frac{dH}{dt}$  yields the following system:

$$\begin{aligned} F &= \Phi + \frac{1}{3} h_0 M_A^{-1} (h_0 M_B \Phi + M_D(H) \Phi) \\ &= \left( I_N + \frac{1}{3} h_0 M_A^{-1} (h_0 M_B + M_D(H)) \right) \Phi \end{aligned} \quad (3.25a)$$

$$M_A \frac{dH}{dt} = h_0 M_B \Phi + M_D(H) \Phi \quad (3.25b)$$

$$M_A \frac{dF}{dt} = -g M_A (H - h_0) - \frac{1}{2} M_E(\Phi) \Phi. \quad (3.25c)$$

where  $I_N$  is the  $[N \times N]$  unity matrix. When  $H(t^n), F(t^n)$  known, we can solve (3.25a) and obtain  $\Phi(t^n)$ . We then can compute (3.25b, 3.25c) in time using an explicit time stepping method.

The spatial averaged energy  $\bar{\mathcal{H}}(t)$  for the Whitham Boussinesq variational formulation is given by:

$$\begin{aligned} \bar{\mathcal{H}}(t) = & \frac{1}{\lambda} \sum_k \int_{K_k} \frac{1}{2} (H_k \theta_0 + H_{k+1} \theta_1) \left( \Phi_k \frac{d\theta_0}{dx} + \Phi_k \frac{d\theta_1}{dx} \right)^2 \\ & + \frac{1}{2} g (H_k \theta_0 + H_{k+1} \theta_1)^2 dx - \frac{1}{6} \left( \frac{dH_k}{dt} \theta_0 + \frac{dH_{k+1}}{dt} \theta_1 \right)^2 \end{aligned} \quad (3.26)$$

### 3.4 Klopman's variational Boussinesq model

In order to solve the weakly nonlinear Klopman variational Boussinesq model numerically we introduce the following expansions for the trial and test functions

$$\begin{aligned} h(x, t) &= \sum_{j=1}^{N+1} \chi_j(x) H_j(t), & \delta h(x, t) &= \sum_{j=1}^{N+1} \chi_j(x) V_j, \\ \phi(x, t) &= \sum_{j=1}^{N+1} \chi_j(x) \Phi_j(t), & \delta \phi(x, t) &= \sum_{j=1}^{N+1} \chi_j(x) W_j, \\ \psi(x, t) &= \sum_{j=1}^{N+1} \chi_j(x) \Psi_j(t), & \delta \psi(x, t) &= \sum_{j=1}^{N+1} \chi_j(x) Z_j. \end{aligned} \quad (3.27)$$

where  $\chi_j$  are linear basisfunctions of degree  $d_p = 1$  that are only non-zero in the elements  $K_{j-1}$  and  $K_j$  as introduced in section 3.2. The seabed slope  $h_0(x)$  is approximated by  $H_0$ , which we will assume constant in the rest of this subsection. We integrate the variational

formulation of the Klopman Boussinesq model (2.37) by parts with respect to time and we have

$$0 = \int_{t_0}^{t_1} \int_{D_h} \delta\varphi \partial_t h - \partial_x \delta\varphi \left[ h \partial_x \varphi - \frac{2}{3} h^3 \partial_x \psi \right] \quad (3.28a)$$

$$- \delta h \partial_t \varphi - \delta h \left( \frac{1}{2} (\partial_x \varphi)^2 - 2h^2 \partial_x \varphi \partial_x \psi + \frac{4}{3} h^4 (\partial_x \psi)^2 + 2h^2 \psi^2 + g(h - h_0) \right) \quad (3.28b)$$

$$+ \partial_x \delta\psi \left[ \frac{2}{3} h^3 \partial_x \varphi - \frac{8}{15} h^5 \partial_x \psi \right] - \frac{4}{3} \delta\psi h^3 \psi \, dx dt. \quad (3.28c)$$

We will now substitute the expansions for our trial and test functions to discretize our weak formulation for each varied variable. Evaluation of the global basisfunction is done over the reference element as described in section 3.2.

### 3.5 Assembly of global nodes

We assemble our system per varied variable at each elements belonging to the tessellation of a periodic domain. We introduce convenient integrals over the elements and collect these contributions per element to solve our system in time.

#### 3.5.1 Assembly for the first part

We first consider part (3.28a), the variation with respect to  $\delta\varphi$ . We have

$$\int_{D_h} \delta\varphi \partial_t h - \partial_x \delta\varphi \left[ h \partial_x \varphi - \frac{2}{3} h^3 \partial_x \psi \right] dx = 0 \Leftrightarrow \quad (3.29a)$$

$$\sum_{j=1}^N \int_{K_j} \delta\varphi \partial_t h - \partial_x \delta\varphi \left[ h \partial_x \varphi - \frac{2}{3} h^3 \partial_x \psi \right] dx = 0. \quad (3.29b)$$

We substitution the expansions (3.27). For convenience we introduce the following integrals at elements  $K_j$  of our tessellation  $\mathcal{T}_h$ ,

$$A(j, i, m) = \frac{|K_j|}{2} \int_{-1}^1 \Theta_i \Theta_m \, d\xi \quad (3.30a)$$

$$B1(j, i, H_L, H_R, \Phi_L, \Phi_R) = \frac{|K_j|}{2} \int_{-1}^1 \frac{d\Theta_i}{dx} (H_L \Theta_1 + H_R \Theta_0) (\Phi_L \frac{d\Theta_1}{dx} + \Phi_R \frac{d\Theta_0}{dx}) d\xi \quad (3.30b)$$

$$C1(j, i, H_L, H_R, \Psi_L, \Psi_R) = \frac{|K_j|}{2} \int_{-1}^1 \frac{d\Theta_i}{dx} (H_L \Theta_1 + H_R \Theta_0)^3 (\Psi_L \frac{d\Theta_1}{dx} + \Psi_R \frac{d\Theta_0}{dx}) d\xi \quad (3.30c)$$

where  $\Theta_i$  represents the expansion of our arbitrary testfunction  $\delta\phi$  and indices  $L$  and  $R$  represent respectively the left ( $x_j$ ) and right ( $x_{j+1}$ ) node of the element concerned. Note that, for fast computation of the integrals,  $\frac{d\Theta_i}{dx} = (-1)^{1-i} \frac{2}{|K_j|}$  for linear polynomials. We collect the integrals above by summation over all elements and add the contributions to the left and right node. We obtain for equation (3.29b)

$$MA \frac{dH}{dt} - MB1 + \frac{2}{3} MC1 = 0 \quad (3.31)$$

where the matrices are found by summation of all contributions from elements  $K_j$ ,  $j = 1, \dots, Ne$  to both nodal values at the left and right boundaries,  $x_j$  and  $x_{j+1}$ , of elements  $K_j$ . They are indicated by  $x_{j+1-i}$ ,  $i = 0, 1$ .

$$MA_{j+1-i, j+1-m} = A(j, i, m) \quad \forall m = 0, 1 \quad (3.32a)$$

$$MB1_{j+1-i} = B1(j, i, H_j, H_{j+1}, \Phi_j, \Phi_{j+1}) \quad (3.32b)$$

$$MC1_{j+1-i} = C1(j, i, H_j, H_{j+1}, \Psi_j, \Psi_{j+1}) \quad (3.32c)$$

Observe that the parameter  $j + 1 - i$  in combination with element  $K_j$  represents the global node, nameley  $\Theta_i = \Theta_1$  refers to the left and  $\Theta_i = \Theta_0$  to the right node of an element. Note that we still have to account for boundary conditions; eg. in case of periodic boundary conditions we concern nodal value  $x_1$  if  $x_{j+1-i} = x_{N_e+1}$  and we add this contribution to the global matrix accordingly.

### 3.5.2 Assembly for the second part

We now consider part (3.28b), the variation with respect to  $\delta\varphi$ . We have

$$\int_{D_h} \delta h \left( \partial_t \varphi + \frac{1}{2} (\partial_x \varphi)^2 - 2h^2 \partial_x \varphi \partial_x \psi + \frac{4}{3} h^4 (\partial_x \psi)^2 + 2h^2 \psi^2 + g(h - h_0) \right) dx = 0 \Leftrightarrow \quad (3.33a)$$

$$\sum_{j=1}^N \int_{K_j} \delta h \left( \partial_t \varphi + \frac{1}{2} (\partial_x \varphi)^2 - 2h^2 \partial_x \varphi \partial_x \psi + \frac{4}{3} h^4 (\partial_x \psi)^2 + 2h^2 \psi^2 + g(h - h_0) \right) dx = 0 \quad (3.33b)$$

and adopt the convenient integrals for our tessellation  $\mathcal{T}_h$

$$A(j, i, m) = \frac{|K_j|}{2} \int_{-1}^1 \Theta_i \Theta_n \, d\xi \quad (3.34a)$$

$$B2(j, i, \Phi_L, \Phi_R) = \frac{|K_j|}{2} \int_{-1}^1 \Theta_i \left( \frac{d\Theta_1}{dx} \Phi_L + \frac{d\Theta_1}{dx} \Phi_R \right)^2 \, d\xi \quad (3.34b)$$

$$C2(j, i, H_L, H_R, \Phi_L, \Phi_R, \Psi_L, \Psi_R) = \frac{|K_j|}{2} \int_{-1}^1 \Theta_i (H_L \Theta_1 + H_R \Theta_0)^2 \left( \Phi_L \frac{d\Theta_1}{dx} + \Phi_R \frac{d\Theta_0}{dx} \right) \left( \Psi_L \frac{d\Theta_1}{dx} + \Psi_R \frac{d\Theta_0}{dx} \right) \, d\xi \quad (3.34c)$$

$$D2(j, i, H_L, H_R, \Psi_L, \Psi_R) = \frac{|K_j|}{2} \int_{-1}^1 \Theta_i (H_L \Theta_1 + H_R \Theta_0)^4 \left( \Psi_L \frac{d\Theta_1}{dx} + \Psi_R \frac{d\Theta_0}{dx} \right)^2 \, d\xi \quad (3.34d)$$

$$E2(j, i, H_L, H_R, \Psi_L, \Psi_R) = \frac{|K_j|}{2} \int_{-1}^1 \Theta_i (H_L \Theta_1 + H_R \Theta_0)^2 (\Psi_L \Theta_1 + \Psi_R \Theta_0)^2 \, d\xi. \quad (3.34e)$$

where  $\Theta_i$  represents the expansion of our arbitrary testfunction  $\delta h$ . We obtain for equation (3.33b)

$$MA \frac{dH}{dt} + \frac{1}{2} MB2 - 2MC2 + \frac{3}{4} MD2 + 2ME2 + gMA(H - H_0) = 0 \quad (3.35)$$

where

$$MA_{j+1-i, j+1-m} = A(j, i, m) \quad \forall m = 0, 1 \quad (3.36a)$$

$$MB2_{j+1-i} = B2(j, i, \Phi_j, \Phi_{j+1}) \quad (3.36b)$$

$$MC2_{j+1-i} = C2(j, i, H_j, H_{j+1}, \Phi_j, \Phi_{j+1}, \Psi_j, \Psi_{j+1}) \quad (3.36c)$$

$$MD2_{j+1-i} = D2(j, i, H_j, H_{h+1}, \Psi_j, \Psi_{j+1}) \quad (3.36d)$$

$$ME2_{j+1-i} = E2(j, i, H_j, H_{j+1}, \Psi_j, \Psi_{j+1}) \quad (3.36e)$$

### 3.5.3 Assembly for the third part

We now consider part (3.28c), the variation with respect to  $\delta\psi$ . We have

$$\int_{D_h} \partial_x \delta \psi \left[ \frac{2}{3} h^3 \partial_x \varphi - \frac{8}{15} h^5 \partial_x \psi \right] - \frac{4}{3} \delta \psi h^3 \psi \, dx = 0 \Leftrightarrow \quad (3.37)$$

$$\sum_{j=1}^N \int_{K_j} \partial_x \delta \psi \left[ \frac{2}{3} h^3 \partial_x \varphi - \frac{8}{15} h^5 \partial_x \psi \right] - \frac{4}{3} \delta \psi h^3 \psi \, dx = 0. \quad (3.38)$$

and use the integrals for our tessellation  $\mathcal{T}_h$

$$C3(j, i, H_L, H_R, \Phi_L, \Phi_R) = \frac{|K_j|}{2} \int_{-1}^1 \frac{d\Theta_i}{dx} (H_L \Theta_1 + H_R \Theta_0)^3 \left( \Phi_L \frac{d\Theta_1}{dx} + \Phi_R \frac{d\Theta_0}{dx} \right) d\xi \quad (3.39a)$$

$$D3(j, i, H_L, H_R, m) = \frac{|K_j|}{2} \int_{-1}^1 \frac{d\Theta_i}{dx} (H_L \Theta_1 + H_R \Theta_0)^5 \frac{d\Theta_m}{dx} d\xi \quad (3.39b)$$

$$E3(j, i, H_L, H_R, m) = \frac{|K_j|}{2} \int_{-1}^1 \Theta_i (H_L \Theta_1 + H_R \Theta_0)^3 \Theta_m \, d\xi \quad (3.39c)$$

where  $\Theta_i$  represents the expansion of our arbitrary testfunction  $\delta \psi$  and with the parameter  $m$  we represent the nodal value of  $\Psi_{j+1-m}$  at  $x_{j+1-m}$ . We obtain for equation (3.38)

$$\frac{2}{3} MC3 - \left( \frac{8}{15} MD3 + \frac{4}{3} ME3 \right) \Psi = 0 \quad (3.40)$$

where

$$MC3_{j+1-i} = C3(j, i, H_j, H_{j+1}, \Phi_j, \Phi_{j+1}) \quad (3.41a)$$

$$MD3_{j+1-i, j+1-m} = D3(j, i, H_j, H_{j+1}, m) \quad (3.41b)$$

$$ME3_{j+1-i, j+1-m} = E3(j, i, H_L, H_R, m) \quad (3.41c)$$

where for periodic boundaries if  $j + 1 - m = Ne + 1$  we have to put  $j + 1 - m = 1$ .

### 3.5.4 Solving the system in time

Since we represent each trial function in terms of polynomial basisfunctions of degree  $d_p = 1$  we have to make sure that our spatial integration routine preserves accuracy. For example integral  $D3$ ; we numerically integrate  $h^5$  over an element. Observe that as a result we obtain polynomials of order at most  $d_p = 5$ .

$$\int_{x_j}^{x_{j+1}} h^5 \, dx \approx \frac{|K_j|}{2} \int_{-1}^1 \left( H_j \left( \frac{1-\xi}{2} \right) + H_{j+1} \left( \frac{1+\xi}{2} \right) \right)^5 d\xi. \quad (3.42)$$

Therefore an integration routine should be chosen that is at least exact for polynomials of degree 5. We choose the three point Gauss quadrature rule, which is exact for polynomials of degree  $d_p = 2 * 3 - 1$ .

Note that we have the following invertible matrices;  $MA$ ,  $MD3$  and  $ME3$  of size  $[Ne * Ne]$ . We have the following vectors of size  $[Ne * 1]$ : the trial function vectors  $H$ ,  $\Phi$  and  $\Psi$ , and the assembly vectors  $MB1$ ,  $MB2$ ,  $MC1$ ,  $MC2$ ,  $MC3$ ,  $MD2$ ,  $MD3$ ,  $ME2$  and  $ME3$ .

When solving the system in time, we first have to solve the third part to obtain  $\Psi$ . Then we obtain our residuals for a time integration method.

$$\Psi = \left( \frac{4}{5} MD3 + 2ME3 \right)^{-1} MC3 \quad (3.43)$$

$$\frac{dH}{dt} = MA^{-1} \left( MB1 - \frac{2}{3} MC1 \right) \quad (3.44)$$

$$\frac{dH}{dt} = MA^{-1} \left( -gMA(H - H_0) - \frac{1}{2} MB2 + 2MC2 - \frac{3}{4} MD2 - 2ME2 \right) \quad (3.45)$$

### 3.6 Time integration

Untill now the time was considered to be continuous. We now discretize our systems with respect to time, to integrate numerically in time from one time step to another. In literature many time integration methods are proposed. Since we consider energy conserved systems, we would particularly like to conserve energy in our numerical scheme. Therefore we consider the Störmer-Verlet method. The two Runge-Kutta methods are considered, since they are high order in time (third- and fourth-order, respectively). However, they are total variation ( $TV$ ) diminishing [14] under the CFL coefficient. For our systems this results in numerical dissipation. The TV diminishing is expressed as follows:

$$TV(u^{n+1}) := \sum_{i \in \mathcal{T}_h} |u_{i+1}^{n+1} - U_i^{n+1}| \leq \sum_{i \in \mathcal{T}_h} |u_{i+1}^n - U_i^n| =: TV(u^{n+1}), \quad (3.46)$$

where  $u(x, t) = u(x_i, t_n)$  is the solution at the  $i^{th}$  node  $x_i$  and at time step  $t_n$  [14]. The CFL conditions states:

$$\Delta t \leq \frac{\max_{j \in \mathcal{T}_h} \Delta x_j}{\max_{j \in \mathcal{T}_h} |u_j^n|}. \quad (3.47)$$

Another result is that a solution of the systems observed only is oscillatory when the numerical solution is representing a discontinuous jump [14], in our case representing the breaking waves.

#### 3.6.1 Störmer-Verlet

Störmer-Verlet is a symplectic method; it is reversible in time and it conserves energy for Hamiltonian systems such as the (non)-linear shallow water equations. [15].

For the linearized Shallow-Water equations:

$$\begin{aligned} H^{n+\frac{1}{2}} &= H^n + \frac{\Delta t}{2} M_B \Phi^n \\ \Phi^{n+1} &= \Phi^n - \frac{\Delta t}{2} M_A H^{n+\frac{1}{2}} \\ H^{n+1} &= H^{n+\frac{1}{2}} + \frac{\Delta t}{2} M_B \Phi^{n+1}. \end{aligned} \quad (3.48)$$

#### 3.6.2 Third order Runge Kutta

We collect the discretized variational formulations in the following system:

$$\partial_t U = R(U), \quad (3.49)$$

with  $U = [H, \Phi]'$  the state vector. We can use the third-order Runge Kutta to discretize the system in time. We compute the new state vector  $U^{n+1}(x)$  at time-step  $t^{n+1} = t^n + \Delta t$  explicetely

$$\begin{aligned} U^{(1)} &= U^n + \Delta t R(U^n, t^n) \\ U^{(2)} &= [3U^n + U^{(1)} + \Delta t R(U^{(1)}, t^n + \Delta t)]/4 \\ U^{n+1} &= [U^n + 2U^{(2)} + 2\Delta t R(U^{(2)}, t^2 + \Delta t/2)]/3. \end{aligned} \quad (3.50)$$

A rough time step estimation is given by

$$\Delta t \leq CFL \min_k (K_k) / c \quad (3.51)$$

with  $CFL$  the Courant-Friedrichs-Lewy number;  $CFL \leq 1$  and  $c$  is a constant velocity, eg.  $c = \sqrt{g h_0}$  in the shallow water case §3.3.1.

### 3.6.3 Fourth-order Runge-Kutta

The classical fourth-order Runge-Kutta formula is [31]:

$$\begin{aligned}
 U^{(1)} &= \Delta t R(U^n, t^n) \\
 U^{(2)} &= \frac{1}{2} \Delta t R(U^n + \frac{1}{2} U^{(1)}, t^n + \Delta t) \\
 U^{(3)} &= \frac{1}{2} \Delta t R(U^n + \frac{1}{2} U^{(2)}, t^n + \Delta t) \\
 U^{(4)} &= \Delta t R(U^n + U^{(3)}, t^n + \Delta t) \\
 U^{n+1} &= U^n + \frac{U^{(1)}}{6} + \frac{U^{(2)}}{3} + \frac{U^{(3)}}{3} + \frac{U^{(4)}}{6}
 \end{aligned} \tag{3.52}$$

### 3.7 Conclusion

In this section we derived for fully nonlinear Whitham variational Boussinesq model a continuous Galerkin finite element method to approximate propagating wave solutions numerically. In the progress of this derivation we have derived a cG FEM for the linear and nonlinear shallow water equations.

Furthermore, we have derived a cG FEM formulation for the weakly nonlinear Klopman variational Boussinesq model for a horizontal seabed.

Finally, we have presented two total variation diminishing in time integration methods, namely the Runge-Kutta methods 3 and 4, and the Störmer-Verlet method, which is a symplectic method.



## 4 Numerical Modeling: Discontinuous Galerkin

### 4.1 Introduction

The first discontinuous Galerkin (DG) method was introduced in 1973 by Reed and Hill [32] in the framework of neutron mass transport, i.e. for hyperbolic equations. Since then DG finite element methods have been developed for a wide range of models and applications. In our model besides hyperbolic terms also elliptic terms appear. The DG method has been developed for purely elliptic problems by Bassi and Rebay [3]. In this report we will follow the approach of Arnold et al. [1] to compute the elliptic terms that appear in the Klopman model. We will use the method of Brezzi et al. which is a local, consistent and conservative method [2]. The discontinuous Galerkin method is particularly useful when hydraulic jumps occur.

The basic idea of the Galerkin method is to multiply the system of partial differential equations by arbitrary test functions. In Discontinuous Galerkin methods we perform a partial integration over each element resulting in a weak formulation. When we discretize the weak formulation the discontinuous Galerkin methods specifically uses a numerical flux at the boundaries of the element that concerns the two neighboring elements. The discontinuity may occur at the element boundaries. The advantage of this method that we can refine  $hp$  locally, which means that we may refine the element size  $h$  of one element or that we may adjust the order of our polynomial expansion  $p$  in an element [38].

In subsection 4.2 we will first introduce the discretization that we will use and we introduce some conventional notations and properties, such as the average  $\{\!\{ \cdot \}\!\}$  and jump  $[\![ \cdot ]\!]$  at a face  $S$  and the global and local lifting operators  $R$  and  $R_s$ .

The DG method is illustrated for the linear shallow water model<sup>9</sup> in subsection 4.3. It is shown how we can design the relations defining the numerical fluxes when energy is conserved, as is the case in our variational models. These fluxes affect the stability and the accuracy of the method. We will follow the approach of Yan and Shu (2002) [38] for KdV type equations to derive conditions for the numerical fluxes.

In subsection 4.4 three basic properties of fluxes are formulated, namely consistency, conservation and stability in time. Furthermore the Rankine-Hugoniot relation is formulated with which we can calculate the propagation speed of the local discontinuity.

Thereafter we present two choices for the fluxes, namely an alternating flux and the simple Lax-Friedrich flux [22].

In subsection 4.5 we illustrate the local discontinuous Galerkin method to compute the elliptic terms on a Poisson equation. In subsection 4.6 we apply the local discontinuous Galerkin method to the linearized equations that were derived from the Klopman variational model. It is in these equations that the elliptic terms appear. It is discussed why the formulation of the primal form as proposed by [38] was not followed and where discrepancies are with Eskillson's work [12, 13].

### 4.2 Finite element discretization

In this section first the finite element discretization is introduced that we will use in the DG method. Second we discretize the trial functions which enables us to solve the system numerically. Third the jump and average over a face are defined and some algebraic properties are given. Fourth the global and local lifting operator are defined, which we will use to solve our elliptic terms.

---

<sup>9</sup>The lsw is a system of hyperbolic equations when written in  $[h, u]$

### 4.2.1 Tesselation of the horizontal domain

The spatial discontinuity in the DG method requires that we discretize the horizontal domain slightly different than in the continuous Galerkin case. Again we partition the horizontal domain  $D_h$  with elements to approximate the solution. We introduce the partitioning  $T_h$  existing of  $N$  open elements  $K_j = \{x | x \in (x_{j-\frac{1}{2}}, x_{j+\frac{1}{2}})\}$  where  $x_{j-\frac{1}{2}}$  and  $x_{j+\frac{1}{2}}$  are the so-called nodes. The result is a tessellation

$$T_h = \{K_j | \cup_{j=1}^N \bar{K}_j = \bar{D}_h \text{ and } K_i \cap K_j = \emptyset \text{ if } i \neq j, 1 \leq i, j \leq N\}. \quad (4.1)$$

with  $\bar{K}_j$  the closure of element  $K_j$ . The discontinuity may occur at the internal faces  $x_{j-\frac{1}{2}}$  and  $x_{j+\frac{1}{2}}$  of element  $K_j$ . Values of  $u$  left and right of face  $x_{j-\frac{1}{2}}$  are therefore denoted by respectively

$$u_{j-\frac{1}{2}}^- := \lim_{x \uparrow x_{j-\frac{1}{2}}} u(x, t) \quad \text{and} \quad u_{j-\frac{1}{2}}^+ := \lim_{x \downarrow x_{j-\frac{1}{2}}} u(x, t) \quad (4.2)$$

as illustrated in figure 4.2.1

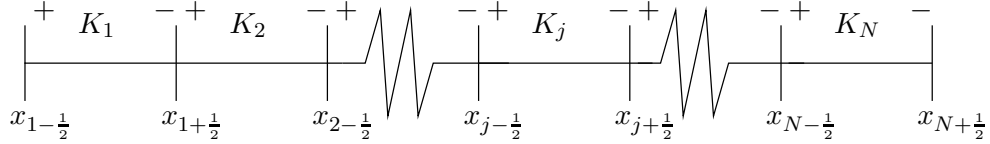


Figure 4.2.1: Spatial discretization of the horizontal domain  $D_h$  for the discontinuous Galerkin finite element method.

### 4.2.2 Discretization

To reduce the partial differential equations of our model explicitly to ordinary differential equations, we choose a finite number of polynomials to expand the variables in each element  $K_j$ . We hereby obtain the so-called trial functions  $u_h(x, t)$  and  $v_h(x, t)$  for the solution  $u(x, t)$  and for test function  $v(x, t)$ , respectively:

$$u_h(x, t) = \sum_{m=0}^{d_P} U_m(x_j, t) \Theta_m(x), \quad w_h(x, t) = \sum_{m=0}^{d_P} W_m(x_j, t) \Theta_m(x), \quad (4.3)$$

with polynomial basis functions  $\theta_m(x) \in P^{d_P}(K_k)$  in which  $P^{d_P}(K_j)$  denotes the space of polynomials in  $K_j$  of degree  $d_P$  and  $u_h, w_h \in V_h$ , with  $V_h = \{v | v|_{K_j} \in P^{d_P}(K_j), k = 1, \dots, N\}$ . The so-called global basis functions  $\Theta_m$  are defined on element  $K_j$  by:

$$\Theta_{m,j}(x) = \begin{cases} 1 & \text{if } m = 0 \\ \theta_{m,j}(x) - \frac{1}{|K_j|} \int_{K_j} \theta_{m,j}(x) dx & \text{if } m > 0. \end{cases} \quad (4.4)$$

with compact support (equal to zero outside the element) and  $\theta_m = \zeta^m$  on the local reference element  $\zeta \in [-1, 1]$ . With a mapping  $x = F_j(\zeta) \in [x_{j-\frac{1}{2}}, x_{j+\frac{1}{2}}]$  with degree  $d_p = 1$  we map from the reference element to the partitioning

$$F_j(\zeta) = \frac{1-\zeta}{2} x_{j-\frac{1}{2}} + \frac{1+\zeta}{2} x_{j+\frac{1}{2}} \quad (4.5)$$

and vice versa from the partitioning to the reference element with its inverse  $F^{-1}(x)$ . Integrals over an element can now be computed with a two-point Gaussian quadrature rule which is

exact for polynomials of degree 1 [28]. An integral over an element can be computed as follows for a smooth function  $g(x) \in V_h$

$$\int_{x_j - \frac{1}{2}}^{x_{j+\frac{1}{2}}} g(x) dx = \frac{|K_j|}{2} \int_{-1}^1 g(F_j(\zeta)) d\zeta = \frac{|K_j|}{2} \left( g(F_j(\frac{-1}{\sqrt{3}})) + g(F_j(\frac{1}{\sqrt{3}})) \right). \quad (4.6)$$

### 4.2.3 Jump and average on a face

The union of the internal faces is denoted by  $\Gamma_i$  and the boundary faces are united in the set  $\Gamma_b$ . All the boundaries are represented by  $\Gamma = \Gamma_i \cup \Gamma_b$ . At an internal face  $S$  we define the jump  $[[\cdot]]$  and the average  $\{\{\cdot\}\}$

$$[[v]] = v^- n^- + v^+ n^+ \quad \text{for } S \in \Gamma_i \quad (4.7a)$$

$$\{\{v\}\} = \frac{1}{2}(v^- + v^+) \quad \text{for } S \in \Gamma_i. \quad (4.7b)$$

with  $n^-$  and  $n^+$  the outward normal with respect to the left and right element of face  $S$ . At  $S \in \Gamma_b$  the jump is  $v^+ n^+$  or  $v^- n^-$  and the average equals the internal value  $v^+$  at the left boundary or  $v^-$  at the right boundary of the domain. Note that in the 1D case  $n^- = -1$  and  $n^+ = +1$ .

We state some algebraic properties that we will use in the following subsections. For  $v_i^-, w_i^-$  at the left and  $v_i^+, w_i^+$  at the right of face  $S_i$  we have that

$$v^-(w^- n^-) + v^+(w^+ n^+) = \{\{v\}\}[[w]] + [[v]]\{\{w\}\} \quad \text{at } S \in \Gamma_i \quad (4.8)$$

and at the left or right boundary, we have that

$$v^\pm(w^\pm n) = \{\{v\}\}[[w]] = [[v]]\{\{w\}\} \quad \text{at } S \in \Gamma_b. \quad (4.9)$$

with  $n$  the outward unit normal. Observe that the following relations hold for the jump average

$$\begin{aligned} \{\{v+w\}\} &= \{\{v\}\} + \{\{w\}\}, & [[v+w]] &= [[v]] + [[w]], \\ \{\{\{v\}\}\} &= \{\{v\}\} & \text{and } [[\{\{v\}\}]] &= 0. \end{aligned} \quad (4.10)$$

### 4.2.4 Lifting operator

To deal with elliptic terms in our systems first the global and local lifting operators are defined [3] in this subsection. Then they are discretized and rewritten as a linear system [34]. The global lifting operator  $\mathcal{R}(p)$  is defined with an arbitrary test function  $v \in \mathcal{T}_h$  as follows:

$$\int_{D_h} v \mathcal{R}(p) dx := \int_{\Gamma} \{\{v\}\} p ds. \quad (4.11)$$

The local lifting operator at face  $S$  is  $\mathcal{R}_s(p)$ . It has compact support outside the elements  $K_j, K_{j+1}$  adjacent to the face  $S = x_{j+\frac{1}{2}} = \bar{K}_j \cap \bar{K}_{j+1}$  is defined as:

$$\int_{D_h} v \mathcal{R}_s(p) dx := \int_S \{\{v\}\} p ds. \quad (4.12)$$

The local lifting operator  $\mathcal{R}_s(p)$  is related to the global lifting operator  $\mathcal{R}(p)$  by:

$$\mathcal{R}(p) = \sum_{S \in \Gamma} \mathcal{R}_s(p). \quad (4.13)$$

We discretize the local lifting operator  $\mathcal{R}_s(p)$  at face  $s$  left or right of element  $K_j$ , by expansion in polynomials of degree  $d_p$  as [34]

$$(\mathcal{R}_s(p))_j = \sum_{i=0}^{d_p} R_i^{s,j} \Theta_i(x) \text{ for } x \in K_j \quad (4.14)$$

in order to solve elliptic terms numerically. Likewise the expansions of our test-function  $v_h(x)$  and trial function  $\psi_h(x)$  read

$$v_h(x) = \sum_{l=0}^{d_p} V_{j,l} \Theta_l(x) \quad \text{and} \quad \psi_h(x) = \sum_{i=0}^{d_p} \Psi_{j,i} \Theta_i(x) \text{ for } x \in K_j. \quad (4.15)$$

We substitute these expansions in the definition for the local lifting operator (4.12) and for a face  $S$  of element  $K_j$

$$\sum_{i=0}^{d_p} R_l^{s_r,j} \left( \int_{K_j} \Theta_l \Theta_i \, dx \right) = \sum_{i=0}^{d_p} \left( \frac{1}{2} \Psi_{k,i} \int_S \Theta_i^- \Theta_l \, ds + \int_S \Theta_i^+ \Theta_l \, ds \right) \text{ for } l = 0, \dots, d_p \quad (4.16)$$

where  $\Theta_i^-$  and  $\Theta_i^+$  represent value at the left and at the right element of face  $S$ , respectively. For convenience we define a matrix  $A^j \in \mathbb{R}^{(d_p+1) \times (d_p+1)}$  at element  $K_j$  and the matrix  $P^{s,j} \in \mathbb{R}^{(d_p+1) \times 2}$  at face  $S$  adjacent to elements  $K_j$  and  $K_{j+1}$  as

$$A_{li}^j = \int_{K_j} \Theta_l \Theta_i \, dx \quad \text{and} \quad P^{s_R,j}(\Psi_{j,i}, \Psi_{j+1,i})_{li} = \frac{1}{2} \Psi_{k,i} \int_{S_r} \Theta_l \Theta_i \, ds. \quad (4.17)$$

Now we can collect the integrals over the elements and over the faces to obtain the following linear system [34]

$$A^j R^{s_R,j} = P^{s_R,j}(\Psi_j, \Psi_{j+1}). \quad (4.18)$$

Similarly, we have on the left face of element  $K_j$ :

$$A^j R^{s_L,j} = P^{s_L,j}(\Psi_{j-1}, \Psi_j) \quad (4.19)$$

Note that, since the basis functions  $\Theta_i$  are orthogonal, automatically yields  $A^j$  is invertible. Finally the lifting operator coefficients  $R^{s,j}$  are found for a left or right face  $s = \{S_L, S_R\}$  by inversion of  $A^j$  and the expansion of the trial function for the local lifting operator now reads

$$(\mathcal{R}_s)_j = \sum_{i=0}^{d_p} R_i^{s,j} \Theta_i = \sum_{i=0}^{d_p} (A^j)^{-1} P^{s,j} \Theta_i \quad (4.20)$$

for face  $S$  left or right of element  $K_j$ .

### 4.3 Linear shallow water system

In this subsection we apply the discontinuous Galerkin method on the linear shallow water equations over a flat seabed and illustrate how our numerical fluxes can be chosen such that energy is conserved. First we start with our system of equations, which are

$$\partial_t h + h_0 \partial_x u = 0 \quad (4.21a)$$

$$\partial_t u + g \partial_x h = 0. \quad (4.21b)$$

We multiply with arbitrary test functions  $v(x), w(x) \in C^\infty(K_j)$  on a certain element  $K_j$  and integrate by parts over each element  $K_j \in \mathcal{T}_h$ . For convenience, we write  $v_x = \frac{dv}{dx}$  for the first order spatial derivative with respect to its only argument. At each element we have

$$\int_{K_j} v \partial_t h - v_x h_0 u \, dx + v h_0 u|_{x_{j+\frac{1}{2}}}^- - v h_0 u|_{x_{j-\frac{1}{2}}}^+ \quad (4.22a)$$

$$\int_{K_j} w \partial_t u - w_x g \partial_x h \, dx + w g h|_{x_{j+\frac{1}{2}}}^- - w g h|_{x_{j-\frac{1}{2}}}^+ \quad (4.22b)$$

where we have taken the internal element values at each face as in (4.2). Since the system  $[h, u]$  can be discontinuous at a face the limit solutions of  $h$  and  $u$  may not exist at the element boundaries  $\partial K_j = S \in \Gamma$ . Instead, we introduce the numerical fluxes  $\hat{h}_i = \hat{h}(h_i^-, h_i^+)$  and  $\hat{u}_i = \hat{u}(u_i^-, u_i^+)$  for all faces  $S_i \in \Gamma$ . Summation over all elements  $K_j$  results in the discontinuous Galerkin weak formulation over the whole tessellation  $\mathcal{T}_h$ .

$$\sum_{j=1}^N \left\{ \int_{K_j} v \partial_t h - v_x h_0 u \, dx + v_{j+\frac{1}{2}}^- h_0 \hat{u}_{j+\frac{1}{2}} - v_{j-\frac{1}{2}}^+ h_0 \hat{u}_{j-\frac{1}{2}} \right\} = 0 \quad (4.23a)$$

$$\sum_{j=1}^N \left\{ \int_{K_j} w \partial_t u - w_x g \partial_x h \, dx + w_{j+\frac{1}{2}}^- g \hat{h}_{j+\frac{1}{2}} - w_{j-\frac{1}{2}}^+ g \hat{h}_{j-\frac{1}{2}} \right\} = 0. \quad (4.23b)$$

Now we will derive conditions for the fluxes that we introduced. Remember that we have an energy conserving system and at a certain horizontal domain  $D_h$  we have  $\partial_t \mathcal{H} = 0$ . We manipulate the system such that we end up with an alternative expression for energy conservation. By addition of (4.23a) and (4.23b) we obtain the following bilinear form:

$$\begin{aligned} \sum_{j=1}^N \{B_j(h, u; v, w)\} &= \sum_{j=1}^N \left\{ \int_{K_j} v \partial_t h - h_0 v_x u \, dx + h_0 \hat{u}_{j+\frac{1}{2}} v_{j+\frac{1}{2}}^- - h_0 \hat{u}_{j-\frac{1}{2}} v_{j-\frac{1}{2}}^+ \right. \\ &\quad \left. + \int_{K_j} w \partial_t u - g \partial_x h w \, dx + g \hat{h}_{j+\frac{1}{2}} w_{j+\frac{1}{2}}^- - g \hat{h}_{j-\frac{1}{2}} w_{j-\frac{1}{2}}^+ \right\}, \end{aligned} \quad (4.24)$$

which is equal to zero for all  $v, w \in C^\infty(K_j)$ , since the solutions  $h$  and  $u$  of the bilinear form also satisfy the system (4.23). We then take<sup>10</sup>

$$v(x) = gh(x, t) \quad \text{and} \quad w(x) = h_0 u(x, t) \quad (4.25)$$

at a certain time  $t$ . Using  $-\int h \partial_x u + u \partial_x h \, dx = -uh|_{j+\frac{1}{2}}^- + uh|_{j-\frac{1}{2}}^+$  we obtain the following relation on element  $K_j$

$$B_j(h, u; gh, h_0 u) = \frac{d}{dt} \int_{K_j} \frac{1}{2} h_0 u^2 + \frac{1}{2} g h^2 \, dx + \hat{H}_{j+\frac{1}{2}} - \hat{H}_{j-\frac{1}{2}} + \hat{\Theta}_{j-\frac{1}{2}} \quad (4.26)$$

with

$$\hat{H}_i = -F(x_i^-) + gh_0 \hat{u}_i h_i^- + gh_0 \hat{h}_i u_i^- \quad (4.27)$$

and

$$\hat{\Theta}_i = [F(x_i)] - 2gh_0 \hat{u}_i \{h\}_i - 2gh_0 \hat{h}_i \{u\}_i \quad (4.28)$$

where

$$F(x_i^\pm) = gh_0 [hu]_{x=x_i^\pm}. \quad (4.29)$$

<sup>10</sup>Yan and Shu (2002) proposed this procedure for the KdV equations where cell entropy is conserved [38].

Say  $\mathcal{T}_h$  is a periodic domain. We may sum  $B_j$  over all elements  $K_j \in \mathcal{T}_h$  and it is still equal to zero. Remember that we have energy conservation and that we have  $\partial_t \mathcal{H} = 0$  or

$$\partial_t \mathcal{H} = \partial_t \int_{D_h} \frac{1}{2} h_0 u^2 + \frac{1}{2} g h^2 \, dx = 0. \quad (4.30)$$

Summing  $B_j(h, u; gh, h_0 u)$  over the periodic domain cancels the  $\hat{H}_i$ -terms, since they were constructed such that alternately a contribution of one element is canceled by a contribution of another element.

$$\sum_{j=1}^N B_j = \frac{d}{dt} \int_{D_h} \frac{1}{2} h_0 u^2 + \frac{1}{2} g h^2 \, dx + \sum_{j=1}^N \hat{\Theta}_{j-\frac{1}{2}} = 0 \quad (4.31)$$

Then we substitute  $\partial_t \mathcal{H} = 0$  and we observe that only  $\hat{\Theta}_i$ -terms remain. Thus for all faces holds

$$\begin{aligned} \hat{\Theta}_i &= g h_0 \{ \llbracket h_i u_i \rrbracket - 2 \hat{u}_i \{ \{ h_i \} \} - 2 \hat{h} \{ \{ u_i \} \} \} = 0 \Leftrightarrow \\ g h_0 \{ h^- u^- - h^+ u^+ - \hat{u} (h^- + h^+) - \hat{h} (u^- + u^+) \} &= 0 \quad \text{at face } x_i. \end{aligned} \quad (4.32)$$

What is left is to choose proper fluxes for  $\hat{u}_i$  and  $\hat{h}_i$  such that this equality holds (besides consistency and conservation, see the following subsection). The non-linear shallow water equations are formulated in discretized in appendix A.

#### 4.4 Numerical Fluxes

Numerical fluxes are used for inter-cell communication. At a face the solution of a system can be discontinuous. The basic idea of a numerical flux is to treat these values as a local Riemann problem and solve it numerically. The local Riemann problem can be solved analytically, but it can be quite expensive in terms of computational effort [4]. So we should use an approximate Riemann solver, eg. HLL or HLLc, to simulate the propagation of the discontinuous jump. First we will state three requirements that should be satisfied by our numerical fluxes and then two examples are presented, namely an alternating flux and the Lax-Friedrich flux [38]. We require that a numerical flux  $\hat{f}(u^-, u^+)$  is consistent, i.e.

$$\hat{f}(u, u) = f(u). \quad (4.33)$$

Furthermore we require that the flux is locally conservative, i.e.

$$\hat{f}(u^+, u^-) + \hat{f}(u^-, u^+) = 0. \quad (4.34)$$

Finally we require that energy is conserved as illustrated in subsection 4.3, which leads to  $L^2$  stability in time

$$B(h, u; v, w) - \partial_t \mathcal{H} = 0 \quad (4.35)$$

for an appropriate  $v, w \in H^1(D_h)$ .

In literature several numerical fluxes are proposed satisfying the three requirements stated above. Whether to choose the right or the left value at a face depends mainly on the propagation speed  $s$  of the solution of the local Riemann problem. We have  $s = dx/dt$  and it can be found by the Rankine-Hugoniot relation [5]

$$0 = \lim_{\epsilon \downarrow 0} \int_{x-\epsilon}^{x+\epsilon} \partial_t \mathbf{u} + \partial_x \mathbf{f}(\mathbf{u}) \, dx = -s \llbracket \mathbf{u} \rrbracket + \mathbf{f}(\{ \mathbf{u} \}), \quad (4.36)$$

where  $\mathbf{u} = [h, u]^T$  and  $\mathbf{f}(\mathbf{u}) = [h_0 u, gh]$  in the linear shallow water case.

For a system with two equations such as (4.23) in the shallow water case, we may choose an alternating flux. For the shallow water case it is sufficient to evaluate  $f(u)$  for the first equation at the left of a face and for the second equation at the right of a face (or vice versa). This choice satisfies the above requirements for linear systems.

Another simple flux is the Lax-Friedrich flux. It satisfies above requirements, but is found to be quite dissipative [38]. It reads

$$f(u^-, u^+) = \{ \{ f(u) \} \} - \frac{1}{2} \alpha \llbracket u \rrbracket, \quad \alpha = \max_u |\partial_u f(u)|, \quad (4.37)$$

where the maximum is taken over a relevant  $u$ , which in practice is the maximum is taken over the elements sharing the respective face. Note that the value of the flux on a boundary face  $S \in \Gamma_d$  is attained by evaluation of the internal boundary value with the respective normal direction.

## 4.5 Elliptic equations

We follow the approach of Arnold et al.[1] to apply the method of Brezzi et al.[2] to the elliptic terms that appear in the Euler-Lagrange equations of the Klopman model [19]. For convenience we consider the Poisson equation:

$$f - \partial_x^2 \psi = 0 \quad (4.38)$$

to illustrate the method, with  $f \in L^2(\Omega)$ . We introduce an auxiliary variable  $\sigma = \partial_x \psi$  and we rewrite the equation to a system of first order equations:

$$f - \partial_x \sigma = 0, \quad (4.39a)$$

$$\sigma - \partial_x \psi = 0. \quad (4.39b)$$

We may now formulate a weak formulation over a subset  $K \in D_h$  by multiplying by test function  $w \in C^\infty(K)$ . From now on  $\sigma$  and  $\psi$  represent the trial functions for the solutions  $\sigma$  and  $\psi$  respectively. For equation (4.39b) we obtain after partial integration twice (forwards and backwards) in space

$$\int_K w \sigma \, dx = \int_K w \partial_x \psi \, dx \quad (4.40a)$$

$$= - \int_K w_x \psi \, dx + \int_{\partial K} w \hat{\psi} n \, ds \quad (4.40b)$$

$$= \int_K w \partial_x \psi \, dx + \int_{\partial K} w (\hat{\psi} - \psi) n \, ds, \quad (4.40c)$$

with  $n$  the outward normal vector to  $\partial K$ . Note that when we integrate by parts with respect to  $\psi$  we have to introduce the numerical flux  $\hat{\psi}$  since  $\psi$  can be discontinuous at the faces, provided that the face is an internal face. For convenience we choose the consistent flux  $\hat{\psi} = \{ \{ \psi \} \}$ . The test functions are still arbitrary. Summation over all elements  $K_j \in \mathcal{T}_h$  gives the weak formulation

$$\int_{D_h} w \sigma \, dx = \int_{D_h} w \partial_x \psi \, dx + \sum_{j=1}^N \int_{\partial K_j} w (\hat{\psi} - \psi) n \, ds. \quad (4.41)$$

We transform this weak form using algebraic property (4.8) into:

$$\int_{D_h} w \sigma \, dx = \int_{D_h} w \partial_x \psi \, dx - \int_{\Gamma} \{ \{ w \} \} \llbracket \psi \rrbracket \, ds + \int_{\Gamma_i} \llbracket w \rrbracket \{ \{ \hat{\psi} - \psi \} \} \, ds. \quad (4.42)$$

Since the numerical flux  $\hat{\psi}$  is consistent at the internal faces  $\Gamma_i$  we have the relation  $\{\{\hat{\psi} - \psi\}\} = 0$ . We now rewrite  $\sigma$  by means of the global lifting operator (4.11) to

$$\int_{D_h} w \sigma \, dx = \int_{D_h} w \partial_x \psi - w \mathcal{R}([\psi]) \, dx \quad (4.43)$$

and we obtain:

$$\sigma = \partial_x \psi - \mathcal{R}([\psi]). \quad (4.44)$$

Similarly we obtain a weak formulation for the first equation (4.39a) of our system by multiplying with a test function  $v \in C^\infty(K)$ . We introduce the numerical flux  $\hat{\sigma}$  and sum over all elements. After application of (4.8) we have:

$$\int_{D_h} v f + v_x \sigma \, dx = \int_{\Gamma} \{\{v\}\} [\hat{\sigma}] \, ds + \int_{\Gamma_i} [v] \{\{\hat{\sigma}\}\} \, ds. \quad (4.45)$$

Substitution of equation (4.44) in: (4.45) for our auxiliary variable  $\sigma$  results in

$$\int_{D_h} v f + v_x (\partial_x \psi - \mathcal{R}([\hat{\psi} - \psi])) \, dx = \int_{\Gamma} \{\{v\}\} [\hat{\sigma}] \, ds + \int_{\Gamma_i} [v] \{\{\hat{\sigma}\}\} \, ds \quad (4.46)$$

and we obtain, after using the relation (4.13) for the local lifting operator, the primal formulation [1]:

$$\int_{D_h} v f + v_x \partial_x \psi \, dx - \sum_{S \in \Gamma} \int_{D_h} v_x \mathcal{R}_s([\psi]) \, dx = \int_{\Gamma} \{\{v\}\} [\hat{\sigma}] \, ds + \int_{\Gamma_i} [v] \{\{\hat{\sigma}\}\} \, ds. \quad (4.47)$$

We choose the stable and consistent numerical flux proposed by Brezzi et al.[2] such that  $[\hat{\sigma}] = 0$

$$\hat{\sigma} = \{\{\partial_x \psi - \eta^e \mathcal{R}_s([\psi])\}\} \quad (4.48)$$

where the global lifting operator  $\mathcal{R}$  was approximated by the local lifting operator  $\mathcal{R}_s$  and  $\eta^e$  should be strictly larger than the number of faces per element.

## 4.6 Linearized Klopman model

In this subsection we will first derive a weak formulation for the linearized Klopman model. In subsection 4.6.1 we will discuss why we need a primal formulation to solve the system. Thereafter the primal formulation is presented, where the approach of Arnold et al.[1] is followed. The linearized Euler-Lagrange equations of the Klopman variational model were derived in section 2.3 and read:

$$\partial_t h + h_0 \partial_x u - \frac{2}{3} h_0^3 \partial_x^2 \psi = 0, \quad (4.49a)$$

$$\partial_t u + g \partial_x (h - h_0) = 0, \quad (4.49b)$$

$$\frac{4}{3} h_0^3 \psi + \frac{2}{3} h_0^3 \partial_x u - \frac{8}{15} h_0^5 \partial_x^2 \psi = 0. \quad (4.49c)$$

For the elliptical terms  $\partial_x^2 \psi$  we introduce the auxiliary variable  $\sigma = \partial_x \psi$  and we follow the approach of Arnold et al.[1] as described in the previous subsection. We multiply with arbitrary test functions  $v(x), w(x), \varsigma(x) \in C^\infty(K_j)$ . The weak formulation at each element  $K_j$ , after simplification, reads:

$$\int_{K_j} v \partial_t h - h_0 v_x u + \frac{2}{3} h_0^3 v_x \sigma \, dx + \int_{\partial K_j} (h_0 v \hat{u} - \frac{2}{3} h_0^3 v \hat{\sigma}) n \, ds = 0, \quad (4.50a)$$

$$\int_{K_j} w \partial_t u - g w_x (h - h_0) \, dx + \int_{\partial K_j} g w (\hat{h} - h_0) n \, ds = 0, \quad (4.50b)$$

$$\int_{K_j} 2\varsigma \psi - \varsigma_x u + \frac{4}{5} h_0^2 \varsigma_x \sigma \, dx + \int_{\partial K_j} (\varsigma \hat{u} - \frac{4}{5} h_0^2 \varsigma \hat{\sigma}) n \, ds = 0. \quad (4.50c)$$

and summation over all elements of  $\mathcal{T}_h$  gives us the weak formulation of the whole system. Note that to solve our system we would need an extra equation  $\sigma = \partial_x \psi$ . However this would yield solving the system globally as we will discuss in next subsection. A LDG approach is proposed by Cockburn and Shu [10], which eliminates  $\sigma$  locally. A more easy approach is eliminating the auxiliary variable globally following the Arnold et al. approach as sketched in the previous subsection on elliptic terms.

#### 4.6.1 Primal formulation

To solve system (4.50) numerically at a certain time step  $t^{n+1}$  we have data available from the previous time step  $t^n$  and information on how  $h$  and  $u$  progress in time, namely according to a first order time-derivative. We can observe that to solve the system per element at a time step  $t^{n+1}$  we also need information of how  $\psi$  evolves in time at every element to obtain  $\psi$  at  $t^{n+1}$ . This is not expressed explicitly so we have to obtain this information from our third equation (4.49c) with the  $u$  at the new time step  $t^{n+1}$ . This quantity is known from the second equation (4.49b), but  $\partial_x^2 \psi$  and  $\psi$  are still unknown. Solving this elliptic equation can be done with a continuous Galerkin method as Eskilsson & Sherwin [12] do for a Boussinesq-type equation or with a local Discontinuous Galerkin method as proposed by Cockburn and Shu [10]. The approach of Cockburn and Shu is similar to the approach of Brezzi [1], but with a much more complex formulation for the auxiliary variable. Therefore the more simple approach of Brezzi et al. [2] is used, which can be replaced by a purely local DG method. The approach of Brezzi et al. is able to approximate the propagation of discontinuities in time, where the continuous Galerkin method is not.

We will now derive the primal formulation for the linearized Klopman Variational Boussinesq equations. As seen in section 4.5 we could substitute our auxiliary variable  $\sigma$ :

$$\sigma = \partial_x \psi - \mathcal{R}(\llbracket \psi \rrbracket) \quad (4.51)$$

and its flux  $\hat{\sigma}$

$$\hat{\sigma} = \llbracket \sigma - \eta^e \mathcal{R}_s(\llbracket \psi \rrbracket) \rrbracket = \llbracket \partial_x \psi - \eta^e \mathcal{R}_s(\llbracket \psi \rrbracket) \rrbracket \quad (4.52)$$

in the weak formulation (4.50). As a result we have a primal formulation which we can solve at a certain timestep  $t^{n+1}$  with the values of  $h, u, \psi$  and  $\partial_x \psi$  known at time-step  $t^n$ . It reads

$$\begin{aligned} \int_{K_j} v \partial_t h - h_0 v_x u + \frac{2}{3} h_0^3 v_x (\partial_x \psi - \mathcal{R}(\llbracket \psi \rrbracket)) \, dx \\ + \int_{\partial K_j} (h_0 v \hat{u} - \frac{2}{3} h_0^3 v \llbracket \partial_x \psi - \eta^e \mathcal{R}_s(\llbracket \psi \rrbracket) \rrbracket) n \, ds = 0, \end{aligned} \quad (4.53a)$$

$$\int_{K_j} w \partial_t u - g w_x (h - h_0) \, dx + \int_{\partial K_j} g w (\hat{h} - h_0) n \, ds = 0, \quad (4.53b)$$

$$\begin{aligned} \int_{K_j} 2\varsigma \psi - \varsigma_x u + \frac{4}{5} h_0^2 \varsigma_x (\partial_x \psi - \mathcal{R}(\llbracket \psi \rrbracket)) \, dx \\ + \int_{\partial K_j} (\varsigma \hat{u} - \frac{4}{5} h_0^2 \varsigma \llbracket \partial_x \psi - \eta^e \mathcal{R}_s(\llbracket \psi \rrbracket) \rrbracket) n \, ds = 0 \end{aligned} \quad (4.53c)$$

and after application of the definition of the global lifting operator (4.11) we have

$$\int_{K_j} v \partial_t h - h_0 v_x u + \frac{2}{3} h_0^3 v_x \partial_x \psi \, dx + \int_{\partial K_j} h_0 v \hat{u} n - \frac{2}{3} h_0^3 \llbracket v_x \rrbracket \llbracket \psi \rrbracket$$

$$-\frac{2}{3}h_0^3 v \{ \{ \partial_x \psi - \eta^e \mathcal{R}_s(\llbracket \psi \rrbracket) \} \} n \, ds = 0, \quad (4.54a)$$

$$\int_{K_j} w \partial_t u - g w_x (h + h_b) \, dx + \int_{\partial K_j} g w (\hat{h} - h_0) n \, ds = 0, \quad (4.54b)$$

$$\int_{K_j} 2\varsigma \psi - \varsigma_x u + \frac{4}{5} h_0^2 \varsigma_x \partial_x \psi \, dx + \int_{\partial K_j} \varsigma \hat{u} n - \frac{4}{5} h_0^2 \{ \{ \varsigma_x \} \} \llbracket \psi \rrbracket - \frac{4}{5} h_0^2 \varsigma \{ \{ \partial_x \psi - \eta^e \mathcal{R}_s(\llbracket \psi \rrbracket) \} \} n \, ds = 0, \quad (4.54c)$$

where we used that  $\llbracket \hat{\psi} \rrbracket = 0$ . Summation over all elements gives us the desired discretization. Note that, when we assume that vertical velocity profile of the fluid, governed by the term  $\psi$ , is equal everywhere, we re-obtain our linearized shallow water system that we considered in subsection 4.3.

#### 4.6.2 DG discretization on the Klopman model

To solve the primal formulation numerically we use the tessellation proposed in subsection 4.2.1. We discretize the trial- and test-functions as proposed in subsection 4.2.2 and we expand our functions as in equation (4.3) with polynomials of degree  $d_P$ . We obtain the following expansions for the trial and test functions

$$\begin{aligned} h_h(x, t) &= \sum_{i=0}^{d_p} H_{j,i}(t) \Theta_i(x), & v_h(x) &= \sum_{i=0}^{d_p} V_{j,i} \Theta_i(x), \\ u_h(x, t) &= \sum_{i=0}^{d_p} U_{j,i}(t) \Theta_i(x), & w_h(x) &= \sum_{i=0}^{d_p} W_{j,i} \Theta_i(x), \\ \psi_h(x, t) &= \sum_{i=0}^{d_p} \Psi_{j,i}(t) \Theta_i(x), & \varsigma_h(x) &= \sum_{i=0}^{d_p} Z_{j,i} \Theta_i(x) \end{aligned} \quad (4.55)$$

for  $x \in K_j$ . We discretize the lifting operator  $\mathcal{R}_s$  as in section 4.2.4, equation (4.20), with expansion coefficients  $(\mathcal{R}_s)_j$  with respect to element  $K_j$  and its faces  $S \in \partial K$

$$(\mathcal{R}_s)_j = \sum_{i=0}^{d_p} R_i^{s,j} \Theta_i = \sum_{i=0}^{d_p} (A^j)^{-1} P^{s,j} \Theta_i. \quad (4.56)$$

We substitute the expansions introduced above in equation (4.54) and we obtain

$$\begin{aligned} &\sum_{i=1}^{d_p} \sum_{l=1}^{d_p} \int_{K_j} V_{j,i} \Theta_i \frac{dH_{j,l}}{dt} \Theta_l - h_0 V_{j,i} \frac{d\Theta_l}{dx} U_{j,l} \Theta_l + \frac{2}{3} h_0^3 V_{j,i} \frac{d\Theta_i}{dx} \frac{d\Theta_l}{dx} \Psi_{j,l} \, dx \\ &\quad + \int_{\partial K_j} h_0 V_{j,i} \Theta_i \left( \hat{u} - \frac{2}{3} h_0^2 \left( \{ \{ \Psi_l \frac{d\Theta_l}{dx} \} \} - \{ \{ \eta^e R_i^{s,j} \Theta_i \} \} \right) \right) n_j \\ &\quad + \frac{2}{3} h_0^2 \{ \{ V_{j,i} \frac{d\Theta_i}{dx} \} \} \llbracket \Psi_i \Theta_i \rrbracket \, ds = 0, \end{aligned} \quad (4.57a)$$

$$\begin{aligned} &\sum_{i=1}^{d_p} \sum_{l=1}^{d_p} \int_{K_j} W_{j,i} \Theta_i \frac{dU_{j,l}}{dt} \Theta_l - g W_{j,i} \frac{d\Theta_i}{dx} H_{j,l} \Theta_l \, dx \\ &\quad + \int_{\partial K_j} g W_{j,i} \Theta_i (\hat{h} - h_0(x_j)) n_j \, ds = 0, \end{aligned} \quad (4.57b)$$

$$\begin{aligned} &\sum_{i=1}^{d_p} \sum_{l=1}^{d_p} \int_{K_j} 2Z_{j,i} \Theta_i \Psi_{j,l} \Theta_l - Z_{j,i} \frac{d\Theta_l}{dx} U_{j,l} \Theta_l + \frac{4}{5} h_0^2 Z_{j,i} \frac{d\Theta_i}{dx} \frac{d\Theta_l}{dx} \Psi_{j,l} \, dx \\ &\quad + \int_{\partial K_j} Z_{j,i} \Theta_i \left( \hat{u} - \frac{4}{5} h_0^2 \left( \{ \{ \Psi_l \frac{d\Theta_l}{dx} \} \} - \{ \{ \eta^e R_i^{s,j} \Theta_i \} \} \right) \right) n_j \\ &\quad + \frac{4}{5} h_0^2 \{ \{ Z_{j,i} \frac{d\Theta_i}{dx} \} \} \llbracket \Psi_i \Theta_i \rrbracket \, ds = 0, \end{aligned} \quad (4.57c)$$

where  $s$  as superscript in  $R_i^{s,j}$  refers to the faces  $S_L$  and  $S_R$  of  $\partial K_j$ . Note that the average  $[\![\Psi_l \frac{d\Theta_l}{dx}]\!]_l$  and jump  $[\![\Psi_l \Theta_l]\!]_l$  are over the elements adjacent to the face. Using that the test functions are arbitrary on every element  $K_j \in \mathcal{T}_h$  we obtain a linear system and we may sum over all elements over our domain  $D_h$ . This system is written out further for polynomials of degree  $d_p = 1$  in appendix B.

### 4.6.3 Total energy

The total energy of the linearized system over a horizontal domain  $D_h$  is given by

$$\mathcal{H} = \int_{D_h} \frac{1}{2} h_0 \left[ u - \frac{2}{3} h_0^2 (\partial_x \psi) \right]^2 + \frac{2}{45} h_0^5 (\partial_x \psi)^2 + \frac{2}{3} h_0^3 \psi^2 + \frac{1}{2} g (h - h_0)^2 \, dx \quad (4.58)$$

$$(4.59)$$

which can be approximated on our tessellation  $\mathcal{T}_h$  with our polynomial expansion of degree  $d_p = 1$  by

$$\begin{aligned} \mathcal{H} = \sum_j^N \frac{K_j}{2} \int_{-1}^1 \frac{1}{2} h_0 (\bar{U}_j + \xi \hat{U}_j - \frac{2}{3} h_0^2 (\frac{2}{|K_j|} \hat{\Psi}_j)^2 + \frac{2}{45} h_0^5 (\frac{2}{|K_j|} \hat{\Psi}_j)^2 \\ + \frac{2}{3} h_0^3 (\bar{\Psi}_j + \xi \hat{\Psi}_j)^2 + \frac{1}{2} g (\bar{H}_j + \xi \hat{H}_j - \bar{H}_0)^2 \, d\xi. \end{aligned} \quad (4.60)$$

### 4.6.4 Choice of numerical flux for KVBM

Since we consider an energy conserving system, we do not adopt the Lax-Friedrich flux. We observe a linear system of equations and therefore we simply choose an alternating flux:

$$\hat{h}_i = H_L - \bar{H}_0 \text{ at face } S_i \quad (4.61)$$

$$\hat{u}_i = U_R \text{ at face } S_i \quad (4.62)$$

which could be interchanged by  $H_R - \bar{H}_0$ ,  $U_L$  respectively. Note that, to solve  $\Psi$  in the third equation of our system, we have to use the same choice for  $\hat{u}$  for consistency reasons, since  $u - \frac{3}{4} h_0^2 \partial_x \psi$  combine to the depth averaged fluid velocity, as stated in the conservation of mass equation (4.49b).

### 4.6.5 Time integration

To solve this system propagating in time we start with initial data at a certain time step  $t^n$ . With equation (4.57) and  $U^n$  known we can compute the values of  $\Psi^n$ . With the values  $H^n, U^n$  and  $\Psi^n$  we can compute (a,b) of (4.57) and obtain  $H^{n+1}, U^{n+1}$  using for example *RK3* or *RK4*, cf. §3.6. Then again with (4.57) we can compute the value of  $\Psi^{n+1}$  at time step  $t^{n+1}$ .

## 4.7 Conclusion

In this section a discontinuous Galerkin approach was proposed to solve the (non)linear shallow water equations numerically. An energy conservation restriction for the numerical flux was formulated.

The discontinuous Galerkin finite element method was then applied on the linear equations of the Klopman variational Boussinesq model. The system describing the KVBM has an elliptic equation in space, which is solved numerically using Brezzi's approach [2]. Since the  $\partial_x^2 \psi$ -term, which appears in the linear equations, appears in a similar way in the weakly nonlinear [19] and the fully nonlinear Klopman variational Boussinesq equations [20], the latter two models can be implemented fairly easily using the proposed discontinuous Galerkin

method. However, the choice of the flux should be considered in the nonlinear case. One might try the more complex HLLC flux for nonlinear shallow water systems [4], where the knowledge of the linear dispersion relation might be helpfully in the determination of the local wave speeds.

## 5 Verification

### 5.1 Introduction

In this section the verification of our numerical models is presented. We verify our numerical results against (semi-)analytical solutions.

Firstly we investigate our shallow water models. We consider wave propagation and energy conservation for linear and nonlinear shallow water waves, simulated numerically with the continuous (see sections 3.3.1 and 3.3.2) and discontinuous (section 4.3) Galerkin finite element methods. Then we verify the time integration methods that have been proposed in section 3.6. Numerical dissipation and a numerical phase shift are illustrated for periodic linear waves that are propagating for a very long time. Next, we investigate the breaking of periodic nonlinear shallow water waves propagating over a horizontal seabed.

Secondly, we will verify our results obtained with the continuous Galerkin (CG) finite element method for the nonlinear Whitham variational Boussinesq model (WVBM).

Thirdly, we will present the verification of the linear Klopman variational Boussinesq model (KVBM) propagating in time over a horizontal seabed. We will verify the results computed by the DG method with the analytical solution. Then we compare the results computed with the CG FEM for the weakly nonlinear model against linear solutions for small amplitude waves.

### 5.2 Shallow water equations

In this section we will verify the numerical implementation of our shallow water models over a horizontal seabed with still water depth  $h_0$ . First the linear shallow water model is implemented to investigate the time integration methods for the continuous Galerkin finite element methods. Then we present the verification for the nonlinear shallow water model, numerically implemented with the continuous and discontinuous Galerkin FEM.

For shallow water we have the energy density  $\mathcal{H}$  given by

$$\mathcal{H} = \int_{D-H} \frac{1}{2} h (\partial_x \phi)^2 + \frac{1}{2} g (h - h_0)^2 \, dx, \quad (5.1)$$

which results, as the basis of our variational principle, in the following Euler-Lagrange equations

$$\partial_t h = -\partial_x [h \partial_x \phi], \quad \partial_t \phi = -g(h - h_0) - \frac{1}{2} (\partial_x \phi)^2, \quad (5.2)$$

or more conveniently for our DG FEM, after substitution of  $u \equiv \partial_x \phi$ ,

$$\partial_t h = -\partial_x [hu], \quad \partial_t u = -\partial_x [gh + \frac{1}{2} u^2]. \quad (5.3)$$

#### 5.2.1 Linear shallow water

We linearize (5.3) and we have:

$$\partial_t h = -h_0 \partial_x^2 \phi, \quad \partial_t \phi = -g(h - h_0). \quad (5.4)$$

As periodic analytical solutions we take

$$h(x, t) = a \cos(\kappa x - \omega t) + h_0, \quad \phi(x, t) = \frac{ag}{\omega} \cos(\kappa x - \omega t), \quad (5.5)$$

where  $a$  is the wave amplitude,  $\kappa$  the wave number and  $\omega = \sqrt{gh_0}$  is the (dispersionless) wave speed. The initial wave profile is plotted in figure 5.2.1

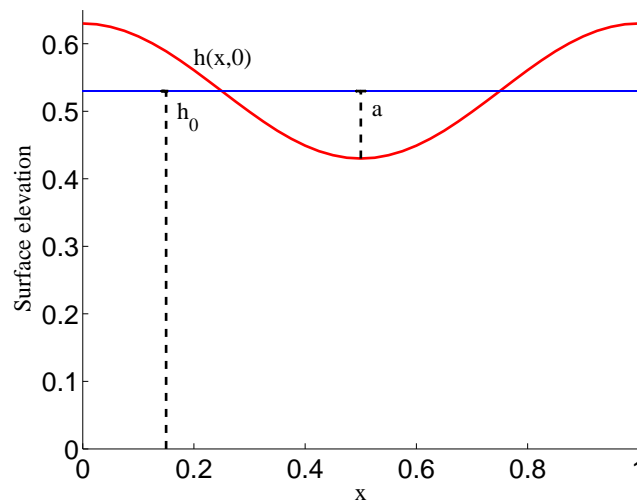


Figure 5.2.1: *Initial sinusoidal wave profile;  $a/h_0 = 0.19$ ;  $k_0 h_0 = 0.53\pi$ ; deep water.*

We now consider a linear wave solution, approximated numerically, which is propagating for a long time period over a horizontal seabed. In figure 5.2.2 we see the surface elevation after a large number of wave periods, i.e. 0, 50, 100, 150, 200 and 250 times wave period  $T = 2\pi/\omega$ . The non-dimensional value of the total energy computed analytically is  $2.1125 \cdot 10^{-3}$  per unit length and per unit mass (for non-dimensional values of  $g$ ,  $h_0$ ). Observe that the RK4 has a phase shift that is almost equal to RK3, but is far less dissipative than RK3. Observe that Störmer-Verlet is second-order conservative in time, but has a bigger phase shift than the RK methods.

### 5.2.2 Nonlinear shallow water

The nonlinear shallow water equations are given in (5.3). We consider a sinusoidal initial wave profile, in order to investigate breaking behavior of a traveling wave described by nonlinear models [36]. The initial solutions are obtained from linear theory equation (5.5) and the initial wave profile is plotted in figure 5.2.1.

We investigate shallow water waves with an initial wave steepness  $k_0 a = 0.53\pi$ , using the continuous Galerkin FEM. The numerical approximation in time is plotted in figure 5.2.3. Observe that the water level approximation becomes oscillatory (Gibbs phenomenon) when a hydraulic jump appears. Observe that the value of the total energy (rapidly) decays when the wave starts to break. Before that, the value of the nondimensionalized energy is similar to the ones plotted for the linear shallow water equations; cf. figure 5.2.2.

We now investigate the same initial wave profile numerically approximated with the discontinuous Galerkin FEM. For our numerical flux we use both the simple alternating flux and the Lax-Friedrich flux (see section 4.4). Observe from the results, presented in figure 5.2.4, that the Lax-Friedrich flux is able to cope with a discontinuous jump, while the alternating flux is not. However, the alternating flux is conservative (except for numerical dissipation by the RK4 time integration method) as was shown in section 4.4. The initial value of the nondimensionalized energy is  $2.1125 \cdot 10^{-3}$  per unit length and per unit mass, the same as for the linear case. Note that the numerical dissipation of energy when simulating an hydraulic jump is not an unwanted effect since breaking waves dissipate energy in nature.

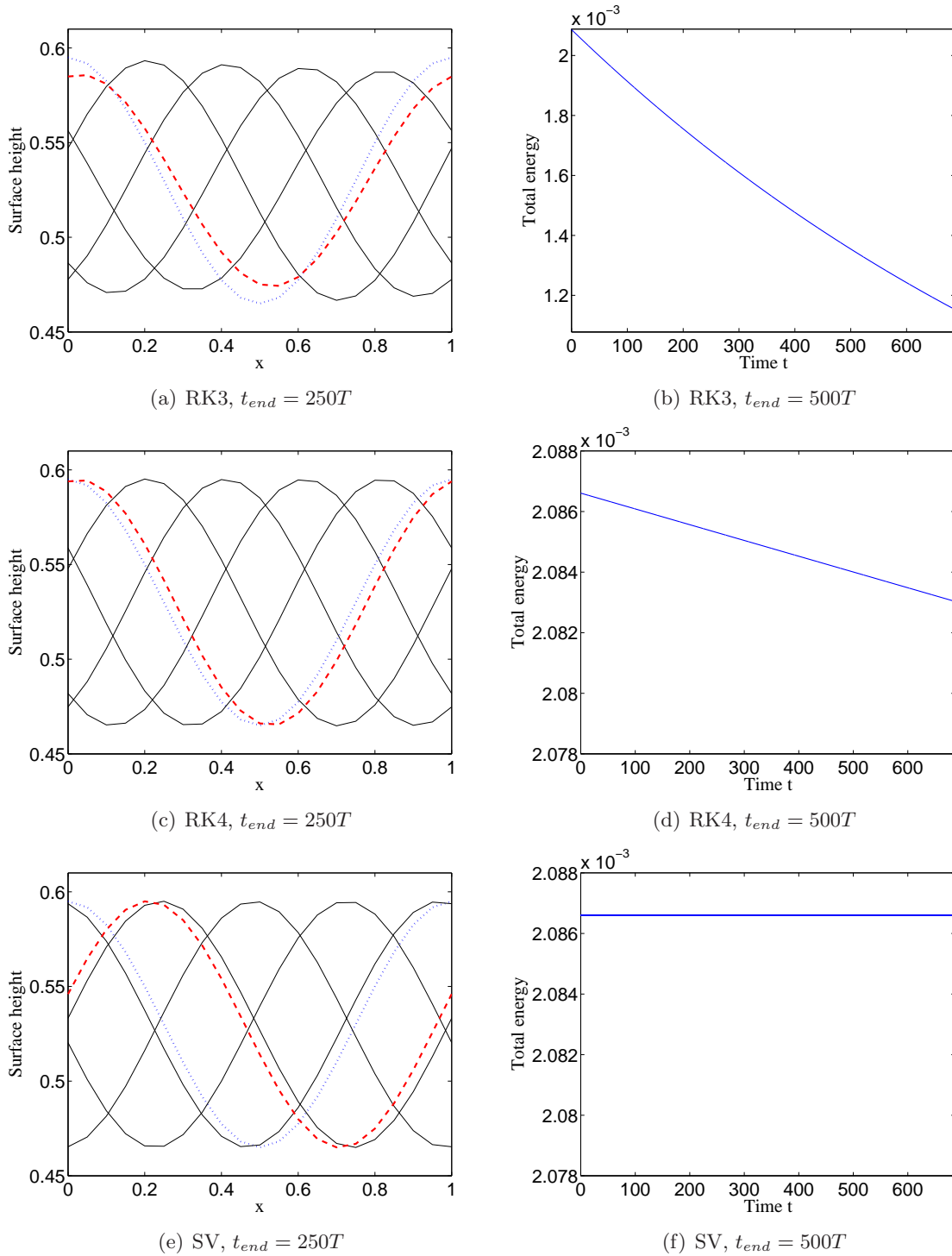


Figure 5.2.2: Runge Kutta 3, RK4 and Störmer-Verlet time integration methods for the linear shallow water equations with periodic boundary conditions; CG FEM. Water height  $h(x, t)$  are plotted for time  $t \in [0, t_{end}]$  at time steps  $n50T$ ,  $n = 0, 1, \dots, 5$ , with  $T = 2\pi/(\kappa\omega)$ . Initial condition is ( $\kappa = 2\pi$ ):  $h(x, 0) = a \cos(\kappa x) + h_0$ ,  $\phi(x, 0) = \frac{a}{\omega} \sin(\kappa x)$ , with  $a = 0.065$  and  $h_0 = 0.53$  (deep water),  $g = 1$  and  $\lambda = 1$ . The thick dotted line is the initial condition and the thick dashed line is at  $t = t_{end}$ . The total energy is plotted up to  $t_{end} = 500T$  and number of elements is 20.

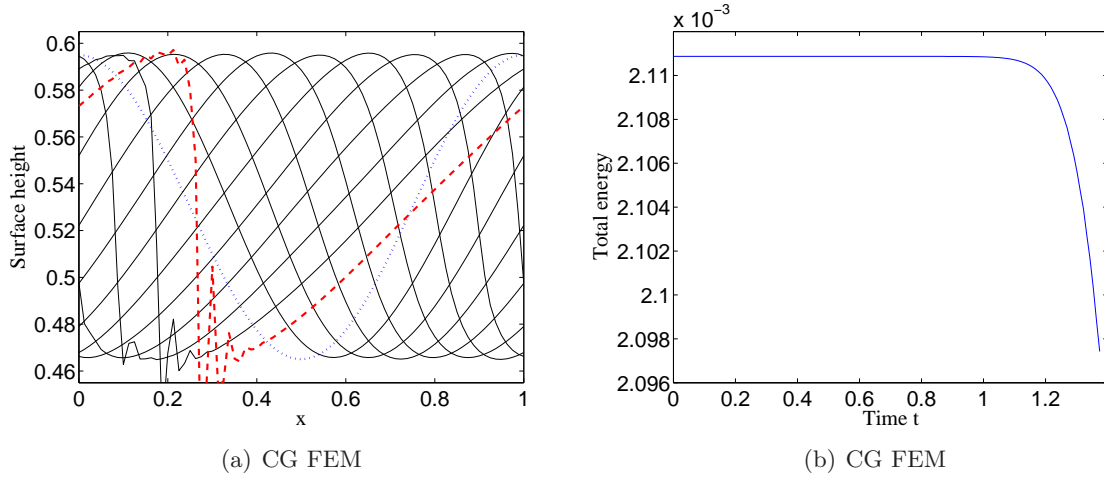


Figure 5.2.3: Nonlinear shallow water equations for a ratio  $kh_0 = 0.53 \cdot (2\pi)$  (deep water, CG FEM),  $a = 0.065$ ,  $g = 1$   $\lambda = 1$  and  $h_0 = 0.53$ . The dotted line is the initial condition as equation (5.5). Number of elements is 80, CFL = 0.5. The wave height is plotted up to  $t_{end} = 1.37$  (dashed line).

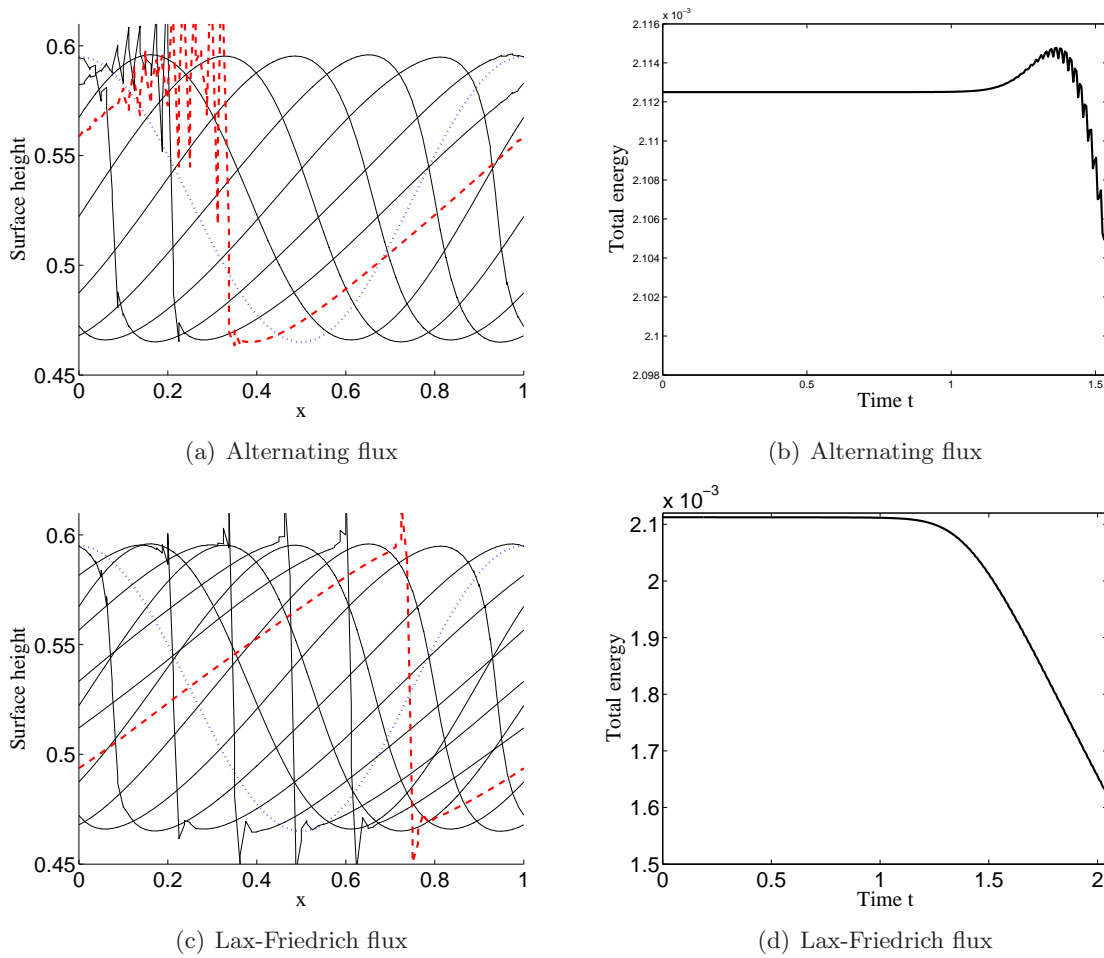


Figure 5.2.4: Nonlinear shallow water equations for a ratio  $kh_0 = 0.53 \cdot (2\pi)$  (deep water, DG FEMs),  $a = 0.065$ ,  $g = 1$   $\lambda = 1$  and  $h_0 = 0.53$ . The initial condition (5.5) is the dotted line. Number of elements is 80, CFL = 0.3. The wave height is plotted up to  $t_{end} = 1.54$  for the alternating flux (dashed line) and up to  $t_{end} = 2.05$  for the Lax-Friedrich flux (dashed line).

### 5.3 Whitham's variational Boussinesq model

In this subsection we will verify the numerical implementation of the Whitham variational Boussinesq model. Firstly, we will scale the model to the domain as depicted in figure 5.2.1 but now for a small wave amplitude  $a/h_0 = 0.01$ . We compute the total energy and wave-propagation over a long time stretch. Secondly, we will compare with a semi-analytical periodic solution for the full nonlinear case.

The energy  $\mathcal{H}$  for the WVBM was given by:

$$\mathcal{H} = \int_{D_h} \frac{1}{2} h (\partial_x \phi)^2 - \frac{1}{6} h_0 (\partial_t h)^2 + \frac{1}{2} g (h - h_0)^2 \, dx, \quad (5.6)$$

which results, from our variational principle, in the following Euler-Lagrange equations:

$$\partial_t h = -\partial_x [h \partial_x \phi], \quad \partial_t \phi = -g(h - h_0) - \frac{1}{2} (\partial_x \phi)^2 - \frac{1}{3} h_0 \partial_t^2 h. \quad (5.7)$$

This is rewritten as:

$$\partial_t h = -\partial_x [h \partial_x \phi], \quad \partial_t F = -g(h - h_0) - \frac{1}{2} (\partial_x \phi)^2, \quad (5.8)$$

after introduction of the auxiliary variable  $F = \phi + \frac{1}{3} h_0 \partial_t h$ , in order to facilitate the numerical integration in time.

#### 5.3.1 Small amplitude waves nonlinear WVBM

As initial conditions we take solutions of the linearized WVBM equations, equation (2.53)

$$h(x, t) = a \cos(\kappa x - \omega t) + h_0 \quad (5.9a)$$

$$F = \frac{ag}{\omega} \sin(\kappa x - \omega t) \quad \text{with} \quad \omega^2 = \frac{gh_0 \kappa^2}{1 + \frac{1}{3} (\kappa h_0)^2}. \quad (5.9b)$$

Nonlinear water waves behave like linear waves when considering small amplitude waves over not too long stretches of time [33]. We take  $a/h_0 = 0.01$ ,  $h_0 = 1$ , representing deep water. For one time period  $T = 2\pi/\omega$  the propagating wave is plotted in figure 5.3.1. To compute the the total energy (5.6) we approximate  $\partial_t h(x, t)$  by  $h_0 M_B \Phi + M_D(H)\Phi$ , see equation (3.25). Observe that the total energy is less than the energy of our nonlinear shallow water systems of section 5.2.2 due to the term  $-\frac{1}{6} h_0 (\partial_t h)^2$ .

#### 5.3.2 Nonlinear Whitham variational Boussinesq model

To verify our numerical model for the Whitham variational Boussinesq, we first consider cnoidal waves<sup>11</sup>, for which analytic solutions can be found [11]. Second, we consider semi-analytical periodic-wave solutions to the WVBM, using a standard MATLAB boundary value problem (BVP) solver, see appendix D. Initial profiles of the analytic solution and of the BVP are plotted in figure D.6.1. The initial solutions are obtained semi-analytically as follows, see Dingemans [11], chapter 6.

$$h(x, t) = -a t + H c n^2 \left( 2K(m) \frac{x - ct}{\lambda}; m \right) + h_0(x) \quad (5.10a)$$

$$\lambda = \sqrt{\frac{16h_0^3}{3A} m \left( \frac{c}{\sqrt{gh_0}} \right)^\beta} K(m) \quad (5.10b)$$

<sup>11</sup>A cnoidal wave is a periodic analytical solution of the KdV equations, which behaves like a propagating soliton; shape invariant in time

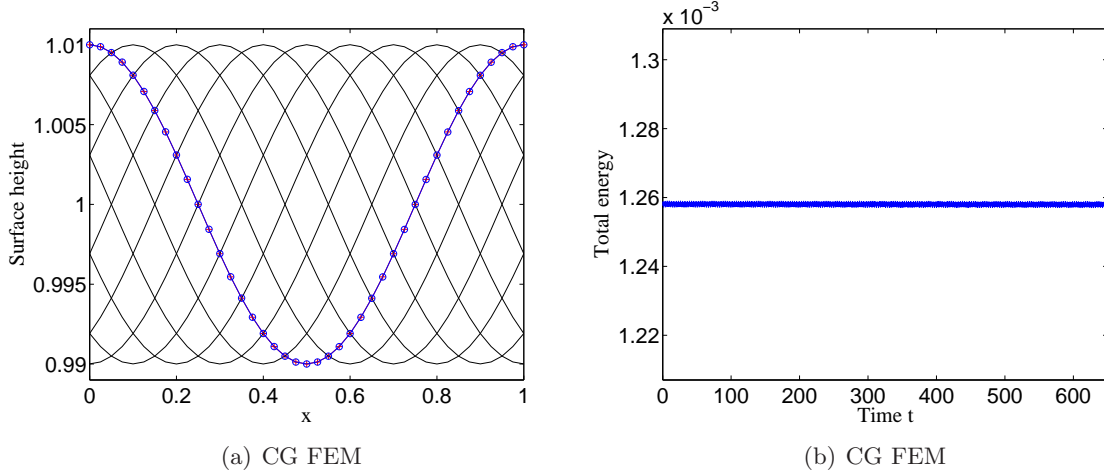


Figure 5.3.1: *Nonlinear WVBM for small amplitude waves  $a/h_0 = 0.01$  computed with CG FEM, for and initial condition (5.9a). Number of elements  $N$  is 40 and  $\Delta t = T/50$ , solutions plotted every  $5\Delta t$ . The energy is computed for  $a = 0.65$ ,  $h_0 = 0.53$ ,  $g = 1$  and  $\lambda = 1$ , time integration method RK4, under time-step restriction CFL = 0.5 up to  $t_{end} = 650$  for  $N = 20$ .*

$$a_c = \frac{A}{m} \left(1 - \frac{E(m)}{K(m)}\right) \quad (5.10c)$$

$$a_t = A - a_c \quad (5.10d)$$

$$c = \left[1 - \frac{A}{2h_0} + \frac{A}{mh_0} \left(1 - \frac{3}{2} \frac{E(m)}{K(m)}\right)\right]^{\frac{1}{\beta}} \sqrt{gh_0}, \quad (5.10e)$$

with  $a_c = \max_{x \in \lambda} (h(x, t) - h_0(x))$  the expression for the crest elevation and  $a_t = \min_{x \in \lambda} (h(x, t) - h_0(x))$  the through depth and  $c$  is the wave celerity;  $cn(\theta; m)$  are Jacobi elliptic functions and  $K(m)$  and  $E(m)$  are complete elliptic integrals of the first and second kind, where  $m_1 = 1 - m$  and  $m$  is the elliptic parameter;  $\beta$  is a value concerning the wideness of the crest.

The initial condition for the velocity potential  $\phi$  can be computed using the mass conservation equation:

$$\partial_t (h - h_0) + \partial_x [h \partial_x \phi] = 0. \quad (5.11)$$

Using that  $\partial_t = -c \partial_x$  for cnoidal waves, gives us:

$$-c(h - h_0) + h \partial_x \phi = \text{constant} = Q. \quad (5.12)$$

which can be rewritten to

$$\partial_x \phi = \frac{Q + c(h - h_0)}{h}. \quad (5.13)$$

Averaging over a wavelength  $\lambda$  yields that equation (5.13) is equal to zero (cnoidal waves are periodic and thus  $\partial_x \phi$  cancels at periodic boundaries at one wavelength) and we obtain

$$Q = -c \left( \overline{\frac{h - h_0}{h}} \right) / \left( \overline{\frac{1}{h}} \right) \quad (5.14)$$

where we define the wavelength average  $\overline{(\cdot)} = \frac{1}{\lambda} \int_0^\lambda (\cdot) dx$ . and  $\phi(x, t)$  is initially given by:

$$\phi = \int_{x_0}^x \frac{Q + c(h(x', t) - h_0(x'))}{h(x', t)} dx'. \quad (5.15)$$

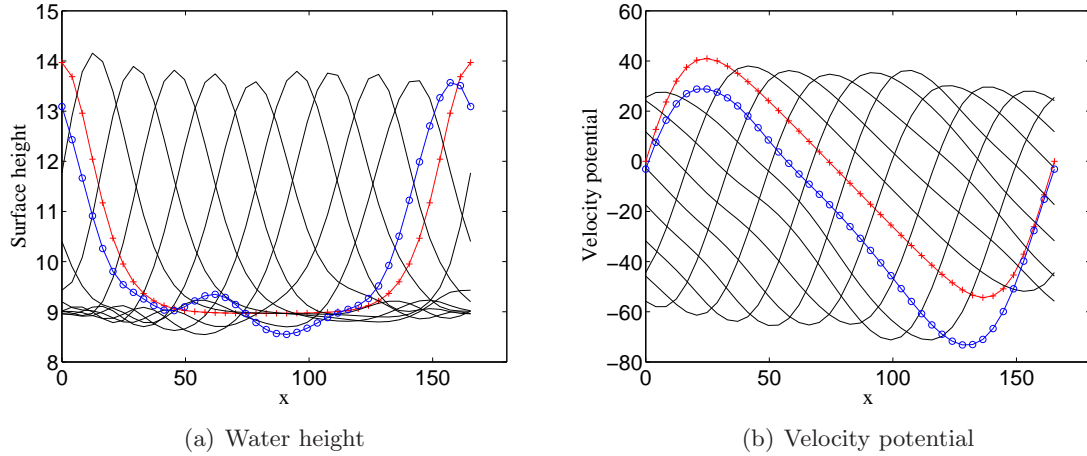


Figure 5.3.2: Cnoidal wave in the WVBM;  $H = 5.0$  m,  $h_0 = 10$  m,  $\lambda = 165.4$  m,  $g = 9.81$   $\text{ms}^{-2}$  and  $m = 0.001$ . The '+' denotes the initial profile as in figure D.6.1 and the 'o' is after one wave period  $T$ . Number of elements  $N = 40$ ,  $\Delta t = T/50$  s.

The numerical solution for one wave period  $T$  is plotted in figure 5.3.2 for parameters  $H = 5.0\text{m}$ ,  $h_0 = 10\text{m}$ ,  $\lambda = 165.4$ ,  $g = 9.81$  and  $m = 0.001$ . Observe that cnoidal wave is not an approximate solution of the Whitham variational Boussinesq model since waves are dispersed. The BVP, see appendix D, gives us, as shown in figure 5.3.3 an exact periodic solution; the initial condition lies on top of the solution at  $t_{\text{end}} = T$ . Note that the total energy was not solved completely correct, since we used an approximation for  $\partial_t^2 \eta$ .

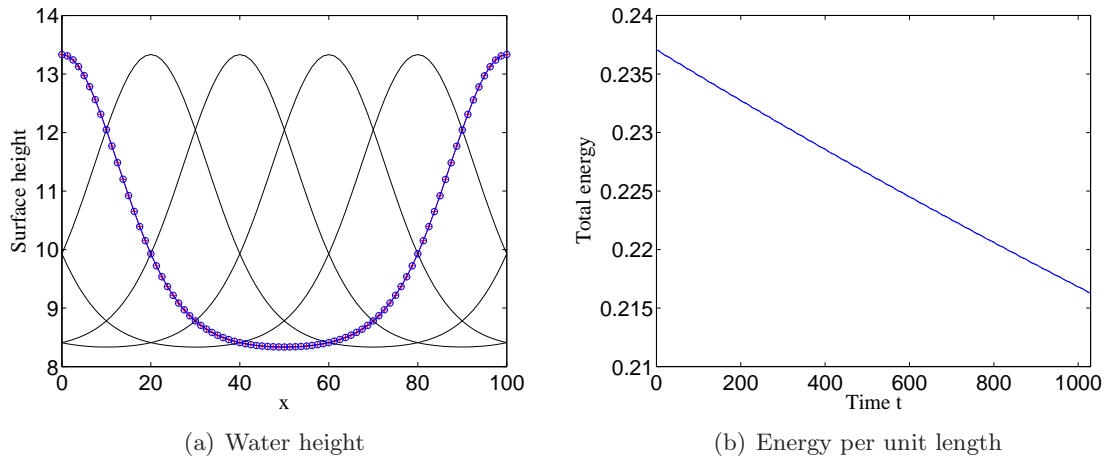


Figure 5.3.3: Nonlinear WVBM with an initial condition solved with the standard matlab boundary value problem solver. Initial values are:  $H = 5.0\text{m}$ ,  $h_0 = 10$  m,  $\lambda = 100$  m,  $g = 9.81$   $\text{ms}^{-2}$  and we had  $m = 0.0334$ . The '+' denotes the initial profile of one wavelength as figure D.6.1 and the 'o' is after one wave period  $T$ . The energy per unit length  $\mathcal{H}/\lambda$  is plotted up to time  $t_{\text{end}} = 100T$  and  $N = 80$ .

## 5.4 Klopman's variational Boussinesq model

In this subsection we will verify the numerical implementation of the Klopman variational Boussinesq model. Firstly, we will scale the model to the domain as depicted in figure 5.2.1 but now for a small wave amplitude  $a/h_0 = 0.01$ . We observe the total energy and wave-propagation for a long time. Secondly, we will consider large amplitude waves for the linear

KVBM computed with the DG FEM.

### 5.5 Small amplitude waves in the Klopman variational Boussinesq model

In this subsection we verify our results obtained for the linear KVBM, numerically computed with the DG method as proposed in section 4.6. The accuracy of our numerical solution of the third elliptic equation of our KVBM system has been verified separately in appendix C. We non-dimensionalize our models by scaling for comparison reasons. We observe periodic waves on the horizontal domain  $x \in [0, 2\pi]$ . When we consider as an initial profile a sinusoidal wave we relate twice the height of the wave  $2a$  to its wavelength  $\lambda$  as follows

$$R = \frac{\Delta z}{\Delta x} = \frac{2a}{\lambda} = \frac{2ak_0}{2\pi}, \quad (5.16)$$

where  $a$  is the amplitude of the wave with wavenumber  $k_0$  as depicted in figure 5.2.1.

For the complete linear KVBM model an analytical solution is given by

$$h(x, t) = a \cos(\kappa x - \omega t) + h_0, \quad (5.17a)$$

$$u(x, t) = a\kappa \cos(\kappa x - \omega t)/\omega, \quad (5.17b)$$

$$\psi(x, t) = -\frac{a\omega\kappa}{\omega(2 + \frac{3}{4}h_0^2\kappa^2)} \sin(\kappa x - \omega t), \quad (5.17c)$$

where  $\omega$  is obtained from the dispersion relation as derived in section 2.3.2 and reads

$$\omega^2 = \frac{g}{h}(\kappa h)^2 \frac{1 + \frac{1}{15}(\kappa h)^2}{1 + \frac{2}{5}(\kappa h)^2}. \quad (5.18)$$

Note that for the continuous Galerkin method we ought to compare  $\phi(x, t) = a \sin(\kappa x - \omega t)/\omega$  instead of  $u(x, t)$ .

After one wave period  $T = 2\pi/\omega$  we have that, for a periodic solution on an horizontal domain  $x \in [0, 2\pi]$ , the solution is ideally the same as the initial condition. Moreover, the shape of wave profile is time invariant (modulo  $T$ ) when propagating over the free surface, as indicated by (5.17). The total energy of the linearized system is given by

$$\mathcal{H}_b = \int_{D_h} \frac{1}{2}h_0 \left[ u - \frac{2}{3}h_0^2\partial_x\psi \right]^2 + \frac{2}{45}h_0^5(\partial_x\psi)^2 + \frac{2}{3}h_0^3\psi^2 + \frac{1}{2}g(h - h_0)^2 dx \quad (5.19)$$

which can be computed analytically for our linear system (5.17) and is approximated numerically by (4.6.3). We now consider a periodic horizontal domain  $L = 2\pi$ , wavenumber  $\kappa = 1$  (such that  $\lambda = 2\pi$ ) and a small amplitude wave  $a \ll h_0$ , for example  $a = 0.01$  with the non-dimensional coefficients  $h_0 = 1$  and  $g = 1$ . The steepness ratio is then given by  $R = \frac{0.01}{\pi}$ . The total (non-dimensional) energy of our system is<sup>12</sup>  $\mathcal{H}_b = 3.142103451$ , which is constant in time. The wave propagation for this linear wave, approximated by the discontinuous Galerkin method for the linearized KVBM (section 4.6), using a time step  $\Delta t = T/48$  with  $T = 2\pi/\omega$ , is plotted in figure 5.5.1a. The total energy of our system at time steps ( $\Delta t = T/48$ , where  $T = 2\pi/\omega$  is our wave period) is plotted for a hundred wave periods in figure 5.5.1b.

When we consider small amplitude water waves, in this case  $a = h_0/100$ , it is observed that the solution of the nonlinear KVBM by the continuous Galerkin method will behave like linear water waves. Nonlinear effects are small compared to the leading linear order [33]. The wave propagation, as approximated with the continuous Galerkin method (section 3.4), is plotted in figure 5.5.1c. The total energy of our system at time steps  $\Delta t = T/24$ , is plotted for a hundred wave periods in figure 5.5.1d.

Note that the plot may suggest that the total energy remains completely constant in time, where in fact energy is dissipated numerically, see table 5.5.1

<sup>12</sup>Solved analytically with maple.

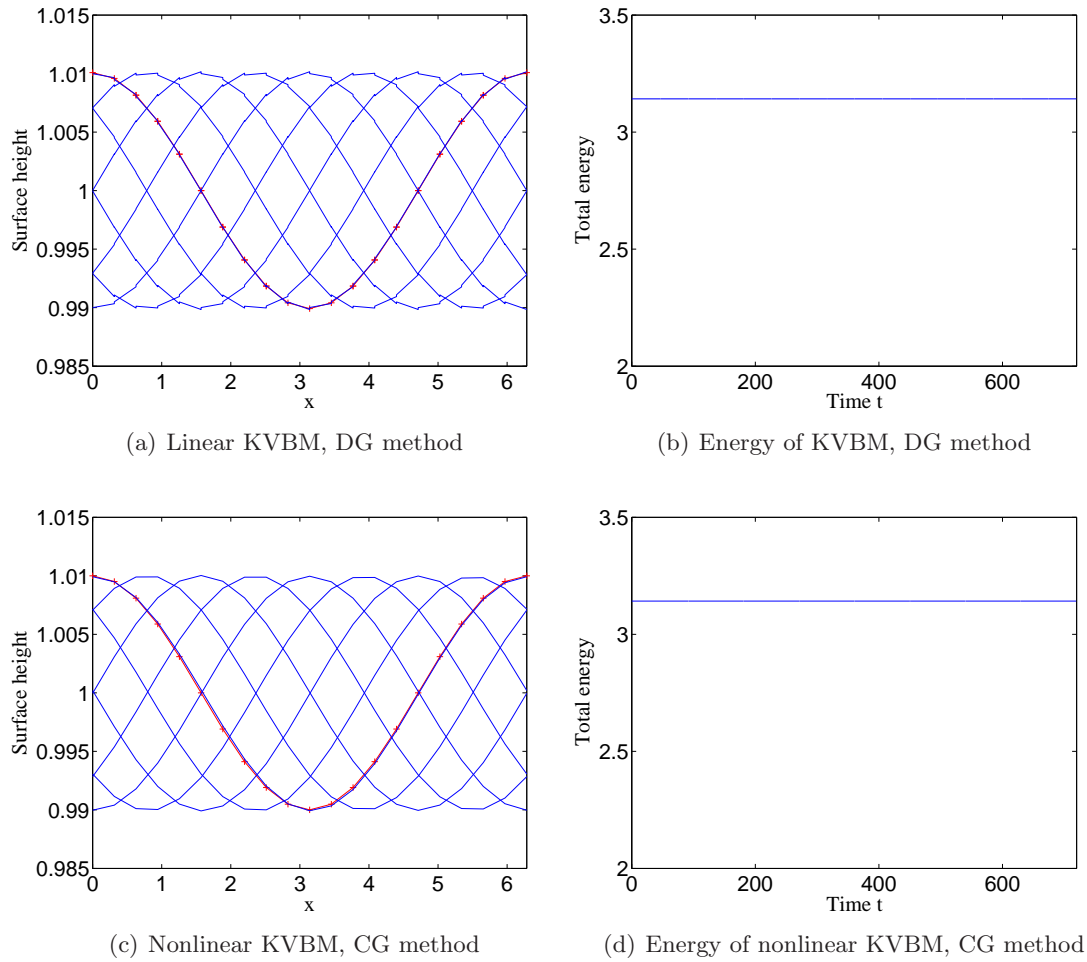


Figure 5.5.1: Small wave amplitude  $a/h_0 = 0.01$ , time integration method is  $RK_4$ . The initial condition is represented with the '+', given by (5.17). For DG we used a time step  $\Delta t = T/48$  and number of elements  $N_e = 20$ . For CG we used  $\Delta t = T/24$  and  $N_e = 20$ . The propagating wave is plotted at time steps  $t = \frac{n}{8}T, n = 0, 1, \dots, 8$ . The total (non-dimensional) energy is plotted for 100 wave periods.

	Lin. KVBM, DG FEM	Nonlin. KVBM, CG FEM
Total energy at $t = 0$	3.141907	3.141952
Total energy at $t = 100T$	3.141864	3.141948
Relative difference	$-1.37 \cdot 10^{-3}\%$	$-1.34 \cdot 10^{-4}\%$

Table 5.5.1: Total energy  $\mathcal{H}$  of the linear and nonlinear KVBM computed with respectively DG and CG FEM.

## 5.6 Large amplitude waves in the Klopman variational Boussinesq model

Verification for large amplitude waves in the the Klopman Boussinesq model can only be done for the linear model, computed with DG FEM. Results for the nonlinear model (CG FEM) will be presented in section 6. We consider very large amplitude waves with  $a/h_0 = 0.4$ . The surface height and velocity potential are plotted in figure 5.6.1. as can be seen, the solution remains sinusoidal, as expected for a linear problem.

## 5.7 Conclusion

In this section we we verified the numerical implementation of the linear and nonlinear shallow water, the nonlinear Whitham variational Boussinesq model and the linear and nonlinear Klopman variational Boussinesq model.

The Runge-Kutta 3 was shown to be more numerically dissipative than the Runge-Kutta 4 time integration method. The Störmer verlet time integration method was shown to be conservative, although it has a bigger phase shift than the Runge-Kutta methods.

The discontinuous Galerkin FEM proved to approximate the propagation of a discontinuous jump in the nonlinear shallow water model better than the continuous Galerkin FEM. When a discontinuous jump occurs, the performance of the discontinuous Galerkin FEM mainly depends on the choice of the flux. The (conservative) alternating flux shows spurious oscillations when the numerical solution follows a propagating shock. The Lax-Friedrich flux only showed unwanted oscillations near the shock.

The cnoidal wave solution showed dispersion effects and it appears that the cnoidal wave does not approximate a periodic solution of the WVBM. The BVP solution of appendix D is shown to be a periodic solution of the nonlinear WVBM. Appart from numerical dissipation, energy is nicely conserved.

The more complex KVBM was solved correctly using the continuous Galerkin FEM for the nonlinear KVBM and using the discontinuous Galerkin FEM for the linear KVBM. Energy was shown to be conserved with the alternating numerical flux.

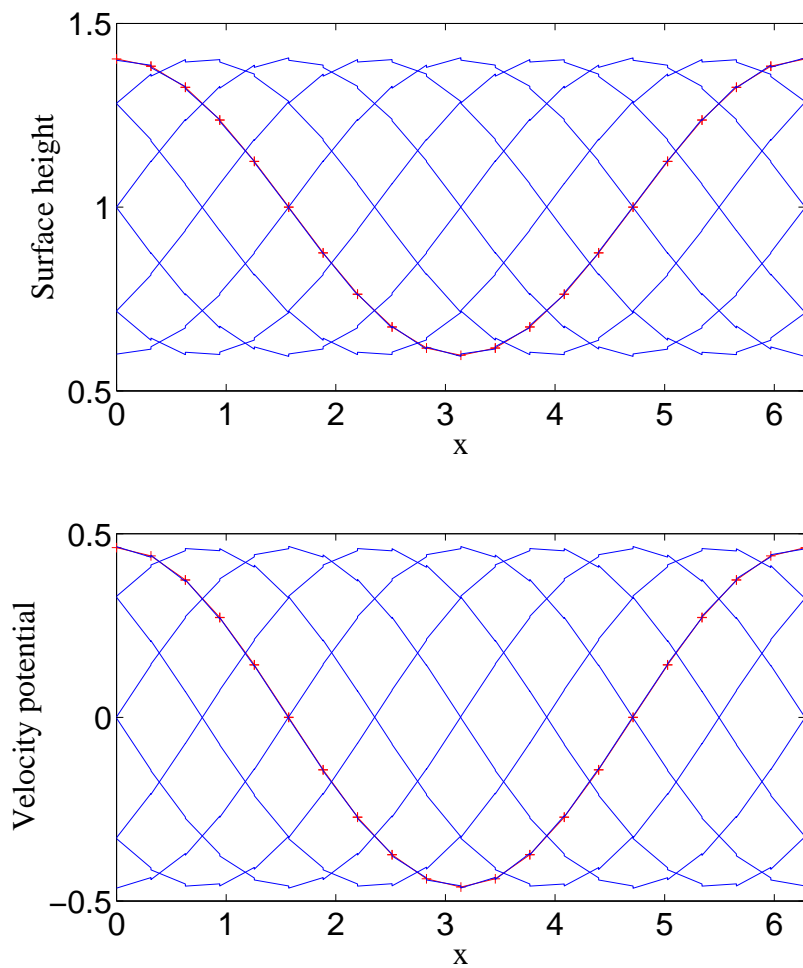


Figure 5.6.1: Large amplitude wave  $a/h_0 = 0.01$ , time integration method is  $RK4$ . The initial condition is represented with the '+', given by (5.17). We used a time step  $\Delta t = T/48$  in  $RK4$  method and number of elements  $N = 20$ . The propagating wave is plotted at time steps  $t = \frac{n}{8}T, n = 0, 1, \dots, 8$ .



## 6 Investigation into wave breaking and linear dispersion

### 6.1 Introduction

In section 2 the following three variational models were studied analytically: Luke's variational principle for potential flow, Klopman's variational Boussinesq model (KVBM) and Whitham's variational Boussinesq model (WVBM). In section 5 we presented the verification of our numerical models. We find that the propagation speed of periodic waves in our numerical models were approximated correctly. In this section we investigate, if in the nonlinear WVBM and weakly nonlinear KVBM breaking waves may occur.

This study is motivated by the fact, that opposite to the nonlinear shallow water equations, waves do not break (i.e. have discontinuous solutions developed from continuous initial solutions) in traditional Boussinesq models. Apparently, the counteracting effect of linear frequency dispersion is too strong for wave breaking to occur. Ofcourse, we know from our own observations at the beach, and from numerical simulations using the full potential flow equations, that real waves may break. Therefore, we will investigate whether the nonlinear WVBM and weakly-nonlinear KVBM allow for breaking waves to develop.

The numerical results are computed with the continuous Galerkin (CG) finite element method for the nonlinear Whitham and Klopman variational Boussinesq models as described in section 3.1.

Firstly, we consider the possibility of wave breaking in the nonlinear Whitham variational Boussinesq model, for waves computed with the CG FEM and propagating over a flat horizontal seabed. The initial wave profile is chosen as in section 5.2.2.

Secondly, we consider the weakly nonlinear Klopman variational Boussinesq model for various wave amplitudes, computed with the CG FEM.

Thirdly we present traveling waves in the linear Klopman variational Boussinesq model numerically computed with the DG FEM.

Conclusions are drawn in next section, section 7.

### 6.2 Wave breaking

#### 6.2.1 Nonlinear Whitham variational Boussinesq model (CG)

In section 5 we have verified that the correct implementation of the nonlinear WVBM. to study the possibility of wave breaking, We now present two test cases for waves propagating over a horizontal seabed. We plot in figure 6.2.1 the (non-dimensionalized) waves propagating for one wave period in deep water,  $h_0\kappa = 0.53 * (2\pi)$  and shallow water  $h_0\kappa = 0.13 * (2\pi)$ . The initial conditions are given by:

$$h(x, t) = a \cos(\kappa x - \omega t) + h_0, \quad (6.1a)$$

$$F = \frac{ag}{\omega} \sin(\kappa x - \omega t) \quad \text{with} \quad \omega^2 = \frac{gh_0\kappa^2}{1 + \frac{1}{3}(\kappa h_0)^2} \quad (6.1b)$$

where  $a = 0.65$ ,  $\kappa = 2\pi$  and  $g = 1$ . To compute the energy we approximate  $(\partial_t h)^2$  as we did in the verification, section 5.3. As can be observed, even for the steepest initial wave profile, the waves do not start to break in the Whitham variational model. As expected for the CG FEM model, energy is almost conserved.

#### 6.2.2 Weakly nonlinear Klopman variational Boussinesq (CG)

To investigate the behavior of the weakly nonlinear Klopman variational Boussinesq model, we start with a sinusoidal wave profile, given by relations (5.17) and plotted in figure 5.2.1, but now for various amplitudes at a water depth  $h_0 = 10$  m, non-dimensionalizing using  $\kappa = 2\pi$  and  $g = 1$ .

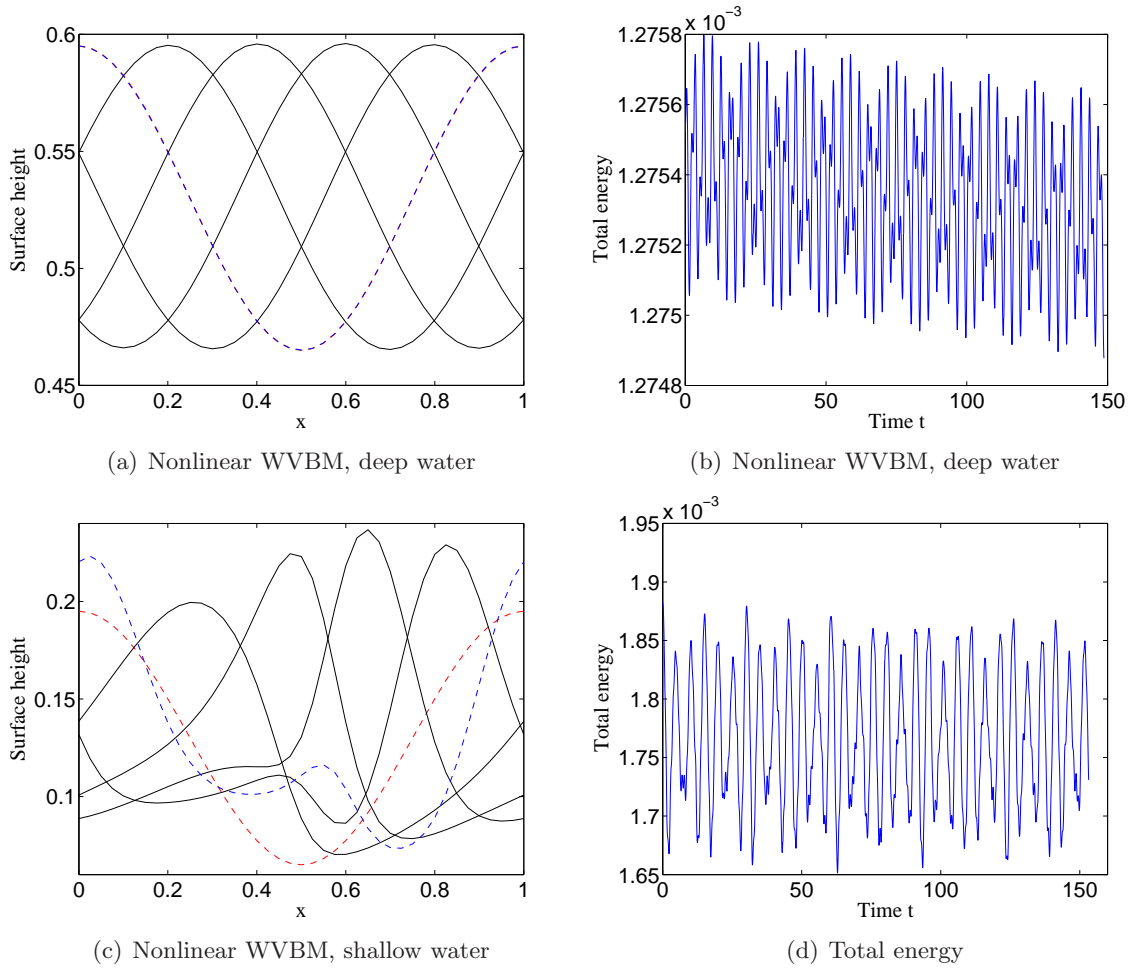


Figure 6.2.1: *Nonlinear WVBM. The initial condition is represented with the dotted line and given by (6.1a). Number of elements  $N = 40$ , time steps  $\Delta t = T/50$ , RK4. The wave ratios  $h_0\kappa$  are for a) the deep water  $0.53 * (2\pi)$  and c) the shallow water  $0.13 * (2\pi)$ . Energy is computed up to  $t_{end} = 50T$ . We have  $g = 1$ ,  $\lambda = 1$ .*

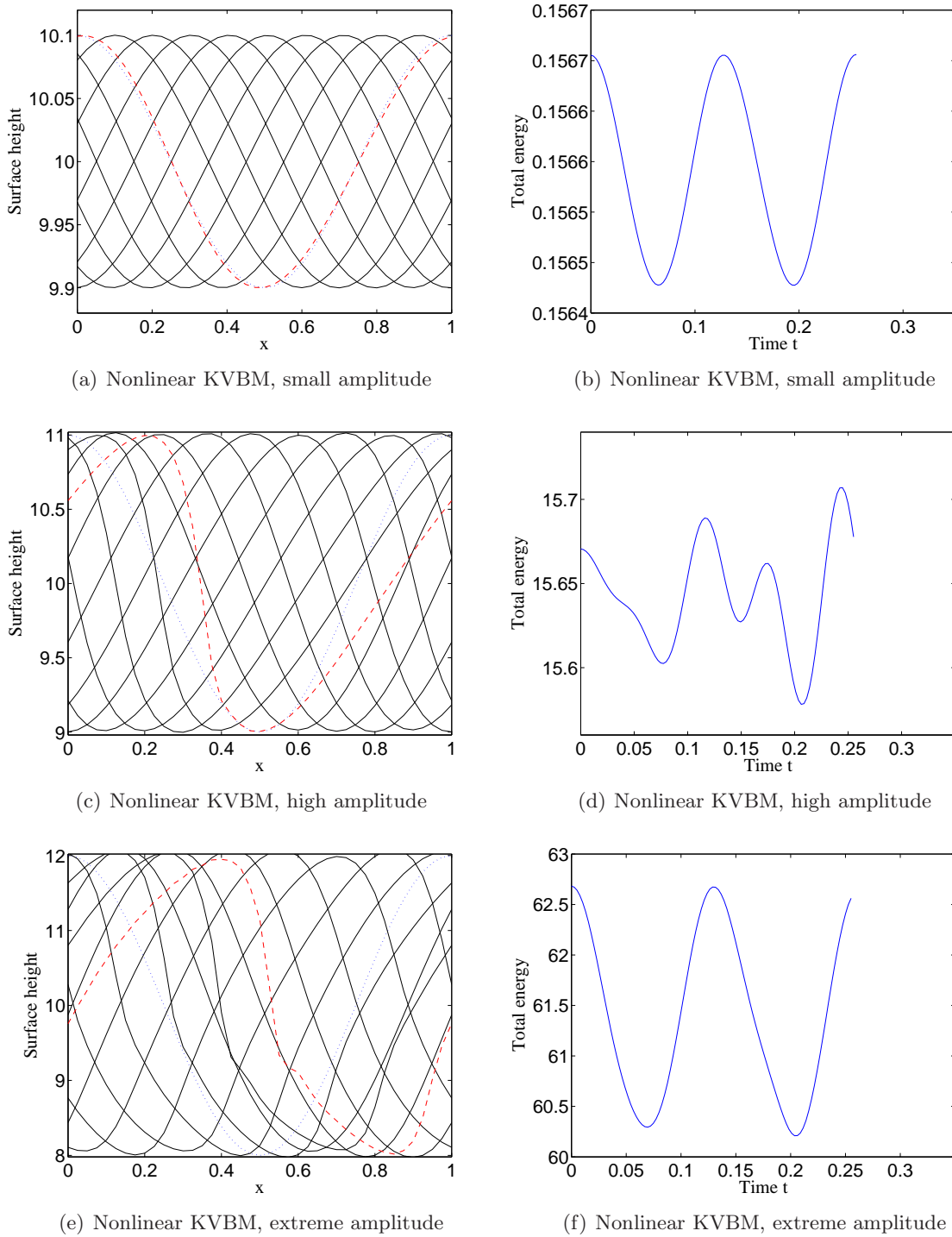


Figure 6.2.2: *Weakly nonlinear KVBM. The initial condition is represented with the dotted line and given by (5.17). Number of elements  $N = 40$ , time steps  $\Delta t = T/100$ , RK4. Water depth  $h_0 = 10$  and the amplitudes are for a)  $a = 0.1$ , c)  $a = 1.0$  and e)  $a = 2.0$ . The energy is computed for one wave period. The dashed line is at  $t_{end} = T$*

At  $t_{end}$ , plot 6.2.2c typically illustrate the behavior of the weakly nonlinear KVBM for extremely high and steep waves. Wave crests are steepening at the front and an extra wave is appearing at the trough due to wave dispersion. This phenomenon is also visible for Rienecker-Fenton<sup>13</sup> initial waves as illustrated in figure 5a of [20]. For high amplitude waves the propagating waves will start to deform strongly, but will not break<sup>14</sup>.

### 6.3 Linear dispersion

To illustrate the effects of dispersion, we now consider the linear KVBM. We consider an initial sinusoidal wave profile, which could represent an initial disturbance of the free surface by, for example, a fast motion of the seabed caused by an earth quake. We consider a flat horizontal seabed of depth  $h_0 = 10$  m. The wave has a wavelength of  $\lambda = 100$  m and amplitudes  $a = 1$  m. The left "fronts" of the wave starts at  $x_0 = 50$  m. The initial disturbance does not affect initially the surrounding fluid, so we choose a zero velocity  $u$  and initial water level  $h_0 = 10$  m. At the initial surface elevation at the bump is given by:

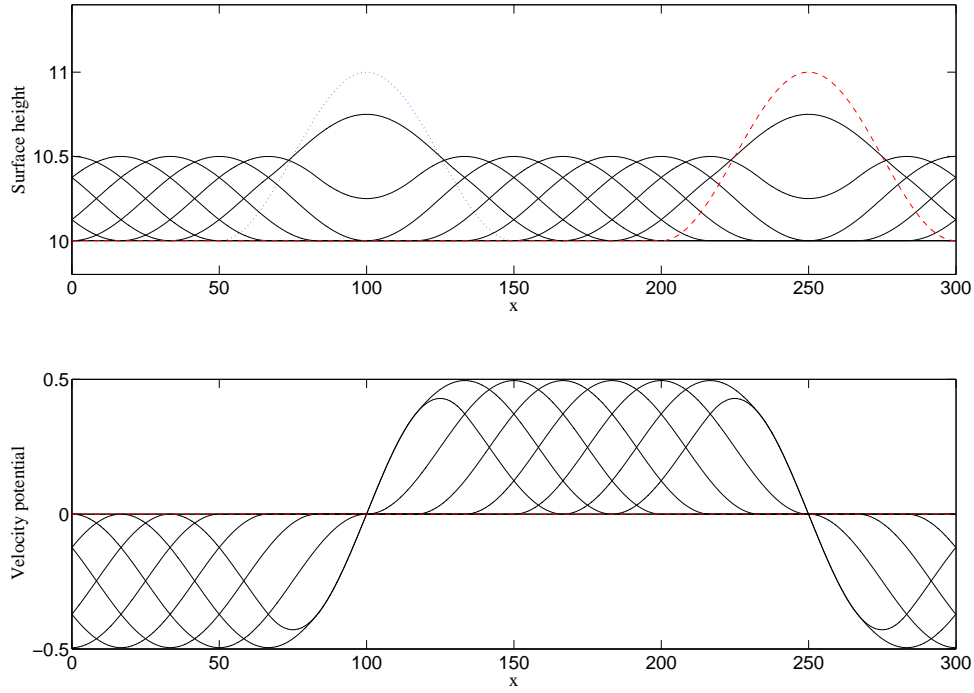
$$h(x, 0) = \frac{a}{2}(1 - \cos(\kappa(x - x_0))) + h_0, \quad \text{and} \quad u(x, 0) = 0. \quad (6.2)$$

In figure 6.3.1 we compare the linear shallow water equations with the linear KVBM to illustrate linear dispersion. The linear shallow case is obtained by assuming that vertical velocity profile of the fluid, governed by the term  $\psi$ , is equal everywhere. We take  $\psi = 0$ . We consider the linear shallow water and the KVBM at periodic boundaries.

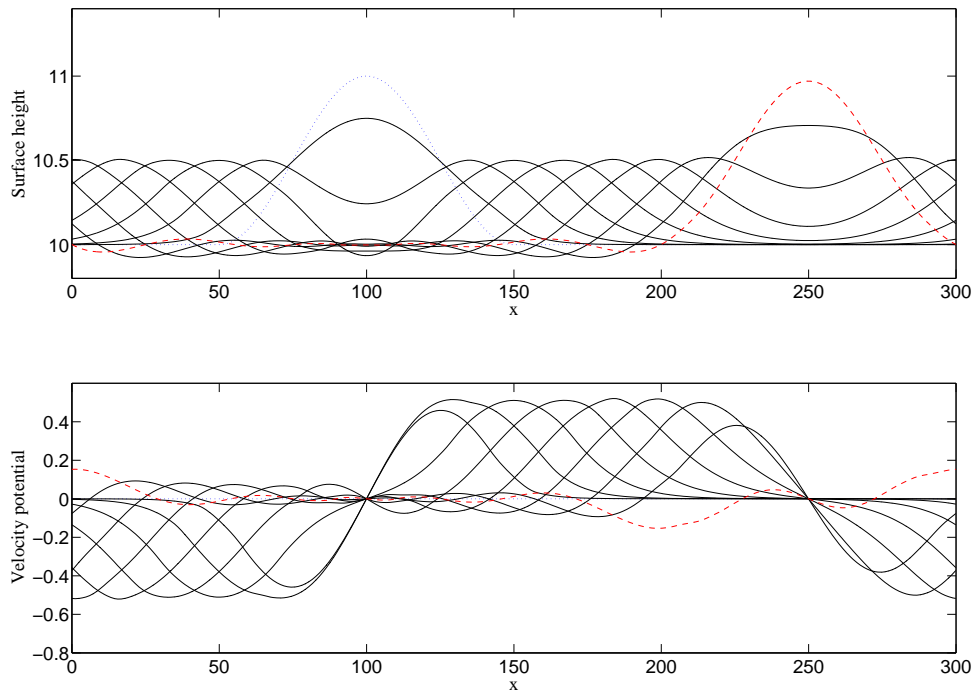
---

<sup>13</sup>Rienecker-Fenton provided a relatively simple method to get a nonlinear potential description of a regular wave in any water depth by means of a Fourier series of the stream function [26].

<sup>14</sup>c.f. the verification in section 5.6



(a) Linear shallow water; dispersionless



(b) Linear KVBM; dispersive

Figure 6.3.1: Linear KVBM computed with the DG method. The initial condition is represented with the dotted line and given by (6.2). Number of elements  $N = 250$ ,  $\Delta x = 300/250$  m and time-integration method is RK4 with time-step  $T/300$ . Water depth  $h_0 = 10$  and the initial amplitude is  $a = 1$  and wave length  $\lambda = 100$ . The surface height and velocity of the fluid are plotted in a) for the linear shallow water ( $T = 10, 10$  s) and in b) for the linear KVBM ( $T = 10, 72$ ) after timesteps  $t = T/6$  and  $t_{end} = 1\frac{1}{2}T$ ; the waves travelling to the left and right meet at  $x_{end} = 300$  m.



## 7 Conclusions

In this report three variational principles modeling free surface waves were studied, namely Luke's variational principle [27] for the full three dimensional potential flow, Klopman's variational Boussinesq model (KVBM) and Whitham's variational Boussinesq model (WVBM). An important property of these models is that energy is conserved by construction and is positive-definite. In this report surface tension is included to the variational principles. By studying the linear dispersion relations, we find that surface tension can not be neglected for short waves,  $\lambda < 10$  cm since it affects the phase speed of the propagating waves.

The KVBM is found to approximate the exact dispersion relation, obtained from Luke's variational principle, better than the WVBM. Furthermore, the Taylor expansion of the KVBM approximates the exact dispersion relation up to the order  $\mathcal{O}(\kappa^{10})$ .

Considering variational principles provide two nice properties. First, moving boundaries have been included in the variational principles describing free surface potential flows. The motion of moving boundaries is obtained by taking variations with respect to time dependent fluid boundaries. Second, variational principles are a logical starting point for the continuous Galerkin finite element weak formulation.

An important question is whether the Boussinesq models allow for the development of breaking (discontinuous) waves. From the numerical computations, see figures 6.2.1 and 6.2.2 it is concluded that the waves described by the nonlinear WVBM and the weakly nonlinear KVBM do not break. In the derivation of the weakly nonlinear KVBM some nonlinear terms were canceled due to the assumption that wave slopes are small  $\partial_x(h + h_b - h_0) \ll 1$ . The dispersion effects in this model might be in balance with the nonlinear terms. The possibility of wave breaking described by this fully nonlinear model should be investigated further, see equations (8.1) from [20].

If the fully nonlinear waves eventually start to break, for waves propagating through the surf-zone, the propagating waves are shown to have a relatively good dispersion with respect to the exact dispersion relation. To be able to simulate the propagation of these waves through the surf zone it is shown that the discontinuous Galerkin method is able to deal with the propagating discontinuous jump. However, the choice of the numerical flux for the fully nonlinear model has not yet been proposed. Dissipation properties of the numerical flux are to be considered, since the model itself does not dissipate energy. The numerical dissipation due to the numerical flux is desired, as illustrated by the the Lax-Friedrich flux in the case of nonlinear shallow water wave and a clever choice can be desirable when waves overturn. In his report an energy conservation restriction for the numerical fluxes have been formulated for the shallow water equations. In a similar way one may be able to construct a restriction on the numerical flux for the fully nonlinear KVBM case.

Besides the advantage of the possibility to cope with breaking waves, the discontinuous Galerkin method has the benefit to locally refine the grid size and the accuracy by locally introducing higher order polynomials [38].

We conclude that the linear KVBM has successfully been implemented in a DG FEM, using linear polynomials to expand the variables. Solving  $\psi$  in the linear KVBM from the elliptic equation, eq. (4.49c), is done using the Brezzi approach [2], see appendix C.



## 8 Recommendations

In this section we discuss some recommendations. We will start with the model assumptions and present possible model extensions. Thereafter we discuss the numerical methods and present some findings.

- When validating the potential flow models against small-scaled laboratory settings one has to include surface tension effects in the variational model, as proposed in this report. The surface tension effects affect the propagation speed of the fluid, and this effect can be easily included in your mathematical model when validating your model with laboratory data.
- In this report we have investigated fluid domains with a constant horizontal water depth  $h_0$  and with periodic boundaries. Further investigation on bathymetry influences, such as steep seabed slopes might be required when simulating waves propagating from the deep oceans to the shores. Furthermore, for practical applications, we may include special boundaries such as ships, sloping beaches and quays in our variational models. Introducing these boundaries means that we have to add additional assumptions at the boundaries for  $\psi$ : i.e. for the vertical velocity  $\partial_z\phi$  at  $z = h(x, t)$ .
- When one considers a broader range of waves than only small-steepness water waves, one has to adopt the fully nonlinear KVBM instead of the weakly nonlinear KVBM. Dropping the assumption that wave slopes are small and allowing waves slopes to be steep may affect the breaking behavior of wave described by the KVBM model heavily. We suggest the discontinuous Galerkin FEM to simulate waves propagating in the surf-zone, and to investigate wave breaking in the fully nonlinear KVBM.
- The continuous Galerkin FEM is derived nicely from the variation of the action functional. It might be worthwhile to investigate further if this may be possible for the discontinuous Galerkin FEM for Lagrangian systems in general. Combining the advantages of these energy conserving system with a highly adaptable computational methods as DG FEM would have many benefits.
- The fully nonlinear equations are, from [20]:

$$\delta h : \partial_t h + \partial_x(hu_p) = 0, \quad (8.1a)$$

$$\delta\phi : \partial_t u + \partial_x \left\{ gh + \frac{1}{2}[u_p - \frac{1}{3}h\partial_x\psi]^2 - \frac{1}{45}[\psi\partial_x h + h\partial_x\psi]^2 + \frac{1}{6}[1 + \frac{1}{5}(\partial_x h)^2]\psi^2 + \partial_x[h(\frac{2}{3}u - \frac{7}{15}\psi\partial_x h - \frac{1}{5}h\partial_x\psi)] \right\} = 0, \quad (8.1b)$$

$$\delta\psi : h\psi \left[ \frac{1}{3} + \frac{7}{15}(\partial_x h)^2 - [\frac{2}{3}hu - \frac{1}{5}h^2\partial_x\psi]\partial_x h + \partial_x \left\{ \frac{1}{3}h^2u - \frac{1}{5}h^2\psi\partial_x h - \frac{2}{15}h^3\partial_x\psi \right\} \right] = 0, \quad (8.1c)$$

where  $u \equiv \partial_x\phi$  and the depth-averaged velocity  $u_p$  is given by

$$u_p = u - \frac{2}{3}\psi\partial_x h - h\partial_x\psi. \quad (8.2)$$

When one constructs a discontinuous Galerkin FEM for the fully nonlinear KVBM, one can still use the Brezzi approach to solve the elliptic equation, since it is linear in  $\psi$  and one still has to solve an elliptical equation. Construction of the weak formulation per element of the fully nonlinear equations (8.1) will give a term over element  $K_j$ , from the last term

$$-\partial_x \left\{ \partial_x \left[ \frac{1}{5}h^2\partial_x\psi \right] \right\} \quad (8.3)$$

in equation (8.1b):

$$\int_{K_j} v_x \partial_x \left[ \frac{1}{5} h^2 \partial_x \psi \right] dx + \text{a flux-term at the element boundaries}, \quad (8.4)$$

which can be solved using the knowledge of  $\sigma = \partial_x \psi$  from (8.1c) from and adopting the degeneration method of Yan and Shu [38] for third order spatial derivatives.

- For the fully nonlinear KVBM, implemented using the discontinuous Galerkin method, we have to investigate the choice of the numerical flux. In this report an alternating flux have been chosen for the linear KVBM. In the shallow water model it is shown that the alternating flux is not able to deal with discontinuous jumps. The Lax-Friedrich flux is too dissipative in the shallow water case. So, for the fully nonlinear KVBM we might want to adopt the HLL or the HLLC flux as proposed by Batten et al.[4], where the wave speed can be approximated locally using the linear dispersion relation. In our linear case the flux choice of the elliptic equation depends on the choice of the numerical flux in the mass-conservation equation, i.e. the determination of  $\partial_t h$ , only. In the nonlinear case the term  $\psi$  comes forth in both equations (8.1a) and (8.1b), so even for an alternating flux the choice of the numerical flux for the third equation (8.1c) is not yet obvious.

## References

- [1] B. Arnold, Brezzi, D.N., B. Cockburn, and D. Marini. Discontinuous Galerkin methods for elliptic problems. In B. Cockburn, G. E. Karniadakis, and C.-W. Shu, editors, *Discontinuous Galerkin Methods: Theory, Computation and Applications*, volume 11, pages 89–101. Springer-Verlag, New York, 2000.
- [2] D.N. Arnold, F. Brezzi, B. Cockburn, and L.D. Marini. Unified analysis of discontinuous Galerkin methods for elliptic problems. *SIAM Journal on Numerical Analysis*, 39(5):1749–1779, 2002.
- [3] F. Bassi and S. Rebay. A high-order accurate discontinuous finite element method for the numerical solution of the compressible Navier-Stokes equations. *Journal of Computational Physics*, 131:267–279, 1997.
- [4] P. Batten, N. Clarke, C. Lambert, and D.M. Causon. On the choice of wavespeeds for the HLLC Riemann solver. *SIAM Journal of Numerical Analysis*, 18(6):1553–1570, 1997.
- [5] O. Bokhove and J.W. Van der Vegt. Introduction to (dis)continuous Galerkin finite element methods. Technical report, Numerical Analysis and Computational Mechanics, Department of Applied Mathematics, Twente University of Technology, 2005.
- [6] S.C. Brenner and L.R. Scott. *The Mathematical Theory of Finite Element Methods*. Springer-Verlag, New York-Berlin-Heidelberg, 1994.
- [7] L.J.F. Broer. On the Hamiltonian theory of surface waves. *Applied Scientific Research*, 29:430–446, 1974.
- [8] L.J.F. Broer. Approximate equations for long wave equations. *Applied Scientific Research*, 31(5):377–395, 1975.
- [9] L.J.F. Broer, E.W.C. van Groesen, and J.M.W. Timmers. Stable model equations for long water waves. *Applied Scientific Research*, 32(6):619–636, 1976.
- [10] C.-W. Cockburn, B. & Shu. The local discontinuous Galerkin method for time-dependent convection-diffusion systems. *SIAM Journal of Numerical Analysis*, 35(6):2240–2463, 1998.
- [11] M. W. Dingemans. *Water wave propagation over uneven bottoms*, publisher = World Scientific Publishing Company, Singapore, year = 1997, key = 2 Parts, 967 pp., volume = 13, OPTnumber = , series = Advanced Series on Ocean Engineering, OPTaddress = , OPTedition = , OPTmonth = , OPTnote = , OPTannotate = .
- [12] E. Eskilsson and S.J. Sherwin. A discontinuous spectral element model for Boussinesq-type equations. *Journal of Scientific Computing*, 17(1-4), 2002.
- [13] E. Eskilsson and S.J. Sherwin. Discontinuous Galerkin spectral/hp element modelling of dispersive shallow water systems. *Journal of Scientific Computing*, 22:269–288, 2005.
- [14] Gotlieb and C.-W. Shu. Total variation diminishing Runge-Kutta schemes. *Mathematics of Computation*, 67(221):73–85, 1998.
- [15] E. Hairer, Ch. Lubich, and G. Wanner. Geometric numerical integration illustrated by the Störmer/Verlet method. *Acta Numerica*, 12:1–55, 2003.
- [16] J.M.J. Journée and W.W. Massie. *Offshore Hydromechanics*. Lecture Notes, Delft University of Technology, 2000.

- 
- [17] J. T. Kirby. *Gravity waves in water of finite depth*, chapter Nonlinear, dispersive long waves in water of variable depth, pages 55–125. Number 10. Computational Mechanics Publications, 1997.
- [18] J.T. Kirby. Boussinesq models and applications to nearshore wave propagation, surfzone processes and wave-induced currents. *Advances in Coastal Modeling, Elsevier*, pages 1–41, 2003.
- [19] G. Klopman, M.W. Dingemans, and E.R. Groesen. A variational model for fully non-linear water waves of Boussinesq type. In *20th. International Workshop on Water Waves and Floating Bodies*, 2005.
- [20] G. Klopman, E.R. Groesen, and M.W. Dingemans. Variational Boussinesq modelling of fully non-linear water waves. *Royal Society (submitted)*, May 2006.
- [21] C. Lanczos. *The variational principles of mechanics*. Dover publications, inc. New York, 4th. edition, 1970.
- [22] R.J. LeVeque. *Numerical methods for Conservation Laws*. Birkhäuser Verlag, Base; Boston; Berlin, 2nd. edition, 1992.
- [23] M.J. Lighthill. *Waves in fluids*. Cambridge University Press, Cambridge, pp. 504, 1978.
- [24] B. Lucquin and O. Pironneau. John Wiley & Sons, Inc., New York etc., pp. 361, 1998.
- [25] P.A. Madsen, R. Murray, and O.R. Sørensen. A new form of the Boussinesq equations with improved linear dispersion characteristics. *Coastal Engineering*, 15:371–388, 1991.
- [26] G. Meskers and R.H.M Huijsmans. Realistic inflow conditions for numerical green water simulations. In *Conference proceedings, 18th. IWWWFB*. The Royal Institution of Naval Architects, 2003. Nantes, France.
- [27] J.W. Miles. On hamilton’s principle for surface waves. *Fluid. Mech.*, 83:153–158, 1977.
- [28] K.W. Morton and D.F. Mayers. *Numerical Solution of Partial Differential Equations*. Cambridge University Press, 1994.
- [29] B.R. Munson, D.F. Young, and T.H. Okiishi. *Fundamentals of Fluid Mechanics*. John Wiley & Sons, Inc., New York etc., pp. 840, 2002.
- [30] D.H. Peregrine. Long waves on a beach. *J. Fluid Mech.*, 27 (4):815–827, 1967.
- [31] W.H. Press, S.A. Teukolsky, Vetterling W.T., and B.P. Flannery. *Numerical Recipes in C++: the art of scientific computing*. Cambridge University Press, 2nd edition, 2001.
- [32] W.H. Reed and T.R. Hill. Triangular mesh methods for the neutron transport equation. Technical Report LA-UR-73-479, Los Alamos scientific laboratory, Los Alamos, NM, 1973.
- [33] J.J. Stoker. *Water waves: the mathematical theory with applications*. Wiley Inter Science, New York, 1957.
- [34] J.J. Sudirham, J.J.W. Van der Vegt, and R.M.J. Van Damme. A study on discontinuous Galerkin finite element methods for elliptic problems. Memoranda 1690, University of Twente, Department of Applied Mathematics, 2003.
- [35] E.R. van Groesen. Applied analytical methods. Lecture notes part 1, Department of Applied Mathematics, Twente University of Technology, 2003.

- 
- [36] T. Vinje and P. Brevig. Numerical simulation of breaking waves. *Advances in Water Resources*, 4(2):77–82, 1981.
- [37] G.B. Whitham. Variational methods and applications to water waves. *Proceedings of The Royal Society, Series A*, Vol. 299, No. 1456:6–25, 1967.
- [38] J. Yan and C.-W. Shu. A local discontinuous Galerkin method for KdV type equations. *Siam J. Numer. Anal.*, Vol 40.(No. 2):pp. 769–791, 2002.

## A Nonlinear shallow water equations with discontinuous Galerkin

### A.1 Non-linear shallow water equations

The non-linear shallow water equations over an horizontal flat seabed are the Euler-Lagrange equations of the following action principle

$$\mathcal{L}(h, \phi) = \int_{D_h} \phi \partial_t h dx - \mathcal{H}(h, \phi), \quad (\text{A.1})$$

where the total energy of the system  $\mathcal{H}$  is given by

$$\mathcal{H} = \int_{D_h} \frac{1}{2} h (\partial_x \phi)^2 + \frac{1}{2} g h^2 dx. \quad (\text{A.2})$$

Imagine  $D_h = K_j$  is an element of our tessalation  $\mathcal{T}_h$ , then taking variations with respect to  $h$  and  $\phi$  gives us our variational weak formulation per element

$$0 = \int_{t_0}^{t_1} \int_{|K_j|} \delta \phi \partial_t h - \frac{d\delta \phi}{dx} [h \partial_x \phi] dx - \int_{|K_j|} \delta h (\partial_t \phi + gh + \frac{1}{2} (\partial_x \phi)^2) dx dt. \quad (\text{A.3})$$

Spatial partial integration and seperation of the two variational derivatives with respect to each variable gives

$$\int_{t_0}^{t_1} \int_{|K_j|} \delta \phi \partial_t h + \delta \phi \partial_x [h \partial_x \phi] dx - \int_{\partial K_j} \delta \phi \widehat{h \partial_x \phi} n ds dt = 0 \quad (\text{A.4a})$$

$$\int_{t_0}^{t_1} \int_{|K_j|} \delta h (\partial_t \phi + gh + \frac{1}{2} (\partial_x \phi)^2) dx dt = 0. \quad (\text{A.4b})$$

where  $\widehat{h \partial_x \phi}$  denotes the numerical flux at the boundary faces. We use the arbitrariness of  $\delta h$  in the set of testfunctions  $C^\infty(K)$  and instead we take  $\frac{d\delta h}{dx} \in C^\infty(K)$ . Substitution of  $u = \partial_x \phi$  and partial integration with respect to space and gives us for

$$\int_{t_0}^{t_1} \int_{|K_j|} \delta \phi \partial_t h + \delta \phi \partial_x [hu] dx - \int_{\partial K_k} \delta \phi \widehat{hun} ds dt = 0 \quad (\text{A.5a})$$

$$\int_{t_0}^{t_1} \int_{|K_j|} \delta h \partial_t u - \partial_x \delta h [gh + \frac{1}{2} u^2] dx + \int_{\partial K_j} \delta h (g\hat{h} + \frac{1}{2} \hat{u}^2) n ds dt = 0. \quad (\text{A.5b})$$

### A.2 DG discretization with polynomials of degree 1

In order to compute the Shallow Water equations we expand the variables with polynomials of degree  $d_p = 1$ . We expand our trial and test functions with polynomials of degree  $d_P = 1$

$$\begin{aligned} h_h(x, t) &= \bar{H}_j(t) + \hat{H}_j(t) \Theta_1(x), & \delta h(x) &= \bar{V}_j + \hat{V}_j \Theta_1(x) \\ u_h(x, t) &= \bar{U}_j(t) + \hat{U}_j(t) \Theta_1(x), & \delta \phi_h(x), &= \bar{W}_j + \hat{W}_j \Theta_1(x) \end{aligned} \quad (\text{A.6a})$$

where for example  $\bar{H}_j$  and  $\hat{H}_j$  are the numerical approximations of the mean and the slope of  $h(x, t)$  at  $x = x_j$ .

### A.3 Algebraic system of equations

$$\int_{K_j} (\bar{V}_j + \hat{V}_j \Theta_1) \frac{d}{dt} (\bar{H}_j + \hat{H}_j \Theta_1) - \hat{V}_j \frac{d\Theta_1}{dx} (\bar{H}_j + \hat{H}_j \Theta_1) (\bar{U}_j + \hat{U}_j \Theta_1) dx$$

$$+ \int_{\partial K_j} (\bar{V}_j + \hat{V}_j \Theta_1) \widehat{h} u n \, ds = 0 \quad (\text{A.7a})$$

$$\int_{K_j} (\bar{W}_j + \hat{W}_j \Theta_1) \frac{d}{dt} (\bar{U}_j + \hat{U}_j \Theta_1) - \hat{W}_j \frac{d\Theta_1}{dx} \left( g(\bar{H}_j + \hat{H}_j \Theta_1) + \frac{1}{2} (\bar{U}_j + \hat{U}_j \Theta_1)^2 \right) dx$$

$$+ \int_{\partial K_j} (\bar{W}_j + \hat{W}_j \Theta_1) \left( g \hat{h} + \frac{1}{2} \hat{u}^2 \right) n \, ds = 0 \quad (\text{A.7b})$$

### A.3.1 Means

We evaluate the integrals over the elements by using the reference element  $\zeta \in [-1, 1]$  and mapping  $x = F_j(\zeta) \in [x_{j-\frac{1}{2}}, x_{j+\frac{1}{2}}]$   $\xi \in [-1, 1]$  as in section 4.2.2. Using the arbitrariness of the test-functions, we first take  $\bar{V}_j = 1, \hat{V}_j = 0$ , and  $\bar{W}_j = 1, \hat{W}_j = 0$ .

$$\frac{d}{dt} \bar{H}_j |K_j| = -\hat{h} u_{j+\frac{1}{2}} + \hat{h} u_{j-\frac{1}{2}} \quad (\text{A.8a})$$

$$\frac{d}{dt} \bar{U}_j |K_j| = -[g \hat{h} + \frac{1}{2} \hat{u}^2]_{j+\frac{1}{2}} + [g \hat{h} + \frac{1}{2} \hat{u}^2]_{j-\frac{1}{2}} \quad (\text{A.8b})$$

### A.3.2 Slopes

Vice versa  $\bar{V}_j = 0, \hat{V}_j = 1$ , and  $\bar{W}_j = 0, \hat{W}_j = 1$

$$\frac{d\hat{H}_j}{dt} \frac{|K_j|}{3} = 2\bar{H}_j \bar{U}_j + \frac{2}{3} \hat{H}_j \hat{U}_j - (\hat{h} u_{j+\frac{1}{2}} + \hat{h} u_{j-\frac{1}{2}}) \quad (\text{A.9a})$$

$$\frac{d\hat{U}_j}{dt} \frac{|K_j|}{3} = 2g\bar{H}_j + \bar{U}_j^2 + \frac{1}{3} \hat{U}_j^2 - \left( [g \hat{h} + \frac{1}{2} \hat{u}^2]_{j+\frac{1}{2}} + [g \hat{h} + \frac{1}{2} \hat{u}^2]_{j-\frac{1}{2}} \right). \quad (\text{A.9b})$$



## B Klopman's variational Boussinesq discontinuous Galerkin discretization

In order to compute the Klopman Variational Boussinesq equations we expand the variables with polynomials of degree  $d_p = 1$  and substitution results in a linear system.

### B.1 DG discretization with polynomials of degree 1

We expand our trial and test functions with polynomials of degree  $d_p = 1$

$$\begin{aligned} h_h(x, t) &= \bar{H}_j(t) + \hat{H}_j(t)\Theta_1(x) & v_h(x) &= \bar{V}_j + \hat{V}_j\Theta_1(x) \\ u_h(x, t) &= \bar{U}_j(t) + \hat{U}_j(t)\Theta_1(x) & w_h(x) &= \bar{W}_j + \hat{W}_j\Theta_1(x) \\ \psi_h(x, t) &= \bar{\Psi}_j(t) + \hat{\Psi}_j(t)\Theta_1(x) & \varsigma_h(x) &= \bar{Z}_j + \hat{Z}_j\Theta_1(x) \end{aligned} \quad (\text{B.1a})$$

where  $\bar{H}_j$  and  $\hat{H}_j$  etc. are the numerical approximations of the mean and the slope of  $h(x, t)$  at  $x = x_j$ . For the lifting operator coefficients  $(\mathcal{R}_s)_j$  at face  $S$  we have (cf. section 4.2.4)

$$R_i^{s,j} = \sum_{i=0}^{d_p} (A^{s,j})^{-1} P^{s,j}, \text{ where } A_{j,li} = \int_{K_j} \Theta_l \Theta_i \, dx, \Rightarrow A_j = |K_j| \begin{bmatrix} 1 & 0 \\ 0 & \frac{1}{3} \end{bmatrix} \quad (\text{B.2})$$

and

$$\begin{aligned} P^{sL}(\Psi_{j-1}, \Psi_j)_i &= \sum_{i=0}^{d_p} \sum_{k=j-1}^j \frac{1}{2} \int_{S_L} \Theta_l \Theta_i \, ds \Rightarrow \\ P^{sL}(\Psi_{j-1}, \Psi_j)_i &= \frac{1}{2} \begin{bmatrix} -1 & -\xi_l \\ -\xi_l & -\xi_l \xi_l \end{bmatrix} \quad \text{and} \quad P^{sR}(\Psi_{j-1}, \Psi_j)_i = \frac{1}{2} \begin{bmatrix} 1 & \xi_r \\ \xi_l & \xi_r \xi_l \end{bmatrix} \\ P^{sL}(\Psi_j, \Psi_{j+1})_i &= \frac{1}{2} \begin{bmatrix} -1 & -\xi_l \\ -\xi_r & -\xi_l \xi_r \end{bmatrix} \quad \text{and} \quad P^{sR}(\Psi_j, \Psi_{j+1})_i = \frac{1}{2} \begin{bmatrix} 1 & \xi_r \\ \xi_r & \xi_r \xi_r \end{bmatrix} \end{aligned} \quad (\text{B.3})$$

### B.2 Algebraic system of equations

$$\begin{aligned} \int_{K_j} (\bar{V}_j + \hat{V}_j\Theta_1) \frac{d}{dt} (\bar{H}_j + \hat{H}_j\Theta_1) - h_0 \hat{V}_j \frac{d\Theta_1}{dx} (\bar{U}_j + \hat{U}_j\Theta_1) + \frac{2}{3} h_0^3 \hat{V}_j \frac{d\Theta_1}{dx} \frac{d\Theta_1}{dx} \hat{\Psi}_j \, dx \\ + \int_{\partial K_j} h_0 (\bar{V}_j + \hat{V}_j\Theta_1) \left( \hat{u} - \frac{2}{3} h_0^2 \left( \left\{ \frac{d\Theta_1}{dx} \hat{\Psi}_j \right\} - \left\{ \eta^e R_i^{s,j} \right\} \right) \right) n \\ + \frac{2}{3} h_0^2 \left\{ \hat{V}_j \frac{d\Theta_1}{dx} \right\} \left[ \bar{\Psi} + \hat{\Psi}\Theta_1 \right] \, ds = 0 \end{aligned} \quad (\text{B.4a})$$

$$\begin{aligned} \int_{K_j} (\bar{W}_j + \hat{W}_j\Theta_1) \frac{d}{dt} (\bar{U}_j + \hat{U}_j\Theta_1) - g \hat{W}_j \frac{d\Theta_1}{dx} (\bar{H}_j + \hat{H}_j\Theta_1) \, dx \\ + \int_{\partial K_j} g (\bar{W}_j + \hat{W}_j\Theta_1) (\hat{h} + h_b) n \, ds = 0 \end{aligned} \quad (\text{B.4b})$$

$$\begin{aligned} \int_{K_j} 2(\bar{Z}_j + \hat{Z}_j\Theta_1) (\bar{\Psi}_j + \hat{\Psi}_j\Theta_1) - \hat{Z}_j \frac{d\Theta_1}{dx} (\bar{U}_j + \hat{U}_j\Theta_1) + \frac{4}{5} h_0^2 \hat{Z}_j \frac{d\Theta_1}{dx} \frac{d\Theta_1}{dx} \hat{\Psi}_j \, dx \\ + \int_{\partial K_j} (\bar{Z}_j + \hat{Z}_j\Theta_1) \left( \hat{u} - \frac{4}{5} h_0^2 \left( \left\{ \frac{d\Theta_1}{dx} \hat{\Psi}_j \right\} - \left\{ \eta^e R_i^{s,j} \right\} \right) \right) n \\ + \frac{4}{5} h_0^2 \left\{ \hat{Z}_j \frac{d\Theta_1}{dx} \right\} \left[ \bar{\Psi} + \hat{\Psi}\Theta_1 \right] \, ds = 0. \end{aligned} \quad (\text{B.4c})$$

### B.2.1 Means

We evaluate the integrals over the elements by using the reference element  $\zeta \in [-1, 1]$  and mapping  $x = F_j(\zeta) \in [x_{j-\frac{1}{2}}, x_{j+\frac{1}{2}}]$   $\xi \in [-1, 1]$  as in section 4.2.2. Using the arbitrariness of the test-functions, we first take  $\bar{V}_j = 1, \hat{V}_j = 0, \bar{W}_j = 1, \hat{W}_j = 0$  and  $\bar{Z}_j = 1, \hat{Z}_j = 0$ .

$$\begin{aligned} \frac{d}{dt} \bar{H}_j |K_j| &= -h_0(\hat{u}_{j+\frac{1}{2}} - \hat{u}_{j-\frac{1}{2}}) + \frac{2}{3} h_0^3 |K_j| (\hat{\Psi}_{j-1} - \hat{\Psi}_{j+1}) \\ &\quad + \frac{2}{3} h_0^3 \frac{\hat{\Psi}_j}{|K_j|} + \frac{1}{3} h_0^3 \eta^e \frac{1}{2} A_j^{-1} [P^{sR}(\Psi_{j-1}, \Psi_j)_0 + P^{sL} \Psi_j, \Psi_{j+1})_0] \end{aligned} \quad (\text{B.5a})$$

$$\frac{d}{dt} \bar{U}_j |K_j| = -g(\hat{h}_{j+\frac{1}{2}} - \hat{h}_{j-\frac{1}{2}} - g(h_{b,j+\frac{1}{2}} - h_{b,j-\frac{1}{2}})) \, ds = 0 \quad (\text{B.5b})$$

$$\begin{aligned} 2\bar{\Psi}_j |K_j| + \frac{4}{5} h_0^2 \frac{\hat{\Psi}_j}{|K_j|} - \frac{4}{5} h_0^2 \eta^e \frac{1}{2} A_j^{-1} [P^{sR}(\Psi_{j-1}, \Psi_j)_0 + P^{sL} \Psi_j, \Psi_{j+1})_0] \\ = (\hat{u}_{j+\frac{1}{2}} - \hat{u}_{j-\frac{1}{2}}) \end{aligned} \quad (\text{B.5c})$$

### B.2.2 Slopes

Vice versa  $\bar{V}_j = 0, \hat{V}_j = 1, \bar{W}_j = 0, \hat{W}_j = 1$  and  $\bar{Z}_j = 0, \hat{Z}_1 = 0$ .

$$\begin{aligned} \frac{d\hat{H}_j}{dt} \frac{|K_j|}{3} &= 2h_0 \bar{U}_j - h_0(\hat{u}_{j+\frac{1}{2}} + \hat{u}_{j-\frac{1}{2}}) - \frac{2}{3} h_0^3 \frac{4}{|K_j|} \hat{\Psi}_j \\ &\quad + \frac{1}{3} h_0^3 \eta^e \frac{1}{2} A_j^{-1} [P^{sR}(\Psi_{j-1}, \Psi_j)_1 + P^{sL}(\Psi_j, \Psi_{j+1})_1], \end{aligned} \quad (\text{B.6a})$$

$$\frac{d\hat{U}_j}{dt} \frac{|K_j|}{3} = 2g\bar{H}_j - g([\hat{h} + h_b]_{j+\frac{1}{2}} + [\hat{h} + h_b]_{j-\frac{1}{2}}), \quad (\text{B.6b})$$

$$\begin{aligned} 2\hat{\Psi}_j \frac{|K_j|}{3} - \frac{4}{5} h_0^2 \frac{4}{|K_j|} \hat{\Psi}_j - \frac{4}{5} h_0^2 \eta^e \frac{1}{2} A_j^{-1} [P^{sR}(\Psi_{j-1}, \Psi_j)_1 + P^{sL} \Psi_j, \Psi_{j+1})_1] \\ = -2\bar{U}_j + (\hat{h}_{j+\frac{1}{2}} + \hat{h}_{j-\frac{1}{2}}). \end{aligned} \quad (\text{B.6c})$$

Note that the two equations, (B.5c) combined with (B.6c), can be solved globally by

$$M\Psi = BU \Rightarrow \Psi = (I_{2N} + M)^{-1} BU \quad (\text{B.7})$$

where  $M$  represents the collection of the lifting operators over the faces and the contribution of  $\partial_x \psi$  and  $I_{2N}$  the "DG-eye" matrix with terms  $1/|K_j|$  on  $I_{2j-1, 2j-1}$  and  $3/|K_j|$   $I_{2j, 2j}$ , which multiply with  $\bar{\psi}$  (B.5c) and  $\hat{\psi}$  (B.6c) respectively.

## C Brezzi's approach

### C.1 Fixed boundary conditions

We test the elliptic system by taking a Dirichlet boundary at the left and a Neumann boundary at the right.

$$\psi - \psi_{xx} = f(x). \quad (\text{C.1})$$

$$\psi(0) = 0, \quad \psi_x(1) = 0 \quad (\text{C.2})$$

We consider the exact solution  $\psi = -\frac{1}{2} + \frac{1}{2} \cos(\pi x)$  on  $x \in [0, 1]$  and for our right-hand-side we have

$$f(x) = -\frac{1}{2} + \frac{1}{2}(1 + \pi^2) \cos(\pi x). \quad (\text{C.3})$$

We obtained the following order of convergence

Ne	$L^2$ error	Order
8	5.4347e-03	0
16	1.4007e-03	1.9561
32	3.5447e-04	1.9824
64	8.9086e-05	1.9924
128	2.2326e-05	1.9965
256	5.5879e-06	1.9983
512	1.3978e-06	1.9992

(C.4)

for lifting parameters  $\eta^e + N_s = 3$ .

### C.2 Periodic boundary conditions

To compute the third equation of the linearized Klopman Euler-Lagrange equations, we have to solve some kind of elliptic system as

$$\psi - c\partial_{xx}\psi = f(x). \quad (\text{C.5})$$

To test the Brezzi method, we take  $c = 1$  and consider the exact periodic solution  $\psi = \cos(2\pi x)$ ,  $x \in [0, 1]$  and right-hand-side

$$f(x) = (1 + (2\pi)^2) \cos(2\pi x). \quad (\text{C.6})$$

We solve the system with the Brezzi method and with a finite difference method. We obtain the following order of accuracy:

Ne	Brezzi		Finite difference	
	$L^2$ error	Order	$L^2$ error	Order
8	3.8095e-02	0	1.7489e-02	0
16	9.6920e-03	1.9747	4.1447e-03	2.1906
32	2.4338e-03	1.9935	1.0222e-03	2.0197
64	6.0914e-04	1.9984	2.5467e-04	2.0049
128	1.5233e-04	1.9996	6.3613e-05	2.0018
256	3.8085e-05	1.9999	1.5900e-05	2.0003
512	9.5213e-06	2.0000	3.9747e-06	2.0001

(C.7)

for lifting parameters  $\eta^e + N_s = 3$ .

### C.3 Conclusion

The Brezzi method is applicable for periodic systems and has second-order convergence for polynomials of degree 1.



## D Periodic wave solutions for WVBM model

*Remark.* The author of this document is Gert Klopman of the group AAMP, University of Twente (date: March 31, 2006). The document has been adapted to fit into this report.

### D.1 Model equations

We use the following variational principle for water waves with surface elevation  $\eta(x, t)$  and velocity potential  $\varphi(x, t)$ :

$$\mathcal{L}(\eta, \partial_t \eta, \partial_x \varphi) = \int \int L(\eta, \partial_t \eta, \partial_x \varphi; x, t) dx dt, \quad (\text{D.1})$$

with the Lagrangian density  $L(\eta, \partial_t \eta, \partial_x \varphi; x, t)$  [37]:

$$L(\eta, \partial_t \eta, \partial_x \varphi; x, t) = -\eta \partial_t \varphi - \frac{1}{2} (h_0 + \eta) (\partial_x \varphi)^2 + \frac{1}{6} h_0 (\partial_t \eta)^2 - \frac{1}{2} g \eta^2, \quad (\text{D.2})$$

where  $g$  is the gravitational acceleration and  $h_0(x)$  is the still water depth: both quantities  $g$  and  $h_0(x)$  are positive. Then from  $\delta \mathcal{L} = 0$  we have the following Euler-Lagrange equations for variations with respect to  $\varphi$  and  $\eta$ , respectively:

$$\partial_t \eta + \partial_x [(h_0 + \eta) \partial_x \varphi] = 0, \quad (\text{D.3a})$$

$$\partial_t \varphi + \frac{1}{2} (\partial_x \varphi)^2 + g \eta + \frac{1}{3} h_0 \partial_t^2 \eta = 0. \quad (\text{D.3b})$$

### D.2 Periodic solutions

We are looking for periodic solutions, with wave length  $\lambda$  and moving with a constant (yet unknown) phase speed  $c$ . The surface elevation itself will be periodic, *i.e.*  $\eta(x - ct)$ , but the potential  $\varphi(x, t)$  may contain a constant drift in space and time:

$$\varphi(x, t) = U x + \gamma t + \phi(x - ct), \quad (\text{D.4})$$

with  $U \equiv \overline{\partial_x \varphi}$  the mean potential-gradient and  $\gamma \equiv \overline{\partial_t \varphi}$  the Bernoulli constant. Both  $\eta(x - ct)$  and  $\phi(x - ct)$  are chosen to have a zero mean value,  $\overline{\eta} = 0$  and  $\overline{\phi} = 0$  respectively:

$$\overline{\eta} \equiv \frac{1}{\lambda} \int_0^\lambda \eta(x - ct) dx = 0 \quad \text{and} \quad (\text{D.5a})$$

$$\overline{\phi} \equiv \frac{1}{\lambda} \int_0^\lambda \phi(x - ct) dx = 0. \quad (\text{D.5b})$$

The flow equations (D.3) become, for the periodic wave case:

$$-c \eta' + \left[ (h_0 + \eta) (U + \phi') \right] = 0, \quad (\text{D.6a})$$

$$\gamma - c \phi' + \frac{1}{2} (U + \phi')^2 + g \eta + \frac{1}{3} h_0 c^2 \eta'' = 0, \quad (\text{D.6b})$$

with an apostrophe denoting differentiation with respect to  $x$ . For the remainder, we consider all quantities at  $t = 0$ , so we can write them as only a function of  $x$ .

### D.3 Integrations

The mass conservation equation (D.6a) can be easily integrated once, giving:

$$-c \eta + (h_0 + \eta) (U + \phi') = Q, \quad (\text{D.7})$$

with the mean mass flux  $Q$  an integration constant. From this, we have for the oscillatory part of the velocity-potential gradient  $\phi'$  :

$$\phi' = \frac{c\eta + Q}{h_0 + \eta} - U. \quad (\text{D.8})$$

This can be used to eliminate  $\phi'$  from the momentum equation (D.6b):

$$\gamma + cU - c \frac{c\eta + Q}{h_0 + \eta} + \frac{1}{2} \left( \frac{c\eta + Q}{h_0 + \eta} \right)^2 + g\eta + \frac{1}{3} h_0 c^2 \eta'' = 0. \quad (\text{D.9})$$

After multiplication with  $\eta'$  we can also integrate this:

$$(\gamma + cU)\eta - \frac{1}{2} \frac{(c\eta + Q)^2}{h_0 + \eta} + \frac{1}{2} g\eta^2 + \frac{1}{6} h_0 c^2 (\eta')^2 = \beta, \quad (\text{D.10})$$

with  $\beta$  another integration constant. This equation looks a bit similar to, but is not the same as the Lagrangian density (D.2). We can write it as:

$$\frac{f(\eta)}{h_0 + \eta} + \frac{1}{6} h_0 c^2 (\eta')^2 = 0, \quad (\text{D.11})$$

with  $f(\eta)$  a cubic polynomial:

$$f(\eta) = \alpha_3 \eta^3 + \alpha_2 \eta^2 + \alpha_1 \eta + \alpha_0, \quad (\text{D.12})$$

where

$$\alpha_0 = -\frac{1}{2} Q^2 - \beta h_0, \quad (\text{D.13a})$$

$$\alpha_1 = (\gamma + cU) h_0 - cQ - \beta, \quad (\text{D.13b})$$

$$\alpha_2 = \gamma + cU - \frac{1}{2} c^2 + \frac{1}{2} g h_0 \quad \text{and} \quad (\text{D.13c})$$

$$\alpha_3 = \frac{1}{2} g. \quad (\text{D.13d})$$

The consequences of  $f(\eta)$  being a cubic polynomial will be examined in more detail later on.

#### D.4 Model closure

To close the system of equations, we average equations (D.8), (D.9) and (D.10):

$$c \frac{\overline{\eta}}{h_0 + \eta} + Q \frac{\overline{1}}{h_0 + \eta} - U = 0, \quad (\text{D.14a})$$

$$\gamma + \frac{1}{2} U^2 + \frac{1}{2} \overline{(\phi')^2} = 0 \quad \text{and} \quad (\text{D.14b})$$

$$-\frac{1}{2} \frac{\overline{(c\eta + Q)^2}}{h_0 + \eta} + \frac{1}{2} g \overline{\eta^2} + \frac{1}{6} h_0 c^2 \overline{(\eta')^2} - \beta = 0. \quad (\text{D.14c})$$

Note that from eq. (D.14b), and from eq. (D.10) for the  $x$ -locations where  $\eta$  is zero, we have:

$$\gamma \leq 0 \quad \text{and} \quad (\text{D.15a})$$

$$\beta + \frac{1}{2} \frac{Q^2}{h_0} \geq 0. \quad (\text{D.15b})$$

From eq. (D.11) we see, that for each  $\eta$  in the periodic wave there are two possible values, a positive and a negative one, for the wave slope  $\eta'$ . So we restrict our search for periodic waves to symmetric waves around the wave crest, which is taken to be at  $x = m\lambda$ ,  $m \in \mathbb{N}$ .

Then the waves are also symmetric around the wave troughs  $x = \frac{1}{2}\lambda + m\lambda$ ,  $m \in \mathbb{N}$ . The surface elevation  $\eta$  is an even function of  $x$  around the crest and trough  $x$ -locations. And the potential  $\phi$  can be taken to be an odd function around crest and trough  $x$ -locations, fixing the level of  $\phi$  at zero at the crests and troughs.

If we take eq. (D.9) as a basis to solve for periodic waves, we have a second-order ordinary differential equation to be solved, with the boundary conditions:

$$\eta' = 0 \quad \text{at} \quad x = 0 \quad \text{and} \quad (D.16a)$$

$$\eta' = 0 \quad \text{at} \quad x = \frac{1}{2}\lambda. \quad (D.16b)$$

Further, if we assume the wave length  $\lambda$ , mean water depth  $h_0$  and gravitational acceleration  $g$  are given, we have the following unknowns parameters: the wave speed  $c$ , the mean depth-averaged velocity  $U$ , the mean discharge  $Q$  and the Bernoulli constant  $\gamma$ . So we need four additional conditions to close the system of equations. First, we have that the mean surface elevation  $\bar{\eta}$  equals zero, eq. (D.5a). Second, we either specify the mean depth-averaged velocity  $U$  or the mean discharge  $Q$ , and third we use eq. (D.14a), to relate them to each other and the phase speed  $c$ . And fourth, we specify the wave height  $H$ :

$$H = \max\{\eta\} - \min\{\eta\} = \eta(0) - \eta(\frac{1}{2}\lambda). \quad (D.17)$$

If we use eq. (D.10) as our flow equation, also  $\beta$  is an unknown, which can be fixed by using eq. (D.14c) as an additional constraint.

Observe that the mean mass-transport velocity is  $Q/h_0$ , which is in general unequal to the mean value of the depth-averaged velocity  $U$ . Also  $U$  is not equal to the mean Eulerian velocity under the trough level. So while specifying the discharge  $Q$  corresponds to Stokes' second definition of wave phase speed, specifying  $U$  does not correspond to Stokes' first definition of phase speed.

### D.5 Further investigation into the periodic wave solutions

Dingemans (section 6.4 [11]) gives a detailed description of how to obtain periodic solutions to (variants of) the Korteweg–de Vries equation, as well as approximate periodic solutions to Boussinesq-type equations.

Starting from eq. (D.12), since  $f(\eta)$  is a real-valued cubic polynomial, it can have either three real-valued roots, or one real-valued root and the other two being a complex-conjugate pair. Since we have at both the wave crest and trough that the wave slope  $\eta'$  is zero, and we assume that they are at two distinct levels  $\eta$ , which must be roots of  $f(\eta)$ , we conclude that  $f(\eta)$  must have three real-valued roots. So from eq. (D.11) we have that there are, for given  $c$ ,  $Q$ ,  $U$ ,  $\beta$  and  $\gamma$ , three levels  $\eta_1$ ,  $\eta_2$  and  $\eta_3$  where  $\eta'$  becomes zero. Without loss of generality, we take  $\eta_1 \geq \eta_2 \geq \eta_3$ , so:

$$f(\eta) = \frac{1}{2}g(\eta - \eta_1)(\eta - \eta_2)(\eta - \eta_3). \quad (D.18)$$

Since  $\bar{\eta} = 0$ , at least one root must be above zero and one below. Further, we see from eq. (D.11), that the part of  $f(\eta)$  for our present interest is the negative part between two zeros, since otherwise  $(\eta')^2$  cannot be positive. Because  $f(\eta)$  is positive above  $\eta = \eta_1$ , we conclude that:

$$\eta_1 > 0, \quad \eta_2 < 0 \quad \text{and} \quad \eta_3 < 0. \quad (D.19)$$

Note that for  $\eta = 0$  we have from eq (D.15b) that  $f(0) < 0$ . The periodic wave solutions are in the range  $\eta_2 \leq \eta \leq \eta_1$ , with  $\eta(0) = \eta_1$  and  $\eta(\frac{1}{2}\lambda) = \eta_2$  being the crest and trough elevation, respectively. Further  $\eta'$  is the negative root of eq. (D.10) in the interval  $x \in [0, \frac{1}{2}\lambda]$ .

Next, it is advantageous to write  $\eta(x)$  as Dingemans (section 6.4 [11]):

$$\eta = \eta_1 - (\eta_1 - \eta_2) \sin^2 \theta(x), \quad (\text{D.20})$$

with  $\theta(x)$  a yet unknown function of  $x$ , varying from  $\theta(0) = 0$  at the wave crest to  $\theta(\frac{1}{2}\lambda) = \frac{1}{2}\pi$  at the wave trough. Then we have:

$$\eta - \eta_1 = -(\eta_1 - \eta_2) \sin^2 \theta, \quad (\text{D.21a})$$

$$\eta - \eta_2 = (\eta_1 - \eta_2) (1 - \sin^2 \theta), \quad (\text{D.21b})$$

$$\eta - \eta_3 = (\eta_1 - \eta_3) - (\eta_1 - \eta_2) \sin^2 \theta \quad \text{and} \quad (\text{D.21c})$$

$$(\eta')^2 = 4(\eta_1 - \eta_2)^2 (\sin^2 \theta) (1 - \sin^2 \theta) (\theta')^2. \quad (\text{D.21d})$$

So, eq (D.11) becomes:

$$\frac{4}{3} \frac{h_0 c^2}{g} (\theta')^2 = \frac{(\eta_1 - \eta_3) - (\eta_1 - \eta_2) \sin^2 \theta}{(h_0 + \eta_1) - (\eta_1 - \eta_2) \sin^2 \theta}. \quad (\text{D.22})$$

From this equation we can solve  $x$  as a function of  $\theta$  in the interval  $\theta \in [0, \frac{1}{2}\pi]$ :

$$\begin{aligned} \sqrt{\frac{3}{4} \frac{g}{h_0 c^2}} x &= \int_0^\theta \sqrt{\frac{(h_0 + \eta_1) - (\eta_1 - \eta_2) \sin^2 s}{(\eta_1 - \eta_3) - (\eta_1 - \eta_2) \sin^2 s}} ds = \\ &= \sqrt{\frac{m_a}{m_b}} \int_0^\theta \sqrt{\frac{1 - m_b \sin^2 s}{1 - m_a \sin^2 s}} ds, \end{aligned} \quad (\text{D.23})$$

where the plus sign branch of  $\theta'$  is taken, since  $\theta$  is increasing from 0 to  $\frac{1}{2}\pi$  for  $x$  from 0 to  $\frac{1}{2}\lambda$ . The coefficients  $m_a$  and  $m_b$  are given by:

$$m_a = \frac{\eta_1 - \eta_2}{\eta_1 - \eta_3} \quad \text{and} \quad (\text{D.24a})$$

$$m_b = \frac{\eta_1 - \eta_2}{h_0 + \eta_1}. \quad (\text{D.24b})$$

Both  $m_a$  and  $m_b$  satisfy

$$0 < m_a < 1 \quad \text{and} \quad 0 < m_b < 1, \quad (\text{D.25})$$

since the wave height  $H = \eta_1 - \eta_2$  is always less than the water depth  $h_0$  for physically meaningful solutions. The integral in eq. (D.23) may be expressible in terms of elliptic integrals, but no sensible analytical solution has been found yet.

## D.6 Numerical solution

For the numerical solution of the periodic wave problem we use eq. (D.9) and solve this using the MATLAB routine `bvp4c`. In order to be able to do so, we have to write the problem as a system of first-order differential equations:

$$\mathbf{y}' = \mathbf{p}(\mathbf{y}), \quad (\text{D.26})$$

with

$$\mathbf{y} = \begin{pmatrix} \eta \\ \eta' \\ Z \\ \phi \end{pmatrix} \quad (\text{D.27})$$

and

$$\mathbf{p}(\mathbf{y}) = \begin{pmatrix} \eta' \\ -\frac{3}{h_0 c^2} \left( \gamma + cU - c \frac{c\eta + Q}{h_0 + \eta} + \frac{1}{2} \left( \frac{c\eta + Q}{h_0 + \eta} \right)^2 + g\eta \right) \\ \eta \\ \frac{c\eta + Q}{h_0 + \eta} - U \end{pmatrix}, \quad (\text{D.28})$$

with

$$Z \equiv \int_0^x \eta(\tilde{x}) \, d\tilde{x}. \quad (\text{D.29})$$

The last two equations are added to be able to ensure that  $\bar{\eta} = 0$  and  $\bar{\phi}' = 0$ . The boundary conditions are:

$$\eta'(0) = 0, \quad (\text{D.30a})$$

$$\eta'(\frac{1}{2}\lambda) = 0, \quad (\text{D.30b})$$

$$Z(0) = 0 \quad \text{and} \quad (\text{D.30c})$$

$$\phi(0) = 0. \quad (\text{D.30d})$$

For given values of the mean water depth  $h_0$ , gravitational acceleration  $g$ , mean depth-averaged velocity  $U$  and wave height  $H \equiv \eta(0) - \eta(\frac{1}{2}\lambda)$ , we have as additional unknowns: the phase speed  $c$ , mean discharge  $Q$ , Bernoulli constant  $\gamma$ . So we have to add three additional constraints, which are:

$$Z(\frac{1}{2}\lambda) = 0, \quad (\text{D.31a})$$

$$\phi(\frac{1}{2}\lambda) = 0 \quad \text{and} \quad (\text{D.31b})$$

$$\eta(0) - \eta(\frac{1}{2}\lambda) - H = 0, \quad (\text{D.31c})$$

the first ensuring that  $\bar{\eta} = Z(\frac{1}{2}\lambda)/(\frac{1}{2}\lambda) = 0$ , the second that  $\phi$  is an odd periodic function ( $\bar{\phi}' = 0$ ) and the last condition demanding the requested wave height  $H$ . As an initial condition, we specify the cnoidal wave solution to the BBM-equation (Dingemans, eq. (6.86) [11]). Some results are shown in figure D.6.1. The input parameters for this case are: mean water depth  $h_0 = 10$  m, wave height  $H = 6$  m, wave length  $\lambda = 100$  m, mean depth-averaged velocity  $U = 0$  m/s and gravitational acceleration  $g = 9.81$  m/s<sup>2</sup>. The computed parameters are: phase speed  $c = 9.83296$  m/s, mean discharge  $Q = 3.71993$  m<sup>2</sup>/s and Bernoulli constant  $\gamma = -1.62375$  m<sup>2</sup>/s<sup>2</sup>. As can be seen from figure D.6.1, there are small, but noticeable differences between the approximate cnoidal wave solution and the ‘exact’ numerical solution.

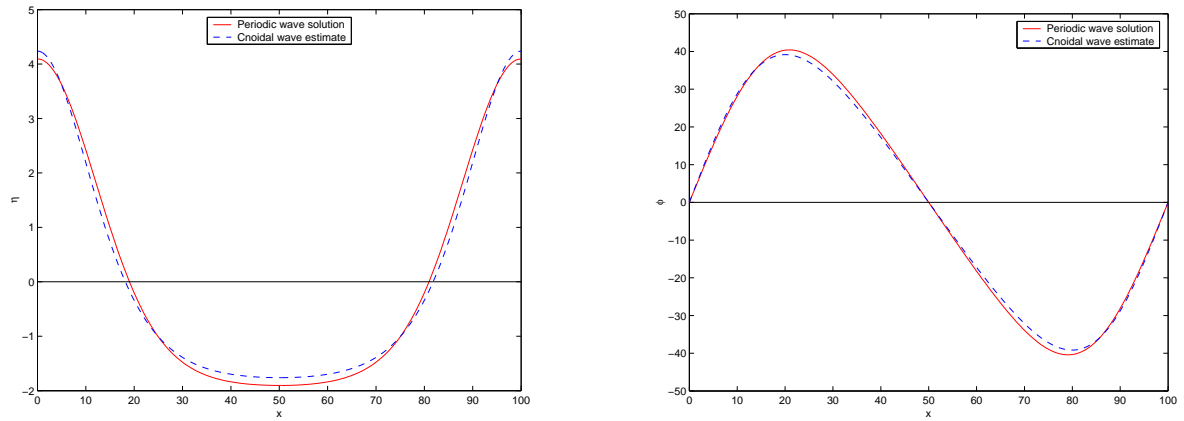


Figure D.6.1: Numerical solution of the periodic wave problem. The parameters are:  $h_0 = 10$  m,  $H = 6$  m,  $\lambda = 100$  m,  $U = 0$  m/s and  $g = 9.81$  m/s<sup>2</sup>. Left is the surface elevation  $\eta(x)$  and right the oscillatory part of the velocity potential  $\phi(x)$ . The drawn red line is the numerical solution obtained with the MATLAB routine `bvp4c`. The dashed blue line is the cnoidal wave solution of the BBM-equation (Dingemans, eq. (6.86) [11]).